HAZARDOUS CONVECTIVE WEATHER IN THE UNITED STATES:

A DYNAMICAL DOWNSCALING APPROACH

by

VITTORIO ANGELO GENSINI

(Under the Direction of Thomas L. Mote)

ABSTRACT

This research uses a high-resolution numerical weather prediction model to resolve hazardous convective weather east of the Continental Divide in the U.S. for two (historical and future) ten-year climate regimes. A regional hazardous convective weather model proxy is used to depict occurrences of tornadoes, damaging thunderstorm wind gusts, large hail at hourly intervals during the period of record. Results from this research provide an objective estimate of the historical occurrence of hazardous convective weather events, and how their spatio-temporal distribution may change in the future. In addition, reanalysis derived proxy soundings are compared to collocated observed soundings for the period 2000–2011. Specifically, important parameters used for forecasting severe convection are examined. These results provide researchers with the potential strengths and limitations of using reanalysis data for the purposes of depicting hazardous convective weather climatologies and initializing model simulations.

INDEX WORDS: Severe Convective Storms, Reanalysis, Dynamical Downscaling, Climatology, Hazards, Extreme Weather

HAZARDOUS CONVECTIVE WEATHER IN THE UNITED STATES:

A DYNAMICAL DOWNSCALING APPROACH

by

VITTORIO ANGELO GENSINI

B.S., Northern Illinois University, 2008

M.S., Northern Illinois University, 2010

A Dissertation Submitted to the Graduate Faculty of The University of Georgia in Partial

Fulfillment of the Requirements for the Degree

DOCTOR OF PHILOSOPHY

ATHENS, GEORGIA

2014

HAZARDOUS CONVECTIVE WEATHER IN THE UNITED STATES:

A DYNAMICAL DOWNSCALING APPROACH

by

VITTORIO ANGELO GENSINI

Major Professor: Thomas L. Mote

Committee: Harold E. Brooks
J. Marshall Shepherd
Andrew J. Grundstein

Electronic Version Approved:

Maureen Grasso
Dean of the Graduate School
The University of Georgia
May 2014

ACKNOWLEDGEMENTS

This dissertation could not have been completed without the enduring love, support, and patience from my wife, Jenna. Thanks for your encouragement, acceptance, and positive attitude during many long nights spent writing in my office. This dissertation is for you.

A sincere thank-you to an amazing supporting cast of friends and family members, especially my parents, Gene and Vicki, along with my second parents Jim and Laura. I cannot think of a better cohort of role models than you four. I am forever indebted to you for your love, support, and encouragement.

I would like to thank all people who have helped and inspired me during my tenure as a student at the University of Georgia. I especially want to thank my advisor, Dr. Tom Mote. I am grateful for his exemplary effort of writing recommendation letters, advice, encouragement, and camaraderie. This dissertation would not have been possible without him. Additional thanks to my committee members – Drs. Harold Brooks, Andy Grundstein, and Marshall Shepherd – for their suggestions, revisions, and insightful conversations. I also appreciate the discussions and assistance I have received from colleagues at UGA, especially in-depth discussions with Craig Ramseyer, Tony Bedel, and Alan Black in the Climate Research Laboratory.

My choice to pursue graduate school was largely a byproduct of discussions with Dr. Walker Ashley during my undergraduate career at Northern Illinois University. Walker believed in my ability to conduct research and is one of the main influences in my early professional career. He has been a brilliant colleague and friend throughout my graduate school journey, and I am very much grateful for his mentorship, friendship, and support.

This work was partially supported by a USDA Forest Service Southern Region cooperative agreement to the University of Georgia Research Foundation, Inc., Thomas L. Mote, PI (SRS 09-CA-1330138-079).

Dr. Vittorio A. Gensini in March of 1987. Go Dawgs!

TABLE OF CONTENTS

LIST OF TABLES

Page

LIST OF FIGURES

Page

CHAPTER 1

INTRODUCTION AND LITERATURE REVIEW

1.1 Introduction

a. Research context

This dissertation research examines historical and future trends of hazardous convective weather (i.e., tornadoes, damaging thunderstorm wind gusts, large hail, and flash flooding; hereafter HCW) in central and eastern portions of the U.S., by dynamically downscaling Global Climate Model (GCM) output. This analysis will provide an objective estimate of the historical occurrence of HCW events, and how their spatio-temporal distribution may change in the future. The motivation for this research stems from a growing vulnerability to severe[1] weather events due to increasing population density, as well as the potential for a greater frequency of these events in future climate regimes.

b. Motivation

Severe thunderstorms during April–May 2011 spawned tornadoes responsible for $17.3 billion in damages and at least 350 fatalities across 20 states. The increasing trend of losses from severe thunderstorms (Changnon 2001) and tornadoes (Brooks and Doswell 2001; Changnon 2009) can be attributed to societal and economic changes rather than an increase in event frequency (Bouwer 2011). However, recent research has indicated that the potential for severe

[1] The current National Weather Service working definition of severe weather is defined as a thunderstorm producing hail that is at least 2.5 cm (1 inch) in diameter or larger, and/or wind gusts to 50 kts (58 mph) or greater, and/or a tornado (rev. Hales 1988).

thunderstorm environments may increase under future climate scenarios (Trapp et al. 2007a; Van Klooster and Roebber 2009). The combination of increasing societal vulnerability (Cutter et al., 2003) and severe thunderstorm frequency may lead to greater HCW impacts in the future.

1.2 Literature review

There is question surrounding the historical record of HCW in the U.S., which is vital to understand if researchers desire to make predictions about future HCW events. In short, spatio-temporal trends of HCW have been difficult to determine reliably due to the subjective nature of the reporting process (Doswell and Burgess 1988; Grazulis 1993; Brooks and Doswell 2001; Brooks and Doswell 2002; Verbout et al. 2006; Doswell 2007). This has left hazards researchers with an observationally biased dataset of reports with unclear trends. To avoid this reporting obstacle, recent research has turned to the environmental ingredients (Doswell et al. 1996) necessary for the formation of severe thunderstorms known as supercells, which are most likely to produce HCW (Doswell et al. 1993; Doswell 2001).

a. HCW environments

In order to attain convection in the atmosphere, several ingredients must be juxtaposed. These include a moist layer of sufficient depth in the low or mid-troposphere, a steep enough lapse rate to allow for substantial convective instability, and sufficient lifting to the level of free convection (Doswell 1987; Johns and Doswell 1992).

Moisture serves as potential energy for convective processes and can be quantified using different techniques. Some common ways to calculate moisture include dewpoint temperature, mixing ratio, and specific humidity. Abundant amounts of moisture can provide a significant positive energy feedback mechanism to convection as condensation releases latent heat, thus increasing the internal temperature of a theoretical parcel.

Convective instability is defined as the ability of a parcel of air to accelerate freely due to its own positive/negative buoyancy. Buoyancy, *B*, can be described[2] as:

$$B \equiv g \frac{T - T'}{T'}$$

where g is the acceleration due to gravity, T is the temperature of a parcel, and T' is the temperature of the surrounding environment. Thus, if T is greater than T', buoyancy will be positive and a parcel will freely accelerate upward due to density differences. Taking the above buoyancy equation and integrating over the distance displaced (typically from the level of free convection [LFC] to the equilibrium level [EL]), yields convective available potential energy (CAPE; Moncrieff and Miller 1976). Measured in $J \cdot kg^{-1}$, CAPE is essentially the amount of energy available to a positively buoyant parcel of air which, in theory, is directly related to updraft velocity (w). CAPE can be calculated using a variety of parcel methods (e.g., mixed-layer, surfaced-based, most-unstable). Different forecasting scenarios utilize different parcel ascent methods. For instance, while thorough boundary layer mixing is occurring in the afternoon hours, a forecaster would likely choose to calculate CAPE based on a mixed-layer parcel over a surface-based parcel because of its greater resemblance of the true thermodynamic condition of the boundary layer. Although the calculation of CAPE using parcel theory has

[2] For a more in-depth discussion on buoyancy, please reference Doswell and Markowski (2004).

limitations (Markowski and Richardson 2011), it is currently the most widely accepted technique to assess potential instability and updraft intensity.

In order for convection to utilize this potential energy in a non-autoconvective environment, a lifting mechanism must supply energy to displace the parcel to its LFC. This negative buoyancy (found by integrating the buoyancy equation between the lifting condensation level [LCL] and LFC) is known as convective inhibition (CIN). Like CAPE, CIN can be calculated using a variety of parcel ascent methods. Lifting mechanisms arise from an array of sources, including topography, frontal boundaries, density discontinuities, upper-level mass divergence, surface mass convergence, etc.

Organized convection (Doswell 2001) forms when another ingredient, wind shear, is also present. Although not mutually exclusive, two types of wind shear exist, and are a key factor in determining convective mode (Weisman and Klemp 1982; 1984; Dial et al. 2010). Speed shear occurs when wind speeds change with height in the atmosphere. This is important in the sustenance of convective activity as it allows the updraft and downdraft to occur in separate regions of the thunderstorm, permitting it to continually ingest less dense, and therefore unstable, surface air. Speed shear also contributes to environmental horizontal vorticity, which can be converted into vertical vorticity if an updraft is introduced (Rotunno 1981; Davies-Jones 1984). Subsequently, directional and speed shear can be quantified using storm relative helicity (SRH; Davies-Jones et al. 1990). SRH is a measure of streamwise vorticity in the inflow region of a convective storm with dimensions $m^2 \cdot s^{-2}$. Often calculated over a vertical layer (typically 0–1 or 0–3 km) by integrating, SRH is easily visualized by forecasters via a hodograph. Recently, Thompson et al. (2007) have developed effective storm relative helicity (ESRH), and documented that ESRH more clearly discriminates between significantly tornadic and nontornadic forms of supercell thunderstorms than the standard 0–1 km and 0–3 km fixed-layer versions of SRH.

b. Organized convection

i. Mesoscale convective systems

First described by Zipser (1982), mesoscale convective systems (MCSs) evolve over 3–6 hour (and longer) time periods, contain both convective and stratiform precipitation regions during some portion of their lifecycle (Smull and Houze 1985; Knupp and Cotton 1987; Biggerstaff and Houze 1991), and have horizontal dimensions of at least 100 km (Houze 2004). Initially, MCS stages (i.e., initiation, growth, maturity, and decay) were described by their infrared satellite characteristics (e.g., cloud shield radius and cloud top temperature), but recently have been categorized by their RADAR attributes (Hilgendorf and Johnson 1998). Additionally, taxonomy was introduced by Parker and Johnson (2000) to classify different types of MCSs based upon stratiform precipitation distribution (e.g., trailing (TS), leading (LS), and parallel (PS) stratiform precipitation. The mesoscale convective complex (MCC), a spatially large and long-lived MCS, has strict qualifications (Maddox 1983).

MCSs tend to favor producing severe weather during early stages of their life cycles, but a few may continue producing large swaths of severe weather (typically wind damage) until they dissipate. For example, MCSs known as bow echoes (Fujita 1978) are well recognized because of their bowing appearance on a two-dimensional planar radar display, and their ability to produce long swaths of damaging winds (Doswell 2001). Occasionally, long-lived windstorms known as derechos occur. Derechos are MCSs that produce severe wind damage over specific spatio-temporal criteria (Johns and Hirt 1987). Ashley and Mote (2005) showed that derechos are a respectable hazard in the U.S. with 153 fatalities and over 2600 injuries occurring over their 18-year study period as a direct result of derechos. Although difficult, differentiating between derecho and ordinary MCS environments appears to reside in different storm-relative vertical wind shear profiles (Evans and Doswell 2001).

ii. Linear organization

While it is the most common form of organized convection, linear organization is typically not responsible for most extreme severe weather events (Doswell 2001). Linear organization is often the result of the vertical wind shear profile, and the lifting mechanism. For example, linear convection tends to dominate if wind shear profiles are aligned parallel to the lifting mechanism. In this scenario, linear structures form as perturbation flows they generate (i.e., updrafts, downdrafts, surface cold pools) interact (Doswell 2001). Therefore, if lift is present in environments characterized by similar thermodynamic properties, linear organization will tend to dominate since most fronts, outflow boundaries, and drylines provide sources of lift that are linear in nature. Although no formal definition exists, a classic example of linear organization is a squall line. The term squall line was first described by the Bergen School of Meteorology in the early twentieth century because of the disruption in calm weather conditions normally present during squall passage (Doswell 2001). Today, squall lines are defined as a type of MCS, and are much longer than they are wide. Squall lines are efficient at relieving convective instabilities on large spatial and temporal scales, as well as providing beneficial precipitation to agriculture.

iii. Supercells

The term supercell first appeared in formal literature in 1962 (Browning 1962). Over the years, studies such as Browning (1977) and Weisman and Klemp (1984) strived to develop a definition of supercells by using different techniques. Doswell (1996) explains uncertainties regarding the true definition of a supercell, but most scientists agree that a supercell must possess a deep, persistent mesocyclone. The identification of a supercell by means of the Lemon technique utilizes three- and four-dimensional RADAR output (Lemon 1977). Currently, supercells are classified along a spectrum in three categories based upon their precipitation distribution: high precipitation (HP), low precipitation (LP), and classic (CL) (Rasmussen and Straka 1998); however, supercells can evolve across this spectrum during their lifecycle (Bluestein and Woodall 1990). Supercells are responsible for a majority of significant severe weather (Church et al. 1993; Doswell 2001); therefore, understanding the environments in which supercells develop is vital to forecasting where and when significant severe weather events will occur.

c. HCW forecasting

Thunderstorm forecasters use three types of forecasting techniques: pattern recognition, climatology, and parameter evaluation (Johns and Doswell 1992). Synoptic pattern recognition of severe weather outbreaks has been documented well (e.g., Miller 1972; Uccellini and Johnson 1979; Doswell 1980; Johns 1982; Johns 1984). In Miller's (1972) study, five synoptic patterns (type A–E) were found most favorable for the development of severe weather events. Miller's patterns are often used as conceptual models for thunderstorm forecasters. Although the specifics of each pattern type differ, the main four ingredients for organized convection are present in each. As Miller's patterns show, early spring severe weather outbreaks typically take place under southwest 500-hPa flow on the east side of a 500-hPa height trough axis. As the convective season progresses, is it common for severe weather outbreaks to transition from southwesterly to northwesterly upper-level 500-hPa flow. Johns (1982, 1984) established that northwest flow severe weather outbreaks occur in environments of abundant low-level moisture, with the 500-hPa wind direction over the expected geographical midpoint of the outbreak from 280º or more. Johns also noted that that low-level moisture transport impinging upon surface boundaries under northwest flow is important in determining areas favorable for severe weather.

Severe weather climatology as a forecast tool is not as apparent as pattern recognition. Issues arise regarding the quality of severe storm reporting in the United States (Doswell and Burgess 1988, Brooks and Doswell 2001), as well as significant events that occur outside of peak climatology. Nevertheless, understanding the climatology of severe weather can assist forecasters by developing an understanding of the relative risk of severe weather events in their respective regions. Perhaps one of the best tools[3] available for forecasters to understand climatologies associated with severe weather events was developed by Brooks et al. (2003a). This interactive web browser allows users to develop probabilities of unique severe weather event occurrence for any U.S. location. From this work, Concannon et al. (2000) showed that the greatest concentrations of significant tornadoes were bounded by an L-shaped region from Iowa to Oklahoma to Mississippi. However, Ashley (2007) has shown that most tornado fatalities from 1880–2005 occurred east of the climatological maximum, where a unique vulnerability exists due to physical and societal factors.

[3] This tool was recently updated and is now available through the Storm Prediction Center's online database: http://www.spc.noaa.gov/new/SVRclimo/climo.php

Parameter evaluation is the most popular and effective technique used in thunderstorm forecasting. Essentially, a forecaster can assess the potential for severe convection by evaluating parameters associated with ingredients necessary for such events (Table 1.1). Diagnostic indices such as CAPE, CIN, SRH, 6BWD, LFC, and LCL are all useful in determining the potential for supercell thunderstorms (Rasmussen and Blanchard 1998; Rasmussen 2003; and Craven et al. 2004). These diagnostic parameters are often analyzed by forecasters in a prognostic sense by extrapolation (i.e., short-term forecasts) and numerical weather prediction. Forecasters typically place thresholds of these parameters on a composite chart (Miller 1972; Crisp 1979) to represent the greatest threat for severe thunderstorms. Quantifications of the overlaying of different ingredients found on composite charts are expressed using composite indices. Several composite indices have been developed to discriminate between atmospheric environments favorable for certain types of severe weather events (Table 1.2). Previous research has used various thunderstorm ingredients to discriminate between significant[4] severe and severe weather environments (Brooks et al. 2003b), supercell and non-supercell environments (Thompson et al. 2003, 2007), and tornado vs. significant tornado environments (Thompson et al. 2003, 2007).

Since organized thunderstorm activity can occur in a variety of atmospheric environments (i.e., from high instability, low shear to low instability, high shear), composite indices evaluated at face value by forecasters can become problematic. For example, if a composite indices' calculation threshold calls for the occurrence of CAPE values greater than 2000 $J \cdot kg^{-1}$, an environment with 1999 $J \cdot kg^{-1}$ of potential energy would be neglected as reaching the threshold. Doswell and Schultz (2006) emphasize that forecasters must exercise caution when employing indices and parameters in an operational setting. They argue that these indices

[4] Significant severe weather is defined as hail at least 5 cm (~2 in.) in diameter, and/or a convective wind gusts ≥120 km h^{-1} (65 kt), and/or a tornado of at least EF2/F2 damage (Hales 1988).

seek to simplify the non-linear atmosphere and should not be treated as a magic solution as to where HCW will occur. Furthermore, it is vital to understand exactly which variables are going into in the calculation of such composite indices in order to understand their strengths and limitations.

d. Using teleconnections to forecast HCW

Hemispheric circulations force favorable synoptic-scale regimes that facilitate mesoscale processes that, in turn, favor HCW development and sustenance. Studies such as Higgins and Schubert (1996) and Deser (2000) have focused on such circulations and their impact on hemispheric jet stream patterns. Since these hemispheric-scale oscillations feed back to the synoptic scale, opportunity arises for forecasters to use these oscillations as possible medium- and long-range predictive tools. Recent attempts to use teleconnection indices such as the Madden-Julian Oscillation (MJO; Madden and Julian 1972) and sea-surface temperature anomalies have shown skill in predicting central U.S. tornado activity in the 4–6 week forecast period (Barrett and Gensini 2013; Elsner and Widen 2013). This enhanced understanding of mid-range HCW evolution and forecasting is improving rapidly and will continue to flourish in the next decade.

e. Evaluating HCW activity using reanalysis

A novel approach by Brooks et al. (2003b) exploited a statistical discriminate relationship between HCW reports and the product of CAPE and 6BWD. They developed spatial distribution plots of global HCW environments for the period 1997–1999 using data from the National Center for Atmospheric Research / National Center for Environmental Prediction (NCAR/NCEP) global reanalysis (Kalnay et al. 1996). HCW environments were concentrated in equatorial Africa, southern Europe, the central U.S., southern Brazil, Australia, northern Argentina, and near the Himalayas, with the highest frequencies found in the central Great Plains region of the U.S. (Brooks et al. 2003b) due to its unique geography (Fig. 1.1). The close proximity to a source of surface moisture (Gulf of Mexico) to the south and steep mid-level lapse rates provided by a north-south oriented mountain chain (Rocky Mountains) to the west comingle to create favorable environments for severe thunderstorms. Because the central U.S. is the home to the highest frequency of HCW on Earth, a higher spatial-resolution analysis of thunderstorm environments was conducted by Gensini and Ashley (2011) using data from the North American Regional Reanalysis (NARR; Mesinger et al. 2006) for the period 1980–2009. This research revealed no significant trend in HCW environmental controls in the U.S. despite a significant increase in severe weather reports over the same period. However, the main caveat with such environmental control analysis is that no research to date (due to the small spatial scale) has been able to account for a lifting mechanism, which is vital in the initiation and sustenance of HCW (Gensini and Ashley 2011; Trapp et al. 2011). This is due to the limited vertical and spatial resolution of most reanalysis datasets, as well as the high spatial variability associated with modeled surface divergence fields.

While reanalysis datasets are currently a popular data source (3140 peer-reviewed journal articles with “reanalysis” in the title or abstract in from 2010–2011), no peer-reviewed research has examined how the filtered nature (e.g., limited vertical levels) of reanalysis data may affect convectively important variables. One major problem of reanalysis for convective purposes is the overestimation of favorable HCW environments in southern Texas (Gensini and Ashley 2011). It is hypothesized here that limited vertical resolution near the reanalysis model surface poorly captures convective inhibition (CIN) produced by an elevated mixed layer, described by

Lanicci and Warner (1991). A recent international study revealed similar problems with CIN calculations over HCW favored regions of Australia (Allen and Karoly 2013).

f. Current limitations

Similar to the historical approaches presented above, some research has used an environmental control approach to simulate potential future changes in HCW using GCM output. Studies such as Del Ginio et al. (2007), Trapp et al. (2007a), Trapp et al. (2009), and Van Klooster and Roebber (2009) all suggest that environmental controls related to HCW will increase in response to elevated greenhouse forcing. While more HCW environments could mean more events in the future, such environments are periods when the atmosphere is favorable for organized HCW, not that it will necessarily occur. A lifting mechanism is essential and was not accounted for in any of the published research employing this methodology.

Despite evidence for increasing HCW environmental controls such as CAPE, climate change assessments have largely avoided any conclusions regarding potential changes of HCW in a future climate (e.g., see discussions in Alley et al. [2007] and Karl et al. [2009]). This is primarily due to problems with the historical record and the large spatial scale in which GCMs operate relative to HCW. As an example of this scale difference, the widely used Community Climate System Model version 3 (CCSM3; Collins et al. 2006) GCM is a spectral model with 85-wavenumber triangular truncation (approximately 1.4° resolution at the equator) in the horizontal (Collins et al. 2006). For comparison, this GCM configuration translates roughly to a 150-km horizontal grid spacing in the central U.S., while explicit resolution of convection should be done at a horizontal grid scale of less than or equal to 4 km (Weisman et al. 1997). Therefore, the resolution of typical GCM output lacks the ability to resolve HCW.

g. Applying dynamical downscaling

Recent exploratory research has indicated dynamical downscaling of GCM data has become possible owing to enhanced model microphysics schemes, faster computer processing, and new GCM data availability. Dynamical downscaling (sometimes referred to as model telescoping) is a method for obtaining high-resolution climate information from relatively coarse-resolution GCM output. Using dynamical downscaling, recent research indicates it is now practical to downscale GCM scale output to the 4 km grid spacing (Trapp et al. 2007b; Trapp et al. 2010; Robinson et al. 2013) required for explicitly resolving convective processes (Weisman et al. 1997). Dynamically downscaled global reanalysis data (similar to the course-resolution of many GCMs) have accurately represented HCW during the peak of the convective season (May–June; Trapp et al. 2010; Robinson et al. 2013). However, no studies have examined historical control runs of GCM output. This is especially important if researchers wish to use a dynamical downscaling technique on future projections from GCM data, as bias correction techniques should be incorporated (Christensen et al. 2008).

1.3 Research questions

The first manuscript (Chapter 2) provides context regarding the similarities and differences between reanalysis derived datasets and observed radiosonde data for convective interests. Although undocumented, it is hypothesized here that limited vertical resolution near the reanalysis model surface poorly captures convective inhibition (CIN) produced by an elevated mixed layer, described by Lanicci and Warner (1991). Quantifying the similarities and differences between historical reanalysis datasets and observed upper-air radiosonde data will permit objective correction techniques for those using reanalysis data to examine HCW. Accordingly, this manuscript will address the following research questions:

- Which convectively important observed variables are most closely represented by reanalysis?
- Which variables are poorly reconstructed by reanalysis?
- Are differences present between observed and derived variables?
- What changes to the reanalysis structure would benefit convective research?

The second manuscript (Chapter 3) assesses a dynamically downscaled reconstruction of HCW from GCM historical control data for the months March–May, 1980–1989. Completion of this objective will establish an objective climatology of HCW from a control GCM simulation. Additionally, results from this section will be used for statistical comparison to fields generated in the third manuscript (Chapter 4) of this dissertation. The following questions will be examined in this manuscript:

- How does the reconstructed HCW proxy distribution compare to observed HCW reports?
- What grid spacing best captures the spatial distribution?
- How do environmental parameters relate to HCW proxy reports?
- Are there any differences in the timing of observed and reconstructed HCW reports?
- How do these reconstructions compare to other studies?

The third manuscript (Chapter 4) assesses a dynamically downscaled reconstruction of HCW from GCM future simulations for the period March–May, 2080–2089. Completion of this objective will establish the first modeled objective climatology of HCW from a GCM run using the SRES (Special Report on Emissions Scenarios) A2 scenario. Results from this section will be used for statistical comparison to fields generated in the second manuscript (Chapter 3) of this dissertation. The following questions will be examined in this manuscript:

- How does the future HCW proxy distribution compare to the historical reconstruction?
- Is there a statistically significant change in future HCW occurrence?
- Can changes in HCW be attributed to changes in the environmental control parameters?
- Are there any differences in the diurnal timing of future and historical HCW reports?
- What are the socioeconomic implications for any potential HCW event changes?

1.4 Summary

Future changes in HCW event occurrence has been a topic of interest for many researchers around the world during the past decade. Solid conclusions have been difficult to formulate, owing to the complex nature of the research question. Most previous studies have narrowed their focus to changes in environmental control parameters that are known to contribute to HCW formation. However, these control parameters only serve to represent a favorable (or non-favorable) HCW environment in the future, not necessarily implying that an HCW event will indeed occur. This assumption can lead to large positive biases of environments favorable for HCW, especially if CIN is ignored. Thus, the foremost part of this dissertation will provide the first documentation of the strengths and limitations of using reanalysis data to approximate HCW environments. This is significant if researchers are to use such data for climatological studies, or to initialize model simulations.

Secondly, a modeled historical climatology of HCW will provide insight into how environmental controls used in previous reanalysis studies were able to capture the distribution of modeled HCW frequency. This portion of the dissertation will contribute to a very limited set of current knowledge regarding the use of dynamical downscaling for purposes of resolving HCW. Additionally, this historical bias-corrected distribution of HCW will provide a baseline with which to compare the future dynamically downscaled simulation.

Arguably the most noteworthy portion of this dissertation will attempt to provide indications of potential changes in distributions of HCW under a future climate scenario. The results from this dissertation will be first application of dynamical downscaling methodology to future output from a GCM. Knowledge of the historical and potential changes in the spatio-temporal distribution of future HCW events is essential if decision makers wish to mitigate socioeconomic impacts of HCW in the future. Most importantly, this dissertation will create knowledge beneficial to a wide variety of researchers (e.g., hydrologists, ecologists, climate modelers, risk analysts) seeking to understand the potential impacts of a shifting climate on HCW.

Table 1.1 Notable severe weather forecasting parameters

Index	Definition	Dimension
Convective Available Potential Energy (CAPE)	Amount of energy available to accelerate a theoretical parcel vertically; directly related to updraft velocity	$J \cdot kg^{-1}$
Convective Inhibition (CIN)	Amount of energy needed to lift the theoretical parcel to its level of free convection	$J \cdot kg^{-1}$
Lifted Index (LI)	Snapshot measure of stability calculated by subtracting the theoretical parcel's temperature from the environment's temperature (usually calculated at 500 hPa)	°C
Lifting Condensation Level (LCL)	Height above ground in which a theoretical parcel becomes saturated due to adiabatic ascent	m
Level of Free Convection (LFC)	Height above ground in which a theoretical parcel vertically accelerates freely due to density differences between the parcel and the environment	m
Storm Relative Helicity (SRH)	Measure of the potential for cyclonic updraft rotation in right-moving supercells. Proportional to streamwise vorticity and the strength of the flow feeding the updraft. Can be calculated over a layer (e.g., 0–1 km) or over the effective inflow layer of the updraft (Effective Storm Relative Helicity [ESRH]).	$m^2 \cdot s^{-2}$ **or** $J \cdot kg^{-1}$
0–6 km Bulk Wind Difference (6BWD)	The surface to 6 km change in wind speed	kts
Mid- / Low-Level Lapse Rates	A measure of the change in temperature per unit of vertical distance. Typically measured in the low-levels (0–3 km) and the mid-levels (700–500 hPa)	$°C \cdot km^{-1}$
2 m θ_e	Temperature that results after all latent heat is released in a theoretical lifted parcel and the then descended dry adiabatically to the 1000 hPa reference level	K

Table 1.2 Notable severe weather forecasting composite indices

Composite Index	Indices Incorporated	Reference(s)
Supercell Composite (SCP)	CAPE, SRH, 6BWD	Thompson et al. (2003, 2007)
Significant Tornado (STP)	CAPE, SRH, 6BWD, LCL	Thompson et al. (2003, 2007)
Energy Helicity Index (EHI)	CAPE, SRH	Hart and Korotky (1991)
Bulk Richardson Number (BRN)	CAPE, 6BWD	Weisman and Klemp (1982)
Craven / Brooks Significant Severe (C)	CAPE, 6BWD	Brooks et al. (2003b)
Non-Supercell Tornado (NST)	CAPE, 0–3 km lapse rate, CIN, 6BWD, Vorticity	Baumgardt and Cook (2006)

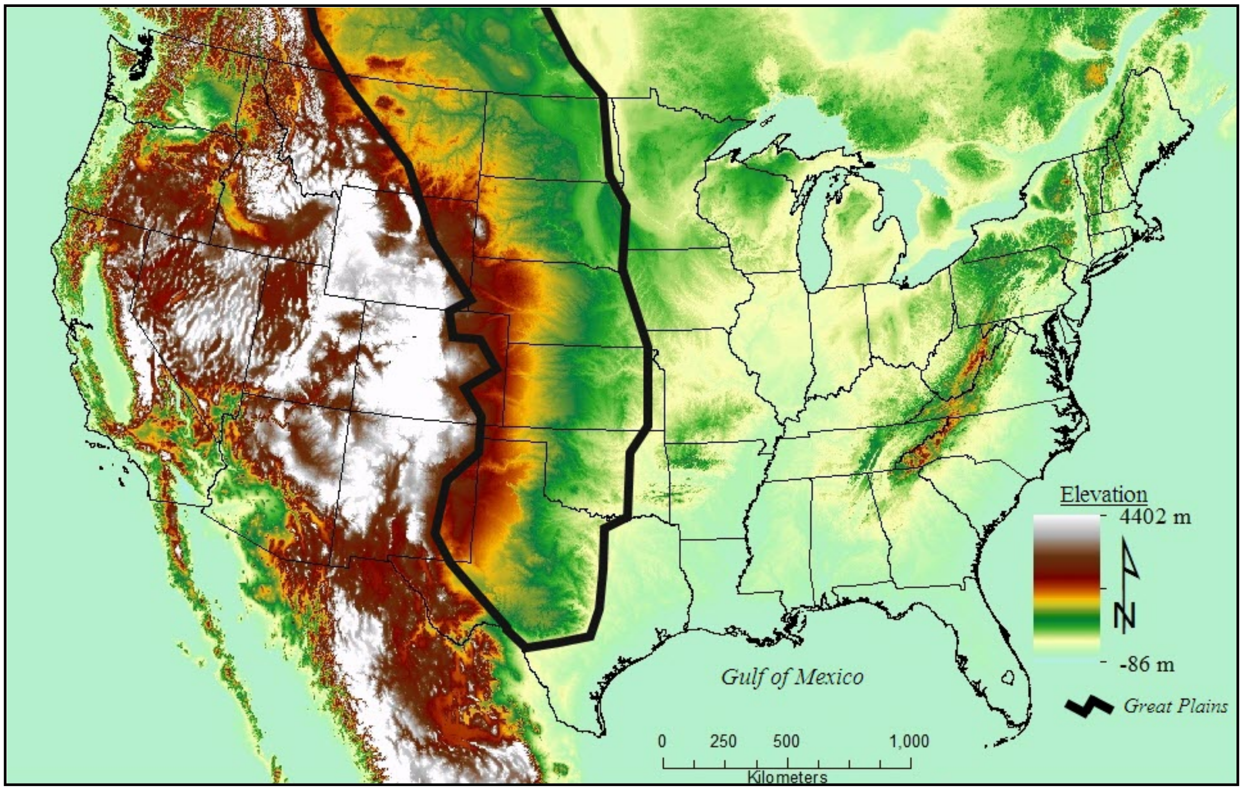

Fig. 1.1. Shaded topographic map of the continental United States. Black polygonal outline indicates the location of the Great Plains.

CHAPTER 2

SEVERE THUNDERSTORM REANALYSIS ENVIRONMENTS AND COLLOCATED RADIOSONDE OBSERVATIONS[1]

[1] Gensini, V. A., C. A. Ramseyer, and T. L. Mote, 2014: Future convective environments using NARCCAP. *International Journal of Climatology*, **34**, 1699–1705. Reprinted here with permission.

Abstract

This research compares reanalysis derived proxy soundings from the North American Regional Reanalysis (NARR) to collocated observed radiosonde data across the central and eastern United States during the period 2000–2011. Specifically, 23 important parameters used for forecasting severe convection are examined. Kinematic variables such as 0–6 km bulk wind shear are best represented by this reanalysis, while thermodynamic variables such as convective available potential energy exhibit regional biases and are generally overestimated by reanalysis. For thermodynamic parameters, parcel ascent choice is an important consideration, owing to large differences in reanalysis vs. observed low-level moisture fields. Results herein provide researchers with potential strengths and limitations of using NARR data for the purposes of depicting hazardous convective weather climatologies and initializing model simulations. Similar studies should be considered for other reanalysis datasets.

2.1 Introduction

Past research using reanalysis data has provided significant insight into the understanding of climatological distributions and trends of parameters associated with severe convective storms (e.g., Brooks et al. 2003; Brooks et al. 2007; Craven et al. 2004; Gensini and Ashley 2011; Allen and Karoly 2013). Essentially a three-dimensional best-guess snapshot of the atmosphere in time, reanalysis aims to provide an objectively modeled baseline dataset that serves to fill data void areas in the coarse-density radiosonde network. The goal of reanalysis is to provide a climatological snapshot of conditions closest to reality by assimilating multiple observation platforms into a numerical weather prediction model (e.g., surface observations, satellite information, radiosonde data). The final product of atmospheric reanalysis is a large (potentially global) dataset that has greater spatio-temporal resolution than observed sounding data. These data are regularly used to conduct historical meteorological analyses, create climatological information and graphics, or initialize boundary conditions for historical model simulations.

While reanalysis datasets are currently a popular data source for researchers (3140 peer-reviewed journal articles with "reanalysis" in the title or abstract from 2010–2011), little peer-reviewed research has examined how the filtered nature (e.g., limited vertical levels) of reanalysis data may affect convectively pertinent variables. For example, a documented problem of reanalysis for convective purposes is the overestimation of favorable hazardous convective weather (HCW) environments in southern Texas (Gensini and Ashley 2011). Thus, it is hypothesized that limited vertical resolution from the reanalysis model surface to ~3000 m AGL poorly captures sharp changes in temperature, affecting the calculation of convective inhibition (CIN) produced by an elevated mixed layer (EML) described by Lanicci and Warner (1991). A recent international study revealed similar problems with CIN calculations over HCW favored regions of Australia (Allen and Karoly 2013). Thus, the purpose of this research is to examine the modeled reanalysis proxy soundings in conjunction with collocated observed sounding data, specifically analyzing key convective variables. Results from this study provide researchers with potential strengths and limitations of using NARR data for purposes of depicting HCW climatologies and initializing model simulations.

2.2 Background

Two other studies have examined the relationship between radiosonde data and reanalysis for purposes of studying severe convection (Lee 2002; Allen and Karoly 2013). Lee (2002) showed that reanalysis proxy soundings provide a reasonable approximation of the convective environment when compared to collocated soundings. Specifically, kinematic variables were found to be best represented by reanalysis, while thermodynamic parameters sometimes contained large differences, owing to errors in low-level moisture fields (Lee 2002). Lee's (2002) research was conducted with coarse-resolution global reanalysis data, whereas this study uses a higher spatial-resolution reanalysis, both in the vertical and horizontal, in an attempt to best compare the observed and reanalyzed convective environment. Allen and Karoly (2013) examined ERA-Interim reanalysis data in comparison to observations for ~20 radiosonde stations and ~3700 soundings over Australia. Results from Allen and Karoly (2013) support the findings shown in Lee (2002).

a. Reanalysis datasets for convective research

Coarse-resolution global reanalysis datasets such as the National Center for Environmental Prediction (NCEP) and National Center for Atmospheric Research (NCAR) global reanalysis (Kalnay et al. 1996) have been utilized (Brooks et al. 2003; Brooks et al. 2007) for global perspectives of severe convective environments over long time periods (available from 1949–present). A higher spatio-temporal reanalysis over North America (North American Regional Reanalysis, NARR; Mesinger et al. [2006]) was used by Gensini and Ashley (2011) to examine severe convective environments over the U.S. in greater detail (available from 1979–present). The NARR provides researchers with a temporally consistent climate data suite for North America (Mesinger et al. 2006) and is preferred to other global reanalysis data for this study due to its superior vertical resolution. Native NARR gridded binary data has a horizontal resolution of 32 km, a vertical resolution of 45 σ layers, and temporal resolution of three hours. NARR uses the 2003 operational Eta Model as part of the assimilation cycle (G. Manikin 2010, personal communication). In comparison, the NCEP/NCAR global reanalysis has a 210 km horizontal resolution, vertical resolution of 28 σ layers and temporal resolution of six hours. While using NARR data for this study provides superior vertical resolution, the corresponding horizontal domain is limited to North America.

2.3 Methodology

0000 UTC raw radiosonde data from 2000–2011 was obtained from the University of Wyoming's online data archive (http://weather.uwyo.edu/upperair/sounding.html) for 21 stations east of the U.S. continental divide (Fig 2.1), where HCW is climatologically favored (Brooks et al. 2003; Gensini and Ashley 2011). Synoptic off-hour (i.e., 1800 UTC, 2100 UTC, etc.) radiosonde launches were omitted from this study due to their limited sample. Reanalysis proxy soundings were obtained by extracting point data from 0000 UTC NARR files using the GRBSND program available in the Weather Processor 6 (WXP) software package via Unisys. Customized Python routines were used to calculate 23 different convectively important variables and composite parameters (Table 2.1), quality control sounding data, and store values in commaseparated values (CSV) format. In an effort to only evaluate surface-based convectively favorable environments, only soundings with non-zero surfaced-based CAPE were considered for this study.

As previously mentioned, low-level thermodynamic errors could be particularly problematic for variables that rely on vertical integration (e.g., CAPE; or any composite parameter that utilizes CAPE in its calculation). This study employs different parcel ascent methods on all thermodynamic parameters to see if a "best choice" exists for researchers using NARR. Thus, two parcel ascent trajectories were calculated (100 hPa mixed layer [ML]; and surface-based [SB]) and applied to all thermodynamic parameters and composite indices. A 100 hPa ML parcel averages the thermodynamic values (i.e., T and T_d) in the lowest 100 hPa of the atmosphere, whereas a SB parcel uses the T and T_d at the surface of the atmosphere (or model) to calculate various indices. The distributed NARR dataset has 5 vertical levels that fall in the lowest 100 hPa of the model (1000, 975, 950, 925, 900 hPa), while a typical radiosonde launch will have ~8 data points in the lowest 100 hPa. Finally, it should be noted that all parcel routines in this study utilize the virtual temperature correction, as they can result in larger and more realistic values of CAPE (Doswell and Rasmussen 1994).

Values of the square of correlation coefficient (R^2) and root-mean-square error (RMSE) (along with standard linear regression slope and y-intercept values) were computed between grouped observed sounding-derived parameter values and the concurrent pair of reanalysis values. RMSE was calculated with the formula (following Wilks 1995):

$$RMSE = \sqrt{\frac{1}{N}\sum(NARRn - OBn)^2}$$

where the sum is from n=1 to N, N is the number of values in each group, *NARRn* is the n^{th} reanalysis value, and *OBn* is the n^{th} observed value. Thus, RMSE represents a typical error (reanalysis minus observed) magnitude for each group of paired observations. To visualize the results, 2-D histograms were plotted for all stations (Fig. 2.1) and all variables (Table 2.1). All 2-D histograms were constructed using Python and the Matplotlib extension library (Hunter 2007). The 1:1 black line on each plot represents a perfect correlation (i.e., NARR value = observed radiosonde value).

2.4 Results

2-D histograms were useful in comparing the distributions between NARR and observed soundings (Fig. 2.2). For example, in Fig. 2.2a, one can see that SBCAPE values at KTOP have a positive bias (i.e., NARR SBCAPE tends to exceed observed SBCAPE values) with a RMSE value of 1637 $J \cdot kg^{-1}$. However, in Fig. 2.2b, good correlation (R^2=.88) is found between NARR and observed 6BWD, exhibiting a RMSE of only 2.7 kts. R^2, RMSE, slope, and y-intercept values can be found for all stations and variables in Tables 2.2, 2.3, 2.4, and 2.5 respectively.

a. Correlation

Table 2.2 displays R^2 values for all 23 parameters and 21 sounding locations. Broadly, R^2 values are found to be higher for kinematic variables such as 6BWD and show less correlation for thermodynamic variables such as SBCAPE. This is an expected result, as R^2 values are typically lower for derived variables and composite parameters, where compounding error (e.g., calculation of a product) reduces correlation values. Out of the 23 parameters examined, FRZGLVL exhibited the highest R^2 values, while STP exhibited the lowest values regardless of station location. Seven variables (7/5LR, FRZGL, 850WND, 500WND, 200WND, 6BWD, CB) exhibited good (≥.75) correlation, nine variables (SBCAPE, SBLI, SBLCL, 03SRH, 01SRH, SCP, 01EHI, $SFCT_d$, Tc) displayed fair (.25>x>.75) correlation, and seven variables (MLCAPE, SBCIN, MLCIN, MLLI, MLLCL, STP, $850T_d$) presented poor (≤.25) R^2 values (Table 2.3).

Perhaps most interesting are the relatively low R^2 values associated with $SFCT_d$ and $850T_d$, as these values are not derived. $SFCT_d$ R^2 values ranged from .37–.63 while $850T_d$ R^2 values ranged from 0–.43, which would be associated with fair to poor agreement (respectively) in this context. This is important, as small errors in the low-level moisture fields may yield large differences in derived quantities such as CAPE. These differences in low-level moisture proved to have an important impact on parcel choice, as all SB parcel parameters exhibited fair correlation, whereas all ML parcel parameters correlated poorly. To visualize this error, consider the differences in the NARR and observed Skew-T/Log-P diagrams from Jackson, MS, valid 20 April 2011 0000 UTC, when an outbreak of severe thunderstorms was observed across portions of the Ohio and Tennessee valley (Fig. 2.3). While SBCAPE calculations were very similar for NARR and observed soundings (3254 and 3035 $J{\cdot}kg^{-1}$ respectively; Fig. 2.4a, Fig. 2.4c), MLCAPE calculations differed by over 1800 $J{\cdot}kg^{-1}$(Fig. 2.4b, Fig. 2.4d).

Such differences in NARR vs. observed low-level moisture fields also influence other variables. In fact, all sites increased correlation values (by an average of .17) when examining SB vs. ML LCL (Fig. 2.5). Examining all 2-D histograms suggests that NARR variance of MLLCL is too small (Fig. 2.5b). This error is due to correlation observed with $850T_d$. While $SFCT_d$ values exhibited fair correlation, $850T_d$ correlation was an average of .36 points lower. Thus, a SB parcel using $SFCT_d$ has a higher probability of lifting a parcel with similar surface moisture values. However, averaging the moisture content of the lowest 100 hPa is more likely to inadequately represent the observed convective environment (especially at higher elevation locations). Consequently, the improvements to correlation for ML over SB versions of LCL, CAPE, and LI are linked to poor representation of lower-tropospheric moisture, especially in the 925–850 hPa levels. The only exception to parcel choice was CIN, where both SB and ML CIN exhibited poor R^2 values (.12 and .11 respectively).

b. Bias / error

Tables 2.4 and 2.5 contain the intercept and slope values for each of the station parameter linear regression lines. These values indicate the bias of each group distribution, as they quantify the difference between the parameter subset regression and the 1:1 line (which has an intercept of zero and a slope of one). Similar to correlation results, it was found that kinematic parameter values agreed better with observations than thermodynamic parameters. Nearly all kinematic variables exhibited a linear regression slope of one and a y-intercept near zero. In addition, parameters related to mid-level environmental conditions performed better than those calculated from near-surface data. Nearly all bias and error can be traced back to errors in the NARR lower-tropospheric moisture fields. For instance, the average RMSE for $850T_d$ at all stations was 9 ºC (Table 2.6). These low-level moisture errors create large RMSE values for variables that depend on the near-surface environment (e.g., SB and MLCAPE station averaged RMSE values of 1465 and 1378 $J \cdot kg^{-1}$ respectively). Such errors are then compounded in composite parameters such as SCP and STP that utilize CAPE as a measure of static stability.

Large bias and error were also found in CIN fields. In particular, NARR fields commonly underestimated the strength of a temperature inversion associated with the EML. Bias is demonstrated by Tc slope values near one, with an average y-intercept near 4 ºC, thus indicating that NARR typically underestimates convective temperature by roughly 4 ºC.

Subjective examination of several comparison soundings suggests that rapid vertical changes in temperature associated with the EML are poorly represented in most NARR soundings. This supports the hypothesis herein that NARR inadequately represents sharp temperature changes associated with the EML and results conveyed in previous research (i.e., Brooks et al. 2003b; Gensini and Ashley 2011; Allen and Karoly 2013). This bias may be explained by the parameterizations used the NARR model assimilation. The NARR employs the Betts–Miller–Janjić (BMJ) convective parameterization (Janjić 1990, 1994). Given that errors in $SFCT_d$ could be considered acceptable, this suggests modeled mixing within the boundary layer is not adequately replicating the convective transport of near-surface moisture throughout the lower troposphere.

2.5 Summary and conclusions

Over 100,000 reanalysis and observed soundings were compared across 21 United States upper-air sites during the period 2000–2011. This analysis was conducted, in part, to examine how well the reanalysis environment depicts observed and derived variables, specifically focusing on variables related to severe storm forecasting. In general, kinematic variables are best represented by NARR, while thermodynamic variables suffer from errors originating in low-level moisture fields. Therefore, when analyzing NARR convective fields, parcel ascent choice is an important consideration. Surface-based parcels performed better than 100-hPa mixed-layer parcels, as less RMSE was found in $SFCT_d$ fields. Variables best resolved by NARR include 7/5LR, FRZGL, 850WND, 500WND, 200WND, 6BWD, and CB. Large RMSE and low correlation values were found with MLCAPE, SBCIN, MLCIN, MLLI, MLLCL, STP, and $850T_d$. Thus, research utilizing NARR low-level fields, and any conclusions drawn from them, should be done with caution.

Overall, NARR provides an invaluable tool to convective researchers as soundings can be derived at spatio-temporal resolutions much greater than the current radiosonde network. This is especially useful for climatological studies wishing to better understand the distribution of environments favorable for severe storms. With these results, bias correction can now be utilized on large-scale climatological studies using similar parameters. Researchers wishing to use NARR fields to initialize model simulations should be aware of potential errors in lower tropospheric moisture values and sharp vertical changes in temperature associated with an EML. When possible, such initializations should try to correct such errors or supplement NARR fields with observed soundings. Finally, any studies examining reanalysis data for dynamical downscaling purposes should be aware of potential errors present in the driving fields.

2.6 References

Allen, J. T., and D. J. Karoly, 2014: A climatology of Australian severe thunderstorm environments 1979–2011: inter-annual variability and ENSO influence. *International Journal of Climatology*, **34,** 81–97.

Brooks, H. E., J. W. Lee, and J. P. Craven, 2003b: The spatial distribution of severe thunderstorm and tornado environments from global reanalysis data. *Atmospheric Research*, **67–68,** 73–94.

Brooks, H. E., A. R. Anderson, K. Riemann, I. Ebbers, and H. Flachs, 2007: Climatological aspects of convective parameters from the NCAR/NCEP reanalysis. *Atmospheric Research*, **83,** 294–305.

Craven, J. P., H. E. Brooks, and J. A. Hart, 2004: Baseline climatology of sounding derived parameters associated with deep, moist convection. *National Weather Digest*, **28,** 13–24.

Doswell III, C. A., and E. N. Rasmussen, 1994: The effect of neglecting the virtual temperature correction on CAPE calculations. *Weather and Forecasting*, **9,** 625–629.

Gensini, V. A., and W. S. Ashley, 2011: Climatology of potentially severe convective environments from the North American Regional Reanalysis. *Electrionic Journal of Severe Storms Meteorology*, **6,** 1–40.

Hunter, J. D., 2007: Matplotlib: A 2D graphics environment. *Computing in Science and Engineering***,** 90–95.

Janjić, Z. I., 1990: The step-mountain coordinate: Physical package. *Monthly Weather Review*, **118,** 1429–1443.

Janjić, Z. I., 1994: The step-mountain Eta coordinate model: Further developments of the convection, viscous sublayer, and turbulence closure schemes. *Monthly Weather Review*, **122,** 927–945.

Kalnay, E., and Coauthors, 1996: The NCEP/NCAR 40-year reanalysis project. *Bulletin of the American Meteorological Society*, **77,** 437–471.

Lanicci, J. M., and T. T. Warner, 1991: A synoptic climatology of the elevated mixed-layer inversion over the southern Great Plains in spring. Part I: Structure, dynamics, and seasonal evolution. *Weather and Forecasting*, **6,** 198–213.

Lee, J. W., 2002: Tornado proximity soundings from the NCEP/NCAR reanalysis data, Meteorology, University of Oklahoma, 61 pp.

Mesinger, F., and Coauthors, 2006: North American Regional Reanalysis. *Bulletin of the American Meteorological Society*, **87,** 343–360.

Wilks, D. S., 1995: *Statistical Methods in the Atmospheric Sciences.* Academic Press, 467 pp.

Table 2.1. Convective variables and composite indices examined in this study.

Abbreviation	Parameter
SBCAPE	Surface-Based Convective Available Potential Energy
MLCAPE	100-hPa Mixed Layer Convective Available Potential Energy
SBCIN	Surface-Based Convective Inhibition
MLCIN	100-hPa Mixed Layer Convective Inhibition
SBLI	Surface-Based Lifted Index (calculated at 500-hPa)
MLLI	100-hPa Mixed Layer Lifted Index (calculated at 500-hPa)
SBLCL	Surface-Based Lifting Condensation Level
MLLCL	100-hPa Mixed Layer Lifting Condensation Level
03SRH	0–3-km Storm Relative Helicity
01SRH	0–1-km Storm Relative Helicity
7/5LR	700–500-hPa Lapse Rate
SCP	Supercell Composite Parameter (using a surface-based parcel)
STP	Significant Tornado Parameter (using a surface-based parcel)
01EHI	0–1-km Energy Helicity Index (using a surface-based parcel)
FRZGLVL	Freezing Level
$SFCT_d$	Surface Dewpoint
$850T_d$	850-hPa Dewpoint
200WND	200-hPa Wind Velocity
500WND	500-hPa Wind Velocity
850WND	850-hPa Wind Velocity
Tc	Convective Temperature
6BWD	0–6-km Bulk Wind Difference
CB	Craven / Brooks Significant Severe Parameter (using a surface-based parcel)

Table 2.2. R^2 values for all parameters and stations analyzed in this study.

	TOP	TBW	RAP	PIT	OUN	OAX	MAF	LZK	LBF	JAN	GRB	FFC	DVN	DNR	DDC	BRO	BNA	BIS	AMA	ALB	*AVG*
SBCAPE	0.43	0.17	0.35	0.24	0.41	0.38	0.13	0.31	0.39	0.21	0.40	0.19	0.37	0.19	0.37	0.33	0.32	0.50	0.33	0.25	*0.31*
MLCAPE	0.19	0.00	0.01	0.15	0.01	0.22	0.00	0.05	0.05	0.00	0.37	0.01	0.33	0.00	0.05	0.20	0.14	0.22	0.00	0.26	*0.11*
SBCIN	0.12	0.12	0.07	0.12	0.20	0.18	0.04	0.05	0.12	0.20	0.16	0.14	0.08	0.00	0.21	0.40	0.05	0.10	0.06	0.06	*0.12*
MLCIN	0.21	0.01	0.11	0.07	0.02	0.09	0.03	0.11	0.13	0.04	0.22	0.00	0.07	0.00	0.13	0.38	0.07	0.16	0.10	0.19	*0.11*
SBLI	0.46	0.27	0.23	0.22	0.46	0.48	0.16	0.35	0.37	0.25	0.39	0.24	0.37	0.14	0.37	0.36	0.31	0.44	0.30	0.23	*0.32*
MLLI	0.20	0.11	0.07	0.18	0.08	0.28	0.05	0.12	0.09	0.08	0.37	0.07	0.37	0.02	0.08	0.25	0.20	0.24	0.05	0.23	*0.16*
SBLCL	0.43	0.19	0.62	0.32	0.59	0.23	0.59	0.39	0.56	0.33	0.17	0.31	0.25	0.65	0.62	0.18	0.41	0.49	0.67	0.27	*0.41*
MLLCL	0.21	0.00	0.28	0.24	0.52	0.26	0.17	0.12	0.36	0.01	0.18	0.00	0.25	0.61	0.55	0.08	0.11	0.28	0.62	0.02	*0.24*
03SRH	0.62	0.55	0.24	0.72	0.56	0.48	0.38	0.73	0.42	0.74	0.58	0.75	0.64	0.32	0.35	0.35	0.78	0.40	0.33	0.68	*0.53*
01SRH	0.52	0.57	0.09	0.62	0.50	0.23	0.16	0.58	0.27	0.73	0.39	0.70	0.55	0.13	0.31	0.33	0.72	0.22	0.31	0.55	*0.42*
7/5LR	0.83	0.64	0.78	0.72	0.85	0.82	0.76	0.76	0.78	0.72	0.74	0.74	0.80	0.81	0.78	0.84	0.76	0.80	0.78	0.62	*0.77*
SCP	0.48	0.43	0.26	0.31	0.53	0.37	0.23	0.47	0.31	0.46	0.58	0.46	0.48	0.13	0.38	0.34	0.46	0.52	0.38	0.32	*0.40*
STP	0.16	0.00	0.00	0.16	0.00	0.06	0.00	0.03	0.00	0.00	0.20	0.01	0.24	0.00	0.01	0.25	0.11	0.05	0.00	0.08	*0.07*
01EHI	0.44	0.12	0.20	0.28	0.43	0.23	0.06	0.36	0.24	0.33	0.36	0.23	0.42	0.03	0.29	0.22	0.36	0.23	0.28	0.41	*0.28*
FRZGLVL	0.96	0.87	0.97	0.94	0.95	0.96	0.92	0.93	0.96	0.91	0.96	0.90	0.95	0.95	0.93	0.90	0.93	0.97	0.94	0.92	*0.94*
SFCTd	0.49	0.42	0.46	0.49	0.49	0.47	0.41	0.46	0.58	0.42	0.63	0.42	0.60	0.38	0.49	0.46	0.51	0.49	0.56	0.49	*0.49*
850Td	0.12	0.00	0.05	0.40	0.12	0.12	0.00	0.04	0.05	0.10	0.29	0.12	0.10	N/A	0.02	0.00	0.33	0.11	0.00	0.44	*0.13*
850WND	0.88	0.76	0.62	0.83	0.87	0.77	0.66	0.83	0.80	0.87	0.84	0.85	0.86	N/A	0.88	0.77	0.88	0.84	0.75	0.82	*0.81*
500WND	0.93	0.88	0.84	0.90	0.92	0.88	0.85	0.90	0.85	0.88	0.87	0.94	0.92	0.74	0.85	0.92	0.93	0.86	0.89	0.90	*0.88*
200WND	0.93	0.90	0.90	0.92	0.93	0.92	0.89	0.92	0.91	0.94	0.91	0.92	0.93	0.89	0.93	0.96	0.93	0.90	0.91	0.93	*0.92*
Tc	0.71	0.03	0.82	0.78	0.53	0.69	0.21	0.61	0.74	0.07	0.72	0.11	0.70	0.64	0.76	0.54	0.66	0.74	0.53	0.62	*0.56*
6BWD	0.88	0.72	0.71	0.86	0.86	0.80	0.78	0.84	0.78	0.81	0.77	0.87	0.86	0.61	0.77	0.90	0.89	0.74	0.80	0.77	*0.80*
CB	0.94	0.56	0.91	0.89	0.94	0.92	0.85	0.87	0.92	0.74	0.90	0.82	0.92	0.91	0.90	0.87	0.89	0.92	0.90	0.84	*0.87*

Table 2.3. Subjective characterization of parameter R^2 values.

Good	Fair	Poor
7/5LR	SBCAPE	MLCAPE
FRZGLVL	SBLI	SBCIN
850WND	SBLCL	MLCIN
500WND	03SRH	MLLI
200WND	01SRH	MLLCL
6BWD	SCP	STP
CB	01EHI	850T_d
	SFCT_d	
	Tc	

Table 2.4. Same as Table 2.2, except for linear regression slope values.

	KALB	KAMA	KBIS	KBNA	KBRO	KDDC	KDNR	KDVN	KFFC	KGRB	KJAN	KLBF	KLZK	KMAF	KOAX	KOUN	KPIT	KRAP	KTBW	KTOP	AVG
SBCAPE	0.34	0.48	0.71	0.33	0.45	0.51	0.55	0.41	0.25	0.39	0.29	0.51	0.35	0.34	0.47	0.50	0.23	0.37	0.27	0.48	**0.41**
MLCAPE	0.41	0.20	0.42	0.26	0.31	0.14	-11.32	0.36	0.05	0.37	0.12	0.15	0.20	-0.07	0.31	0.09	0.18	0.07	0.61	0.26	**-0.38**
SBCIN	0.21	0.37	0.45	0.24	0.68	0.64	-0.02	0.36	0.49	0.44	0.56	0.46	0.31	0.34	0.62	0.63	0.33	0.47	0.44	0.46	**0.42**
MLCIN	0.46	0.27	0.41	0.29	0.90	0.38	0.06	0.75	-0.03	0.96	0.28	0.37	0.28	0.42	0.38	0.12	0.49	0.32	0.14	0.61	**0.38**
SBLI	0.36	0.50	0.67	0.39	0.62	0.59	0.37	0.47	0.35	0.46	0.38	0.57	0.45	0.38	0.57	0.57	0.29	0.33	0.42	0.57	**0.46**
MLLI	0.33	0.16	0.36	0.29	0.41	0.18	0.03	0.45	0.11	0.43	0.16	0.18	0.24	0.14	0.39	0.20	0.24	0.14	0.23	0.31	**0.25**
SBLCL	1.43	0.86	0.63	0.99	0.61	0.71	1.23	0.39	0.59	0.37	0.54	0.74	0.61	0.79	0.37	0.56	1.26	0.75	0.46	0.51	**0.73**
MLLCL	0.34	2.59	1.06	1.12	2.13	2.93	2.89	1.78	0.02	2.07	0.18	3.78	0.63	1.18	3.08	2.70	4.38	0.91	-0.05	1.39	**1.77**
03SRH	0.93	0.75	0.86	1.01	0.73	0.76	0.88	1.00	1.13	1.01	1.02	0.89	1.05	0.78	0.86	0.95	1.05	0.73	1.03	0.96	**0.92**
01SRH	0.87	0.79	0.80	1.03	0.55	0.83	0.59	1.12	1.43	0.80	1.06	0.97	1.22	0.79	0.73	1.25	1.21	0.52	1.18	1.14	**0.93**
7/5LR	0.95	0.97	1.00	0.98	0.99	0.98	1.09	0.98	0.98	0.94	0.96	0.96	0.96	0.92	1.01	1.00	0.96	0.97	0.92	0.99	**0.98**
SCP	0.83	1.08	1.11	0.60	0.43	0.75	1.39	0.68	0.83	0.85	0.90	0.53	0.77	0.74	0.46	0.82	0.40	0.78	1.24	0.58	**0.80**
STP	0.54	-0.57	0.71	0.44	0.24	3.07	0.00	0.61	0.50	0.38	-0.22	0.65	2.30	0.00	1.07	-1.38	0.33	0.04	1.84	1.04	**0.56**
01EHI	0.58	0.57	0.73	0.40	0.30	0.61	0.42	0.64	0.58	0.47	0.59	0.91	0.61	0.50	0.65	0.84	0.41	0.46	0.40	0.69	**0.56**
FRZGLVL	0.99	0.99	0.98	1.01	0.99	0.99	0.98	0.99	0.99	0.99	1.00	0.99	0.96	0.96	0.99	1.01	0.98	0.95	0.98	1.00	**0.99**
SFCTd	0.72	0.82	0.73	0.73	0.67	0.72	0.85	0.71	0.67	0.70	0.65	0.77	0.70	0.64	0.68	0.65	0.68	0.71	0.63	0.68	**0.71**
850Td	0.70	0.01	0.27	0.67	-0.16	0.12	N/A	0.43	0.27	0.63	0.35	0.23	0.15	-0.03	0.38	0.37	0.68	0.17	0.10	0.42	**0.30**
850WND	0.92	0.89	0.95	0.94	1.00	1.01	N/A	0.97	0.97	0.97	0.95	0.93	0.93	0.90	0.86	0.92	0.93	0.82	0.89	0.93	**0.93**
500WND	1.02	0.97	0.96	0.99	1.02	0.94	0.85	0.98	0.99	0.97	0.97	0.91	0.95	0.92	0.97	0.99	0.95	0.97	0.92	1.01	**0.96**
200WND	0.98	0.94	0.95	0.95	0.98	0.96	0.94	0.98	0.93	0.95	0.93	0.95	0.94	0.93	0.94	0.98	0.91	1.00	0.93	0.97	**0.95**
Tc	0.87	0.89	1.03	1.04	1.06	1.07	0.71	0.95	0.31	0.98	0.24	1.06	0.93	0.43	0.94	1.01	1.06	1.02	0.14	0.96	**0.83**
6BWD	1.00	1.02	0.92	1.01	0.99	0.94	0.93	0.99	1.00	0.94	0.98	0.92	0.95	1.00	0.96	0.99	0.98	0.94	0.89	1.01	**0.97**
CB	1.12	1.00	0.99	1.04	0.97	0.96	0.83	1.01	1.00	0.98	0.95	0.95	0.95	0.93	0.98	0.98	1.04	0.97	0.85	1.01	**0.97**

Table 2.5. Same as Table 2.2, except for linear regression y-intercept values.

	KALB	KAMA	KBIS	KBNA	KBRO	KDDC	KDNR	KDVN	KFFC	KGRB	KJAN	KLBF	KLZK	KMAF	KOAX	KOUN	KPIT	KRAP	KTBW	KTOP	AVG
SBCAPE	336.6	98.0	-128.9	173.2	354.8	145.8	319.4	40.9	328.0	62.4	322.9	200.1	198.9	320.7	257.8	201.9	162.2	106.5	425.0	134.6	203.0
MLCAPE	483.9	769.9	656.3	770.5	766.3	839.2	608.2	153.2	892.7	177.5	1162.3	931.3	1049.4	727.0	710.0	1166.3	333.7	692.0	1195.8	745.3	741.5
SBCIN	-27.9	-89.5	-134.1	-36.1	-43.0	-75.3	-56.8	-53.1	-33.2	-47.2	-41.5	-95.3	-53.7	-95.1	-76.6	-82.1	-25.2	-122.5	-45.0	-67.4	-65.0
MLCIN	-28.0	-51.4	-85.0	-30.5	-39.2	-64.1	-101.3	-62.0	-40.7	-49.8	-39.5	-67.4	-38.5	-54.1	-86.5	-65.2	-34.0	-82.6	-40.2	-65.3	-56.3
SBLI	-0.9	-0.5	-0.3	-0.5	-0.2	-0.3	-1.6	-0.4	-0.8	-0.2	-0.7	-0.6	-0.4	-1.0	-0.6	-0.6	-0.4	-1.1	-0.8	-0.3	-0.6
MLLI	-1.6	-2.6	-2.4	-1.9	-1.4	-2.1	-5.2	-0.3	-2.7	-0.5	-3.6	-2.5	-2.7	-3.3	-1.7	-3.1	-0.8	-2.4	-4.7	-1.9	-2.4
SBLCL	571.9	94.5	461.0	567.7	643.6	459.6	203.3	874.6	779.1	956.6	809.9	422.0	729.1	171.2	945.3	661.5	504.2	289.7	744.0	876.5	588.3
MLLCL	784.2	-5892.4	-318.9	-111.9	-732.5	-3914.4	-1191.1	-451.2	1251.1	-721.3	858.2	-5455.2	339.8	-2943.5	-2970.7	-4145.0	-2639.0	-341.8	1204.4	-299.9	-1920.6
03SRH	15.5	56.8	60.9	7.5	39.2	78.3	33.2	18.8	6.1	20.1	11.2	47.1	9.3	28.4	47.0	35.6	4.6	76.0	8.8	35.0	32.0
01SRH	17.8	16.6	35.1	6.8	15.8	15.6	17.6	17.8	9.6	20.6	8.5	37.2	12.6	22.1	35.5	14.4	9.7	42.4	12.0	20.9	19.4
7/5LR	-0.3	-0.2	-0.2	-0.2	-0.1	-0.1	0.7	-0.2	-0.2	-0.4	-0.3	-0.4	-0.4	-0.5	0.0	-0.1	-0.3	-0.4	-0.5	-0.2	-0.2
SCP	0.7	1.6	1.2	0.5	0.9	1.7	1.5	0.8	0.4	0.2	0.2	2.0	0.6	1.3	1.5	1.2	0.6	2.0	0.1	1.0	1.0
STP	0.2	0.1	0.2	0.1	0.1	0.1	2.3	0.1	0.1	0.1	0.2	0.2	0.3	1.8	0.2	0.3	0.1	0.1	0.1	0.2	0.4
01EHI	0.1	0.1	0.2	0.1	0.2	0.1	0.1	0.1	0.1	0.0	0.0	0.2	0.1	0.1	0.2	0.1	0.1	0.1	0.1	0.2	0.1
FRZGLVL	174.6	-1.1	173.4	-52.0	33.6	-0.3	563.1	-27.5	25.2	89.4	11.3	82.6	186.1	243.0	76.3	-34.8	-4.4	102.3	92.0	19.9	87.6
SFCTd	4.4	3.2	5.9	3.7	6.5	4.7	3.5	4.9	5.7	4.9	6.1	5.1	5.1	5.7	6.4	6.8	4.1	4.6	7.7	5.6	5.2
850Td	9.7	10.5	9.0	4.0	12.6	10.7	N/A	5.2	13.6	2.6	17.0	8.7	11.0	11.0	8.8	10.8	3.0	7.7	13.3	8.4	9.4
850WND	1.6	3.2	1.6	1.4	1.9	1.7	N/A	1.7	1.2	1.4	1.3	2.0	1.8	2.7	3.4	1.8	1.5	4.0	2.0	2.2	2.0
500WND	1.4	0.5	1.0	1.2	0.5	1.4	3.1	1.2	1.1	1.8	1.1	1.6	0.7	0.9	0.8	1.0	1.8	0.6	1.7	0.7	1.2
200WND	0.4	1.9	2.0	2.8	1.5	1.3	0.7	1.2	2.4	1.2	2.2	1.9	1.3	1.9	1.2	1.5	2.4	-0.5	1.9	1.9	1.6
Tc	5.3	-0.2	-1.8	-1.4	-0.1	-4.0	6.5	1.8	19.4	2.0	22.7	-2.5	1.5	15.8	1.6	-3.7	-1.0	-3.2	26.1	1.8	4.3
6BWD	2.6	1.0	5.0	1.3	0.2	2.8	2.7	1.1	1.5	3.3	1.2	3.0	1.8	0.8	1.4	0.4	2.2	5.4	2.7	0.9	2.1
CB	166.2	899.6	2298.7	1145.6	617.5	1791.3	298.7	520.9	1651.1	2119.6	2078.7	1457.9	2572.8	1068.8	976.6	564.9	1095.2	2927.8	3936.8	823.3	1450.6

Table 2.6. Same as Table 2.2, except for RMSE values.

	KALB	KAMA	KBIS	KBNA	KBRO	KDDC	KDNR	KDVN	KFFC	KGRB	KJAN	KLBF	KLZK	KMAF	KOAX	KOUN	KPIT	KRAP	KTBW	KTOP	AVG
SBCAPE	1214.8	952.4	1059.2	2013.2	1449.6	1087.6	449.5	2090.2	1689.7	1628.3	2016.7	1118.8	2127.9	944.5	1619.4	1253.5	1915.3	1218.0	1809.2	1653.4	1465.6
MLCAPE	889.2	980.4	1202.5	1170.7	1527.0	1476.2	809.5	2228.2	1395.8	1567.6	1411.3	1455.5	1272.9	950.0	1797.8	1380.1	1676.9	990.9	1434.8	1953.2	1378.5
SBCIN	6.3	8.0	10.4	2.8	4.9	7.7	73.2	4.9	4.5	4.0	5.3	8.4	5.8	8.6	7.9	8.0	5.1	10.3	5.9	6.6	9.9
MLCIN	59.8	64.4	100.5	19.5	88.1	78.3	124.6	115.3	88.8	105.1	85.0	75.4	103.9	106.3	114.2	76.5	79.3	87.5	88.2	106.2	88.3
SBLI	3.0	2.3	2.4	3.7	2.5	2.4	2.2	3.9	3.0	3.5	3.4	2.5	3.7	2.4	3.1	2.5	3.9	3.0	2.8	3.1	3.0
MLLI	3.1	5.6	3.3	2.9	2.8	3.4	2.1	4.2	8.4	3.5	8.9	3.7	3.5	10.4	3.6	4.5	3.7	4.1	11.8	3.8	4.9
SBLCL	598.9	631.6	417.9	1008.4	717.7	357.1	707.6	537.7	767.0	399.3	939.3	438.1	615.8	545.3	592.4	676.1	495.3	613.2	832.0	462.7	617.7
MLLCL	414.4	1147.1	576.3	392.4	305.2	577.7	2494.0	481.4	1196.0	469.3	1331.1	638.6	498.0	2271.2	512.2	726.6	513.8	890.6	1722.6	556.9	885.8
03SRH	48.0	84.5	89.7	42.1	59.4	104.7	76.8	65.6	43.7	61.6	46.2	83.5	54.4	58.6	80.9	75.9	48.6	92.2	45.2	72.6	66.7
01SRH	42.6	45.2	58.0	34.2	38.9	53.3	41.0	57.2	43.7	45.2	35.2	63.6	51.9	44.5	56.3	57.2	44.9	53.5	39.8	60.2	48.3
7/5LR	0.3	0.6	0.3	0.6	0.6	0.3	0.4	0.4	0.5	0.3	0.7	0.4	0.5	0.5	0.4	0.5	0.3	0.4	0.6	0.3	0.4
SCP	2.6	7.0	4.0	5.4	3.9	6.0	3.9	6.1	3.4	2.2	4.8	6.1	5.2	3.4	8.6	6.6	2.8	5.5	2.3	5.7	4.8
STP	0.6	0.4	0.6	0.6	0.8	0.5	0.1	1.3	0.5	0.8	0.8	0.6	1.1	0.3	1.0	1.0	0.6	0.2	0.5	1.0	0.7
01EHI	0.5	0.4	0.6	0.5	0.6	0.5	0.2	0.8	0.3	0.7	0.5	0.6	0.6	0.3	0.8	0.6	0.6	0.3	0.4	0.7	0.5
FRZGLVL	165.4	159.9	104.6	236.6	170.8	89.5	447.9	147.8	219.4	90.2	233.6	101.1	167.0	153.7	116.0	153.4	113.0	106.6	239.6	85.9	165.1
SFCTd	2.0	3.5	2.6	4.8	2.9	1.8	3.0	3.2	3.3	1.5	4.4	2.9	3.1	3.1	3.1	3.3	2.3	3.6	3.4	2.2	3.0
850Td	6.7	11.1	4.5	4.3	14.3	3.6	N/A	4.6	20.8	2.8	20.1	4.6	7.6	16.4	6.1	10.7	1.9	6.4	10.3	15.1	9.0
850WND	4.0	4.1	3.5	3.2	4.2	3.8	N/A	4.1	3.5	4.1	3.4	3.8	4.3	3.8	5.0	3.6	3.7	4.9	4.0	3.9	4.0
500WND	4.8	4.4	4.2	4.1	3.6	4.9	5.5	4.2	3.7	4.9	5.2	4.7	4.8	5.1	4.6	4.3	4.3	4.9	4.3	4.0	4.5
200WND	6.6	6.6	6.3	6.1	5.6	5.6	7.5	6.1	7.0	6.8	6.1	6.3	7.1	8.2	6.3	6.4	7.0	6.7	7.6	6.0	6.6
Tc	3.1	5.5	3.1	2.5	3.8	2.9	4.6	2.8	8.3	2.9	9.9	2.9	3.2	9.1	3.3	5.1	2.0	3.6	10.4	3.1	4.6
6BWD	4.0	3.5	3.7	2.6	2.3	3.4	5.7	2.8	2.8	3.4	3.4	3.3	3.0	3.7	3.0	2.8	2.8	4.5	3.4	2.7	3.3
CB	1834.4	1168.9	1100.9	1345.2	1411.1	1333.8	1144.8	1129.2	1866.1	1367.1	2433.1	1131.2	1397.3	1428.8	1128.3	1089.1	1366.8	1142.8	4797.0	1091.6	1535.4

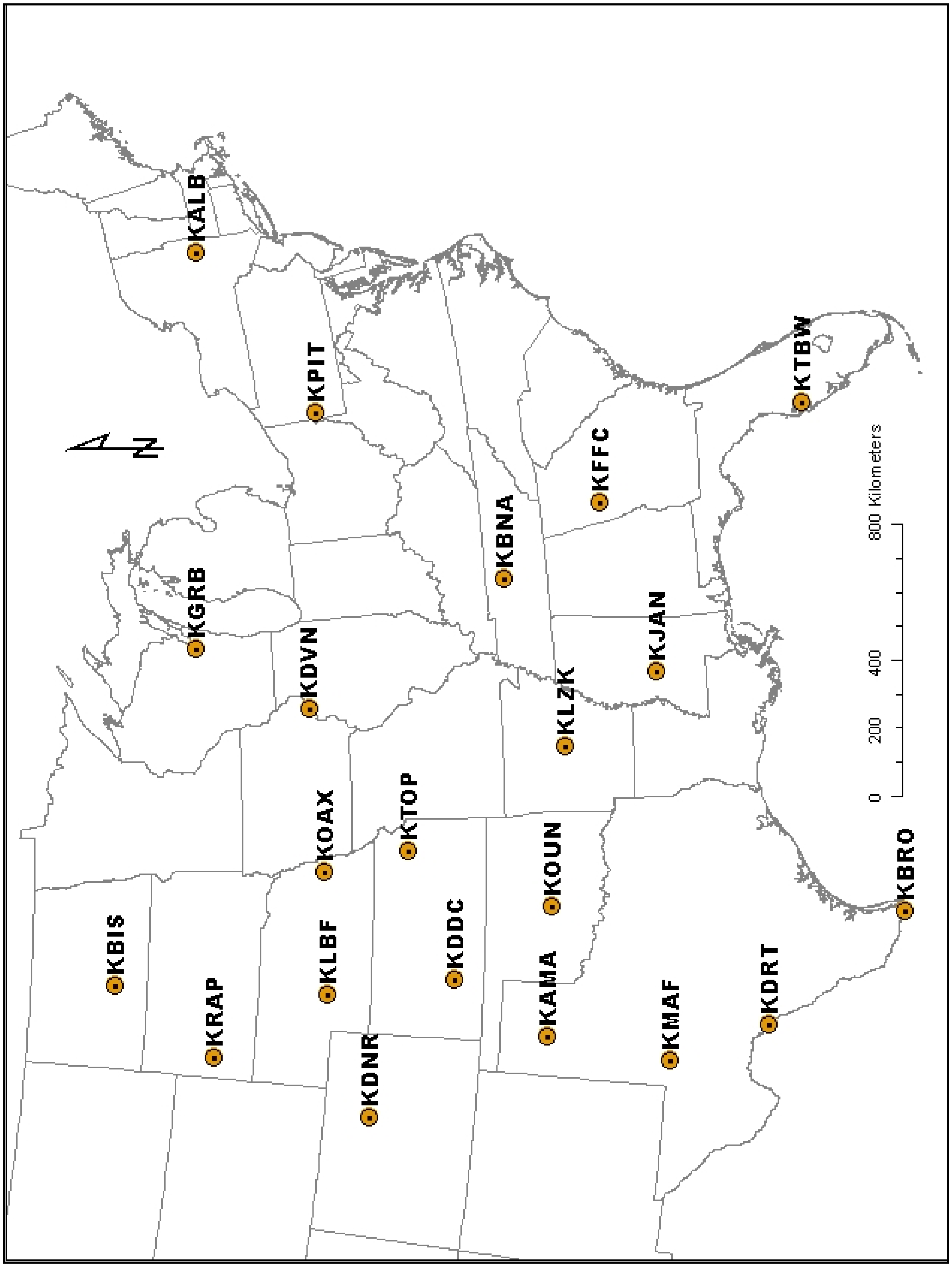

Fig. 2.1. Locations of 21 radiosonde stations used in this study.

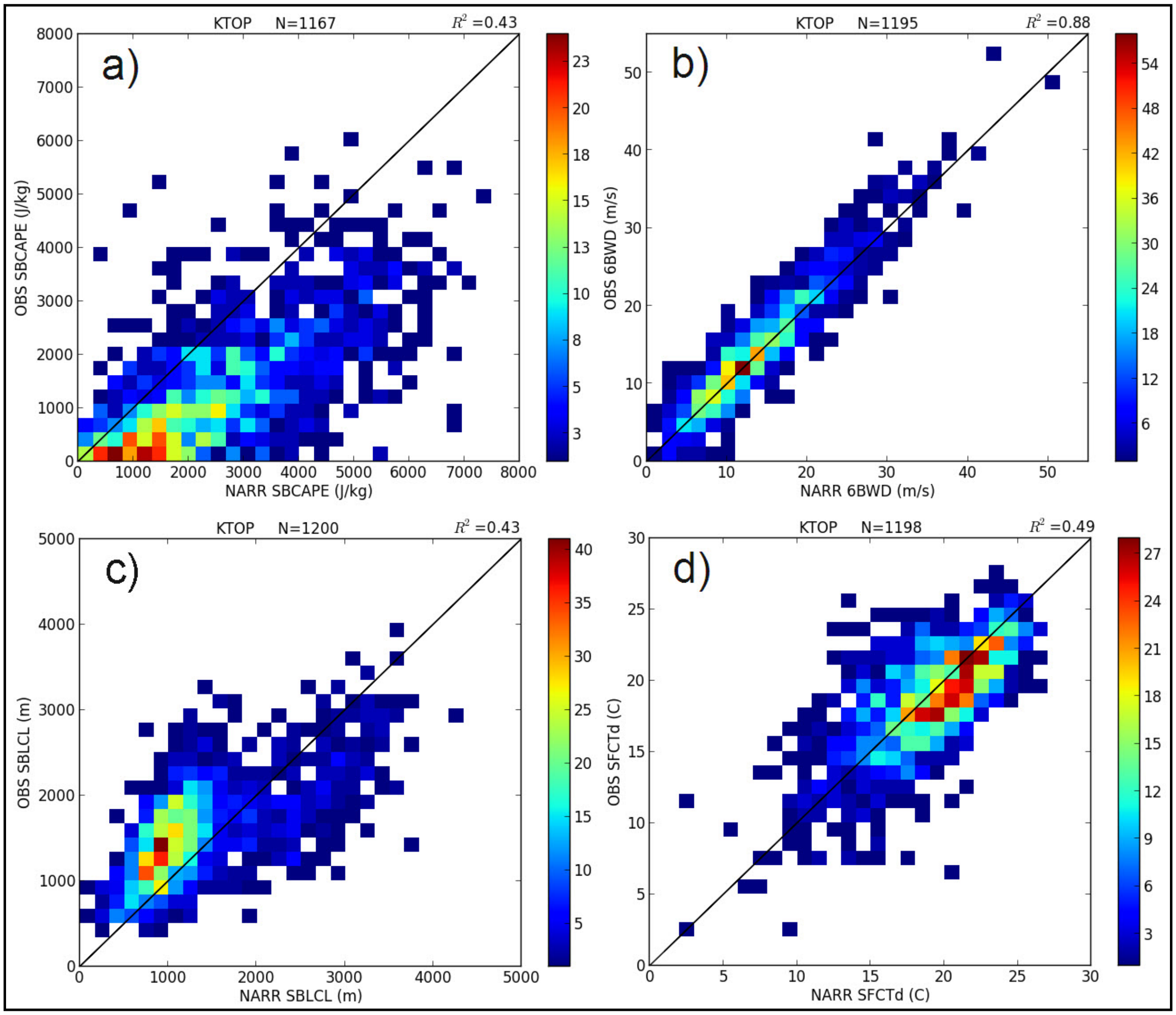

Fig. 2.2. Comparison between NARR and observed a) SBCAPE, b) 6BWD, c) LCL, and d) $SFCT_d$ for all events 2000–2011 $\geq$ 100 J·kg^{-1} SBCAPE at Topeka, KS (KTOP).

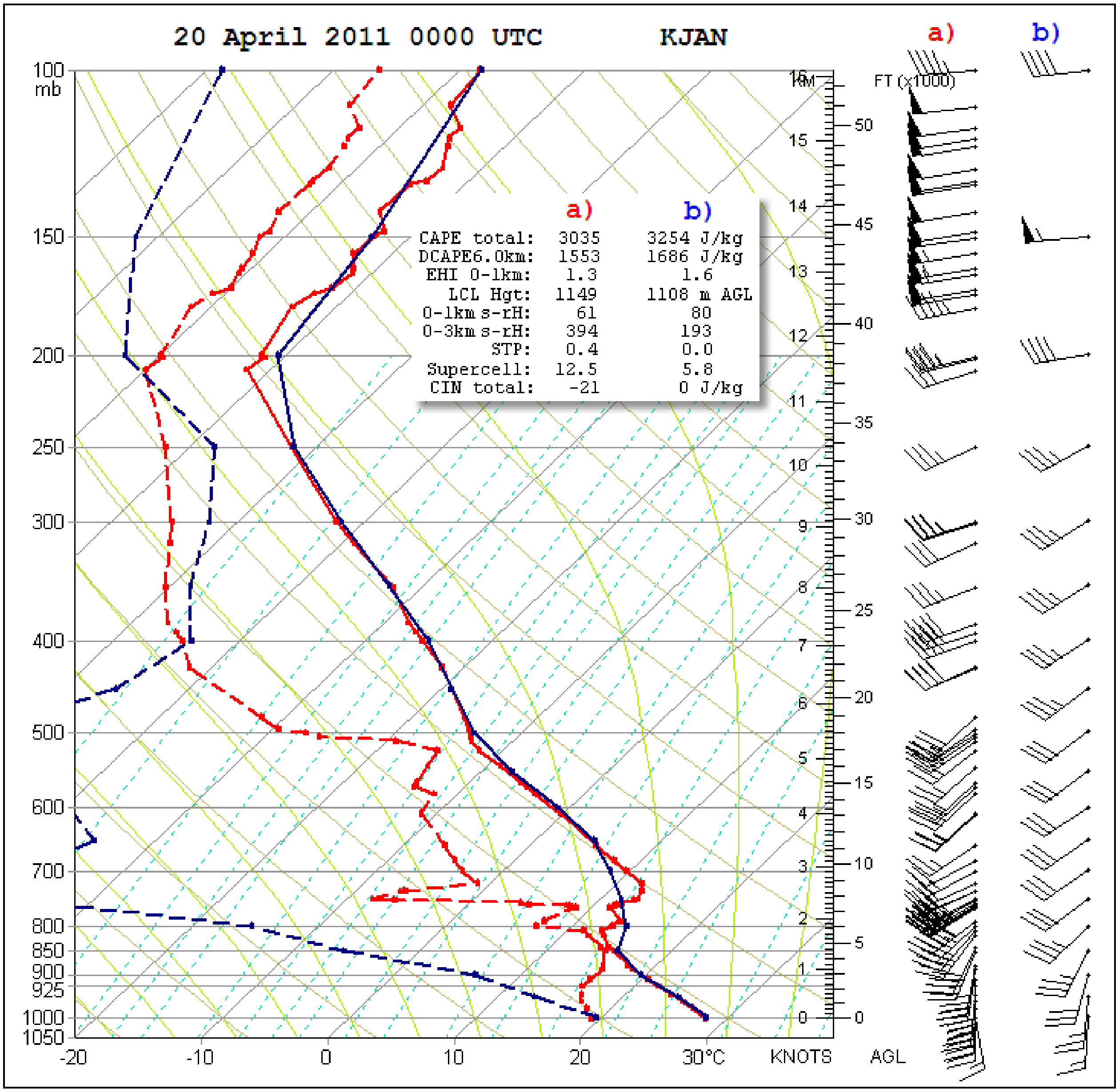

Fig. 2.3. Jackson, MS (KJAN) a) observed (red) and b) NARR (blue) soundings valid 0000 UTC 20 April 2011. Parameters shown are calculated using a surface-based parcel.

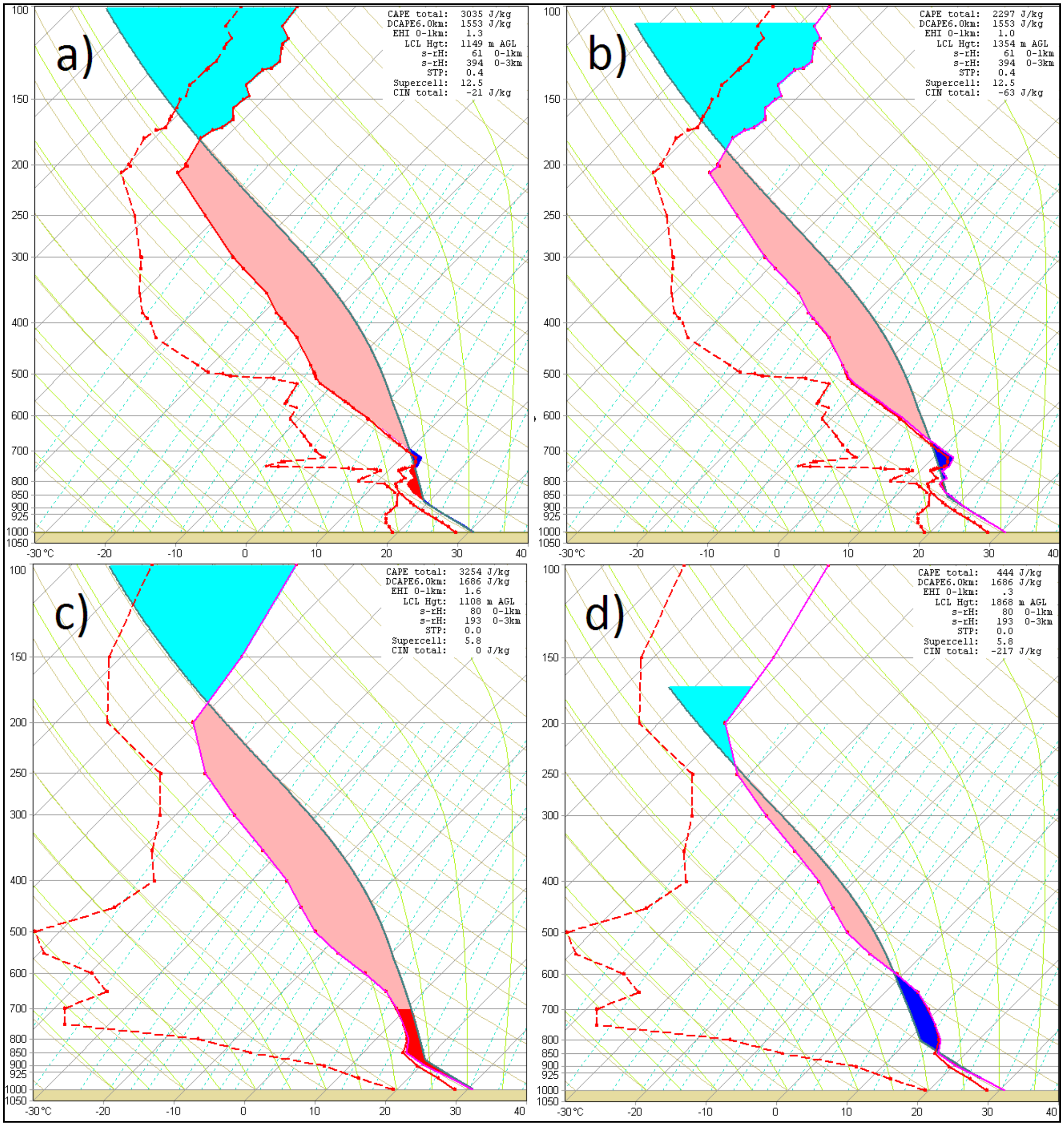

Fig. 2.4. 0000 UTC 20 April 2011 Jackson, MS (KJAN) a) SB parcel observed, (b) ML parcel observed, (c) SB NARR parcel, and (d) ML NARR parcel.

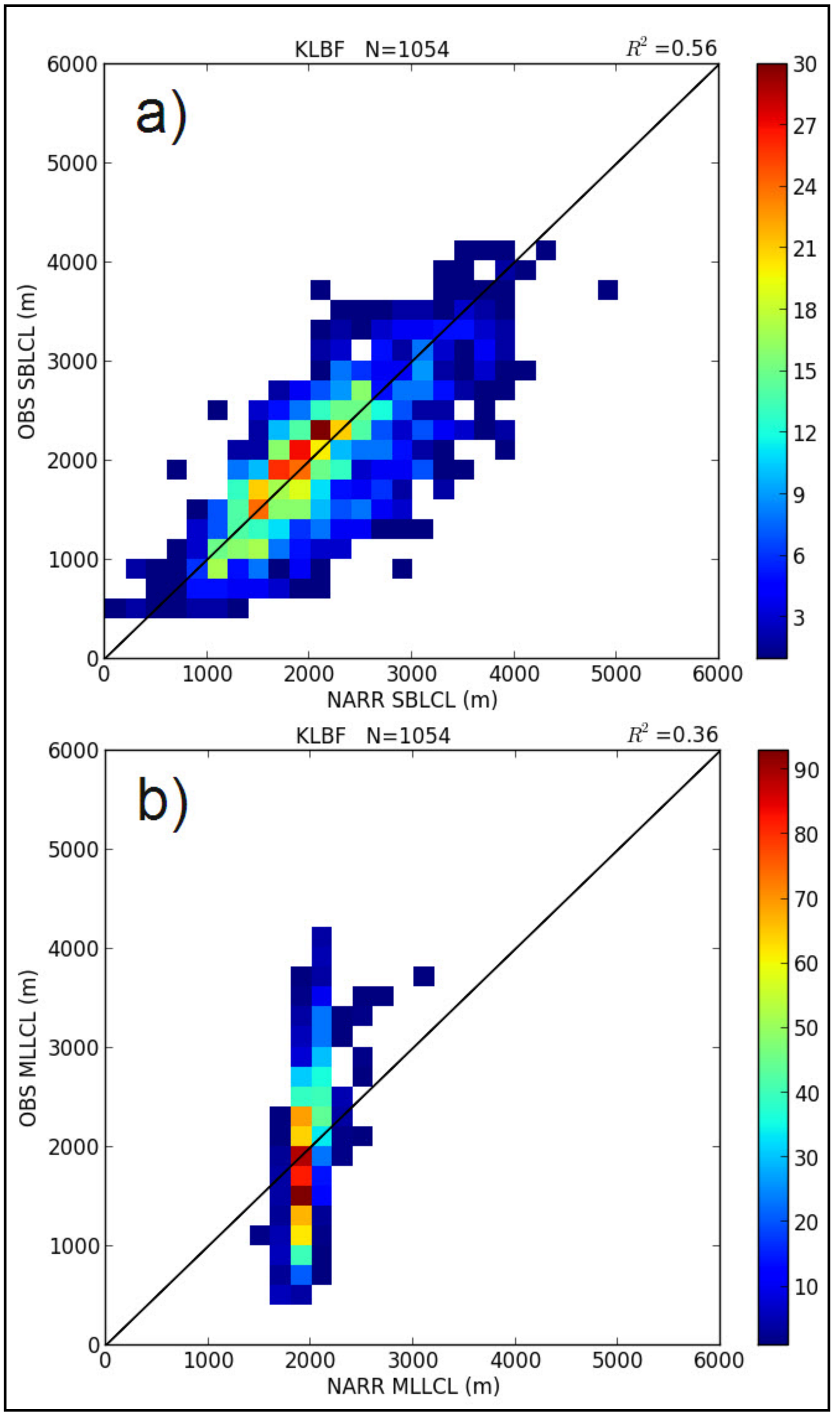

Fig. 2.5. Comparison of NARR and observed a) SBLCL and b) MLCL for North Platte, NE (KLBF) for all events 2000–2011 with ≥ 100 J·kg^{-1} SBCAPE.

CHAPTER 3

EXAMINATION OF HISTORICAL HAZARDOUS CONVECTIVE WEATHER USING DYNAMICAL DOWNSCALING[1]

[1] Gensini, V.A. and T. L. Mote. Submitted to *Journal of Climate* on 12 December 2013.

Abstract

High-resolution (4 km; hourly) regional climate modeling is utilized to resolve March–May hazardous convective weather east of the U.S. Continental Divide for a historical climate period (1980–1990). A hazardous convective weather model proxy is used to depict occurrences of tornadoes, damaging thunderstorm wind gusts, and large hail at hourly intervals during the period of record. Through dynamical downscaling, the regional climate model does an admirable job of replicating the seasonal spatial shifts of hazardous convective weather occurrence during the months examined. Additionally, the interannual variability and diurnal progression of observed severe weather reports closely mimic cycles produced by the regional model. While this methodology has been tested in previous research, this is the first study to use coarse-resolution Global climate model data to force a high-resolution regional model with continuous seasonal integration in the U.S. for purposes of resolving severe convection. Overall, it is recommended that dynamical downscaling play an integral role in measuring climatological distributions of severe weather, both in historical and future climates.

3.1 Introduction

Preliminary research suggests that environmental controls related to hazardous convective weather (tornadoes, severe wind gusts, and large hail; hereafter HCW) will increase in response to elevated greenhouse forcing (Del Ginio et al. 2007; Trapp et al. 2007a; Trapp et al. 2009; Van Klooster and Roebber 2009; Gensini et al. 2013; Diffenbaugh et al. 2013). Despite this evidence, climate change assessments have largely avoided any conclusions regarding potential changes of HCW in a future climate (see discussions in Alley et al. [2007], Karl et al. [2009] and Brooks [2013]). This is primarily due to problems with the historical record of observed HCW reports, the link between HCW reports and associated environmental controls, and the large spatial scale in which Global Climate Models (GCMs) operate relative to HCW.

The widely used Community Climate System Model version 3 (CCSM3; Collins et al. 2006) GCM is a spectral model with 85-wavenumber triangular truncation (approximately 1.4° resolution at the equator) in the horizontal (Collins et al. 2006). This GCM configuration translates roughly to a 150 km horizontal grid spacing in the central U.S., whereas explicit resolution of convection should be done at a horizontal grid scale of less than or equal to 4 km (Weisman et al. 1997). Therefore, the resolution of typical GCM output lacks the ability to resolve HCW. The current understanding of potential changes in future HCW regimes is limited to environmental controls. While more HCW environments could mean more events in the future, such environments are periods when the atmosphere is favorable for organized HCW, not that it will necessarily occur.

Recent exploratory research has indicated dynamical downscaling of GCM data has become possible owing to enhanced model microphysics schemes, increases in computer processing speed, and new GCM data availability (e.g., Trapp et al. 2011; Robinson et al. 2013; Mahoney et al. 2013). Thus, the purpose of this research is to utilize dynamical downscaling to explicitly resolve proxy HCW events using GCM input data. Specifically, this manuscript will examine a GCM historical period (1980–1990) driven via reanalysis in relation to observed HCW reports. This historical baseline will provide a comparison for future period simulations and bias correction estimates.

3.2 Background

Dynamical downscaling is a method for obtaining high-resolution climate information from relatively coarse-resolution GCM output. Using dynamical downscaling, recent research indicates it is now practical to downscale GCM scale output to the 4 km grid spacing (Trapp et al. 2007b; Trapp et al. 2011; Robinson et al. 2013) required for resolving deep convective processes (Weisman et al. 1997). In fact, a recent study has explored the use of dynamical downscaling at a spatial resolution of 1.5 km (Kendon et al. 2012), while several other studies have performed seasonal downscaling at or below 3 km (e.g., Hohenegger et al. 2008; Sato et al. 2009; Langhans et al. 2013; Warrach-Sagi et al. 2013; Prein et al. 2013). Generally, these studies all found utility in the increased spatial resolution provided by dynamical downscaling for their respective research. For severe convection, dynamically downscaled global reanalysis data (similar to the coarse-resolution of many GCMs [~100 km]) has accurately represented HCW during the peak of the convective season (May–June; Trapp et al. 2011; Robinson et al. 2013). However, no studies have examined the use of dynamical downscaling on historical GCM output for HCW purposes in the U.S.

It is important to note that despite a significant increase in HCW reports over the last three decades, research indicates that environmental controls factors (i.e., Convective Available Potential Energy [CAPE] and 0–6 km shear; Gensini and Ashley 2011; Robinson et al. 2013) and modeled proxy reports (Robinson et al. 2013) have exhibited little to no trend. This recent inflation in HCW reports has been extensively documented (Doswell and Burgess 1988; Grazulis 1993; Brooks and Doswell 2001; Brooks and Doswell 2002; Verbout et al. 2006; Doswell 2007). Thus, the recent increase in losses from severe thunderstorms (Changnon 2001) and tornadoes (Brooks and Doswell 2001; Changnon 2009) can be attributed to societal and economic changes rather than an increase in event frequency (Bouwer 2011).

3.3 Methodology

Using 1980–1990 historical data from the CCSM3, a HCW proxy is gridded and summed to create a spatio-temporal climatology for the months March–May. The proxy used in this research will follow that used in Trapp et al. (2011), using hourly thresholds of updraft helicity (UH) and simulated composite radar reflectivity (Z) as described by Kain et al. (2008). UH and Z data are obtained from CCSM3 data by dynamical downscaling, using the non-hydrostatic advanced research core of the Weather Research and Forecasting (WRF-ARW) model (Skamarock et al. 2008). Modeled proxy HCW reports are compared to observed HCW reports over the same period using report data obtained from the Storm Prediction Center (SPC) as compiled for the National Climatic Data Center (NCDC) publication *Storm Data*. Though there are documented problems with using *Storm Data* for convective research purposes (Doswell and Burgess 1988; Brooks 2004), it is currently the most comprehensive source for HCW climatological information.

a. Region

The study region for this research encompasses all points in the U.S. east of the Continental Divide (Fig. 3.1). This domain is centered on the central Great Plains region, which is characterized by the largest HCW frequency on Earth (Brooks et al. 2003b). While it would be ideal to include the entire U.S. in such a study, one must weigh the computational expense of modeling at such a high spatial resolution against the expected benefit of the results. Given that HCW rarely happens west of the Continental Divide (Brooks et al. 2003a; Brooks et al. 2003b; Gensini and Ashley 2011), this region has been omitted.

b. Model diagnostics

i. <u>Parent GCM characteristics</u>

The CCSM3 is a coupled global climate model consisting of atmosphere, land surface, sea-ice, and ocean components (Collins et al., 2006). Available data includes a control run (no changes in external climate forcing), a 20th century simulation (containing the observed changes of greenhouse gases, sulphate aerosols, volcanic aerosols, and solar irradiance from the 20th century), and 21st century scenarios (containing estimated changes in greenhouse gas concentration and aerosol concentrations). For this particular study, 11 years (1980–1990) of a simulation initialized in 1870 and run through the 20th century (CCSM3 b30.030e dataset) was chosen in an effort to assess CCSM3 bias and error relative to actual HCW reports over the same period.

ii. Regional climate model

As previously mentioned, the Regional Climate Model (RCM) used for dynamical downscaling in this study is the non-hydrostatic advanced research core of the Weather Research and Forecasting (WRF-ARW) model (Skamarock et al. 2008). Initial conditions for WRF are provided from CCSM3 at 0000 UTC on March 1st of each year, and integrated over a three-month period, providing CCSM3 boundary conditions every six hours. Parameterizations of physical processes (Table 3.1) and other aspects of the regional climate model configuration are based on WRF-model simulations of HCW in the United States (e.g., Weisman et al. 2008; Kain et al. 2006; Trapp et al. 2011; Robinson et al. 2013). The first six hours and of the simulation are discarded, in addition to the first six lateral-edge domain points, to account for model spin-up (Skamarock 2004). Since a cold start is initialized on March 1st of every HCW season, interannual soil moisture memory is lost, despite the ability to capture seasonal soil moisture feedbacks.

Nine pairs of UH/Z values were tested using fractional gross error (F_E) and mean bias (MB) statistics to determine the most appropriate threshold for HCW proxy occurrence (Fig. 3.2). This analysis suggests the optimal proxy for a HCW event occurs when an hourly model grid point exceeds Z values ≥ 40 dBZ juxtapositioned with UH values ≥ 60 $m^2 \cdot s^{-2}$. This threshold depicts a relative minimum in F_E, but does display a slight positive bias, which changes through the analyzed months. This threshold is slightly different than the 50-40 Z/UH pair used in previous research (Trapp et al. 2011; Robinson et al. 2013). This difference is subtle, considering the differing WRF initial and boundary conditions (NCEP/NCAR Global Reanalysis v. CCSM3) and the examination of an earlier period in the annual convective cycle (March–May v. April–June). The slightly lower Z, but higher UH, values used in our study makes physical sense as earlier months in the annual convective cycle are typically dominated by a low-CAPE and high-shear environment (Brooks et al. 2007) that are strongly synoptically forced (Galway and Pearson 1981).

Although the RCM configuration, study months, and proxy report methodology are similar to previous research (Trapp et al. 2011; Robinson et al. 2013), there is an important difference to note. This study employs a longer (continuous) integration time over the entire three month period, which is different than the 24-h re-initialization used in Trapp et al. (2011) and Robinson et al. (2013). This longer integration time is desirable in climate modeling as it supports a better representation of influences associated with longer-memory processes (e.g., soil moisture) on HCW.

A 50 km fishnet grid was used to evaluate observed and model-simulated HCW events. This grid length is smaller than the ~80 km used in previous severe weather report climatologies (e.g., Brooks et al. 2003a), but greater than the ~38 km grid length used in a similar downscaling study (Trapp et al. 2011). This coarsened grid scale helps compensate for errors in the spatial location of observed HCW reports, and their interpolation to the nearest 4 km RCM grid point.

3.4 Results

Model simulated HCW reports closely mimic the spatial evolution of observed reports for the months analyzed (Fig. 3.3). That is, the RCM reflects an increase in reports and a gradual northward progression of relative maxima consistent with the observed cycle of HCW during this period. These results are consistent with previous downscaling studies that examined April–June (Trapp et al. 2011). In terms of magnitude, March shows little bias relative to observations, whereas April (May) shows a positive (negative) bias (Fig. 3.2). Additionally, RCM simulated and observed HCW exhibit similar interannual variability for the months March–May (Fig. 3.4). For example, March–May 1987 and 1988 are notable in U.S. HCW climatological record for their relatively low report occurrence. The RCM also depicts relative minimums in simulated HCW during these years. While only eleven years are analyzed in this study, and therefore any advanced statistical analysis is inhibited, the historical period run of CCSM3 with the addition of a WRF as a RCM is able sufficiently capture observed variability of HCW at the 4 km, hourly scale during the months examined.

Spatial patterns of bias indicate population density likely plays a role in influencing observed reports relative to those simulated by the RCM (Fig. 3.5). For example, 1980–1990 observed reports are shown to be higher near larger cities such as Dallas-Fort Worth, Oklahoma City, and Shreveport. Meanwhile, magnitudes of observed reports are lower than modeled values on the High-Plains and in portions of Missouri/Arkansas where lack of population (and hence reports) is a key factor. In addition, there is a general underestimation of HCW occurrences by the RCM in many portions of the Southeast U.S. (Fig. 3.5). This underestimation regularly occurs in the month of May and may be attributable to convective mode and scale of forcing for ascent. For example, supercell thunderstorms are most common in the Central Plains of the U.S., and a grid spacing of 4 km better resolves these mesocyclones versus the storm-scale rotation associated with quasi-linear convective severe weather common across the Southeast U.S. Similar biases were found during the months of May and June by Trapp et al. (2011). Using these results, future period simulations can be bias-corrected to account for such errors (Christensen et al. 2008). However, it is unknown if these errors originate from the parent GCM, manifest in the RCM due to choice of model configuration, or are simply errors associated with reporting in *Storm Data*.

To supplement confidence in these simulated reports, environmental controls (i.e., CAPE and 0–6 km shear) known to support HCW were examined (Fig. 3.6). These environmental controls serve as indicators to the climatological locations where one might expect HCW to occur. When restricting analysis of environments to 0000 UTC and resampling RCM output to 3 km grid length (in order to compare to the North American Regional Reanalysis [NARR; Mesinger et al. 2006]), it is shown that the RCM used herein also replicates the interannual variability of proxy significant severe weather environments (Fig. 3.7). Line values shown in Fig. 3.7 are RCM domain-averaged 0000 UTC frequencies of the proxy C composite parameter following the methodology of Gensini and Ashley (2011). While the statistical significance is limited in this relatively short temporal series, it is encouraging to see a historical period RCM run capture the interannual variability of environments favorable for HCW as depicted by the NARR. This strengthens the previous notion that RCMs can adequately capture the interannual variability of observed HCW.

In addition to seasonal spatio-temporal analysis, diurnal convective cycles were also examined (Fig. 3.8). This analysis suggests that high-resolution RCMs can adequately capture the diurnal cycle of HCW. Hourly modeled proxy reports explain 96% of the variability associated with observed reports. In fact, only one hour (0800 UTC) showed no overlap in the 10% error range of hourly observed and simulated HCW. The HCW peak in the RCM occurred at 0000 UTC (2890 reports), whereas observations peaked slightly earlier at 2300 UTC (3157 reports). This is similar to the WRF delayed maximum in rainfall intensity observed by Clark et al. (2007). It should be noted that agreement herein is likely improved due to stronger HCW forcing mechanisms (e.g., fronts) during the months March–May (Galway and Pearson 1981). It is probable that this similarity would diminish as the HCW season progresses into June–August when subtler forcing for ascent is present (Liu et al. 2006).

3.5 Summary and conclusions

We have utilized high-resolution (4 km; hourly) regional climate modeling to simulate a proxy for the variability of tornadoes, damaging thunderstorm wind gusts, and large hail across the eastern two-thirds of the U.S. for the months March–May during the period 1980–1990. This process used GCM output from CCSM3 to drive WRF (the RCM). A proxy for HCW was developed utilizing methodology from Trapp et al. (2011) and Robinson et al. (2013). However, continuous integration over the three-month period was employed in this study to best replicate long-memory processes, a suggestion from previous research.

Overall, proxy HCW events simulated by the WRF as a RCM depict skill in the spatio-temporal distributions of hazardous thunderstorms during the months examined. Proxy report analysis is strengthened using an environmental control parameter that exhibits strong interannual correlation between RCM generated and reanalyzed environments. Spatial biases are present, indicating that evaluating HCW occurrence at small spatial scales should be done with caution. Instead, evaluations HCW occurrence from RCM output may be best done at GCM resolution. Along with studies such as Trapp et al. (2011) and Robinson et al. (2013), this research further indicates that dynamical downscaling of data with relatively coarse grid length to the resolution needed to explicitly resolve HCW is a productive endeavor.

To date, the main limitation of performing dynamical downscaling analysis for purposes of resolving HCW continues to be the lack of temporal length (i.e., we use an eleven-year period), owing to the computationally expensive nature of performing dynamical downscaling.

This will be mitigated in the future as additional years and months are simulated, along with additional parent/child GCMs/RCMs, creating an ensemble estimation of both historical and future HCW occurrence. These GCM-driven dynamically downscaled scenarios must play a vital role in our understanding of potential changes in future HCW distributions and will serve as a comparison to environmental methods (Del Ginio et al. 2007; Trapp et al. 2007a; Trapp et al. 2009; Van Klooster and Roebber 2009; Gensini et al. 2013; Diffenbaugh et al. 2013) used to estimate such changes in previous research.

3.6 References

Alley, R., and Coauthors, 2007: Summary for policymakers. *Climate Change 2007: The Physical Science Basis,* S. Solomon, and Coauthors, Eds., Cambridge University Press, 1–18.

Bouwer, L. M., 2011: Have disaster losses increased due to anthropogenic climate change? *Bulletin of the American Meteorological Society*, **92,** 39–46.

Brooks, H. E., 2004: On the relationship of tornado path length and width to intensity. *Weather and Forecasting*, **19,** 310–319.

——, 2013: Severe thunderstorms and climate change. *Atmospheric Research*, **123,** 129–138.

Brooks, H. E., and C. A. Doswell III, 2001: Normalized damage from major tornadoes in the United States: 1890–1999. *Weather and Forecasting,* **16,** 168–176.

——, 2002: Deaths in the 3 May 1999 Oklahoma City tornado from a historical perspective. *Weather and Forecasting*, **17,** 354–361.

Brooks, H. E., C. A. Doswell III, and M. P. Kay, 2003a: Climatological estimates of local daily tornado probability for the United States. *Weather and Forecasting*, **18,** 626–640.

Brooks, H. E., J. W. Lee, and J. P. Craven, 2003b: The spatial distribution of severe thunderstorm and tornado environments from global reanalysis data. *Atmospheric Research*, **67–68,** 73–94.

Brooks, H. E., A. R. Anderson, K. Riemann, I. Ebbers, and H. Flachs, 2007: Climatological aspects of convective parameters from the NCAR/NCEP reanalysis. *Atmospheric Research*, **83,** 294–305.

Changnon, S. A., 2001: Damaging thunderstorm activity in the United States. *Bulletin of the American Meteorological Society*, **82,** 597–608.

——, 2009: Tornado losses in the United States. *Natural Hazards Review*, **10,** 145–150.

Chen, F., and J. Dudhia, 2001: Coupling an advanced land surface-hydrology model with the Penn State-NCAR MM5 modeling system. Part I: Model implementation and sensitivity. *Monthly Weather Review*, **129,** 569–585.

Christensen, J. H., F. Boberg, O. B. Christensen, and P. Lucas-Picher, 2008: On the need for bias correction of regional climate change projections of temperature and precipitation. *Geophysical Research Letters*, **35,** L20709.

Clark, A. J., W. A. Gallus Jr, and T.-C. Chen, 2007: Comparison of the diurnal precipitation cycle in convection-resolving and non-convection-resolving mesoscale models. *Monthly Weather Review*, **135,** 3456–3473.

Collins, W. D., and Coauthors, 2006: The Community Climate System Model Version 3 (CCSM3). *Journal of Climate*, **19,** 2122–2143.

Del Genio, A. D., M.-S. Yao, and J. Jonas, 2007: Will moist convection be stronger in a warmer climate? *Geophysical Research Letters*, **34,** L16703.

Diffenbaugh, N. S., M. Scherer, and R. J. Trapp, 2013: Robust increases in severe thunderstorm environments in response to greenhouse forcing. *Proceedings of the National Academy of Sciences*, **110,** 16361–16366.

Doswell III, C. A., 2007: Small sample size and data quality issues illustrated using tornado occurrence data. *Electronic Journal of Severe Storms Meteorology*, **2,** 1–16.

Doswell III, C. A., and D. W. Burgess, 1988: On some issues of United States tornado climatology. *Monthly Weather Review*, **116,** 495–501.

Dudhia, J., 1989: Numerical study of convection observed during the winter monsoon experiment using a mesoscale two-dimensional model. *Journal of the Atmospheric Sciences*, **46,** 3077–3107.

Galway, J. G., and A. Pearson, 1981: Winter tornado outbreaks. *Monthly Weather Review*, **109,** 1072–1080.

Gensini, V. A., and W. S. Ashley, 2011: Climatology of potentially severe convective environments from the North American Regional Reanalysis. *Electronic Journal of Severe Storms Meteorology*, **6,** 1–40.

Gensini, V. A., C. Ramseyer, and T. L. Mote, 2014: Future convective environments using NARCCAP. *International Journal of Climatology*, **34,** 1699–1705.

Grazulis, T. P., 1993: *Significant tornadoes: 1680–1991.* Environmental Films, 1326 pp.

Hohenegger, C., P. Brockhaus, and C. Schar, 2008: Towards climate simulations at cloud-resolving scales. *Meteorologische Zeitschrift*, **17,** 383–394.

Hong, S.-Y., and J.-O. J. Lim, 2006: The WRF single-moment 6-class microphysics scheme (WSM6). *Journal Korean Meteorological Society*, **42,** 129–151.

Iacono, M. J., E. J. Mlawer, S. A. Clough, and J. J. Morcrette, 2000: Impact of an improved longwave radiation model, RRTM, on the energy budget and thermodynamic properties of the NCAR community climate model, CCM3. *Journal of Geophysical Research*, **105,** 14873–14890.

Kain, J. S., and Coauthors, 2008: Some practical considerations regarding horizontal resolution in the first generation of operational convection-allowing NWP. *Weather and Forecasting*, **23,** 931–952.

Karl, T. R., J. M. Melillo, and T. C. Peterson, 2009: *Global climate change impacts in the United States.* Cambridge University Press.

Kendon, E. J., N. M. Roberts, C. A. Senior, and M. J. Roberts, 2012: Realism of rainfall in a very high-resolution regional climate model. *Journal of Climate*, **25**, 5791–5806.

Langhans, W., J. Schmidli, O. Fuhrer, S. Bieri, and C. Schar, 2013: Long-Term Simulations of Thermally Driven Flows and Orographic Convection at Convection-Parameterizing and Cloud-Resolving Resolutions. *Journal of Applied Meteorology & Climatology*, **52**, 1490–1510.

Liu, C., M. W. Moncrieff, J. D. Tuttle, and R. E. Carbone, 2006: Explicit and parameterized episodes of warm-season precipitation over the continental United States. *Advances in Atmospheric Sciences*, **23,** 91–105.

Mahoney, K., M. Alexander, J. D. Scott, and J. Barsugli, 2013: High-resolution downscaled simulations of warm-season extreme precipitation events in the Colorado Front Range under past and future climates. *Journal of Climate*, **26**, 8671–8689.

Mellor, G. L., and T. Yamada, 1982: Development of a turbulence closure model for geophysical fluid problems. *Reviews of Geophysics*, **20,** 851–875.

Mesinger, F., and Coauthors, 2006: North American Regional Reanalysis. *Bulletin of the American Meteorological Society*, **87,** 343–360.

Mlawer, E. J., S. J. Taubman, P. D. Brown, M. J. Iacono, and S. A. Clough, 1997: Radiative transfer for inhomogeneous atmospheres: RRTM, a validated correlated-k model for the longwave. *Journal of Geophysical Research*, **102,** 16663–16682.

Prein, A. F., G. J. Holland, R. M. Rasmussen, J. Done, K. Ikeda, M. P. Clark, and C. H. Liu, 2013: Importance of regional climate model grid spacing for the simulation of heavy precipitation in the Colorado Headwaters. *Journal of Climate*, **26**, 4848–4857.

Robinson, E. D., R. J. Trapp, and M. E. Baldwin, 2013: The geospatial and temporal distributions of severe thunderstorms from high-resolution dynamical downscaling. *Journal of Applied Meteorology and Climatology***, 52,** 2147–2161.

Sato, T., H. Miura, M. Satoh, Y. N. Takayabu, and Y. Wang, 2009: Diurnal cycle of precipitation in the tropics simulated in a global cloud-resolving model. *Journal of Climate*, **22**, 4809–4826.

Shepherd, M., D. Niyogi, and T. L. Mote, 2009: A seasonal-scale climatological analysis correlating spring tornadic activity with antecedent fall–winter drought in the southeastern United States. *Environmental Research Letters*, **4,** 7pp.

Skamarock, W. C., 2004: Evaluating mesoscale NWP models using kinetic energy spectra. *Monthly Weather Review*, **132,** 3019–3032.

Skamarock, W. C., J. B. Klemp, J. Dudhia, D. O. Gill, D. M. Barker, W. Wang, and J. G. Powers, 2008: A description of the Advanced Research WRF version 3. NCAR Tech. Note NCAR/TN-475+STR, 113pp.

Trapp, R. J., N. S. Diffenbaugh, H. E. Brooks, M. E. Baldwin, E. D. Robinson, and J. S. Pal, 2007a: Changes in severe thunderstorm environment frequency during the 21st century caused by anthropogenically enhanced global radiative forcing. *Proceedings of the National Academy of Sciences*, **104,** 19719–19723.

Trapp, R. J., B. A. Halvorson, and N. S. Diffenbaugh, 2007b: Telescoping, multimodel approaches to evaluate extreme convective weather under future climates. *Journal of Geophysical Research*, **112,** D20109.

Trapp, R. J., N. S. Diffenbaugh, and A. Gluhovsky, 2009: Transient response of severe thunderstorm forcing to elevated greenhouse gas concentrations. *Geophysical Research Letters*, **36,** L01703.

Trapp, R. J., E. Robinson, M. Baldwin, N. Diffenbaugh, and B. Schwedler, 2011: Regional climate of hazardous convective weather through high-resolution dynamical downscaling. *Climate Dynamics*, **37,** 677–688.

Van Klooster, S. L., and P. J. Roebber, 2009: Surface-based convective potential in the contiguous United States in a business-as-usual future climate. *Journal of Climate*, **22,** 3317–3330.

Verbout, S. M., H. E. Brooks, L. M. Leslie, and D. M. Schultz, 2006: Evolution of the U.S. tornado database: 1954–2003. *Weather and Forecasting*, **21,** 86–93.

Warrach-Sagi, K., T. Schwitalla, V. Wulfmeyer, and H.-S. Bauer, 2013: Evaluation of a climate simulation in Europe based on the WRF–NOAH model system: precipitation in Germany. *Climate Dynamics*, **41,** 755–774.

Weisman, M. L., W. C. Skamarock, and J. B. Klemp, 1997: The resolution dependence of explicitly modeled convective systems. *Monthly Weather Review*, **125,** 527–548.

Weisman, M. L., C. Davis, W. Wang, K. W. Manning, and J. B. Klemp, 2008: Experiences with 0–36-h Explicit Convective Forecasts with the WRF-ARW Model. *Weather and Forecasting*, **23,** 407–437.

Table 3.1. Relevant regional model configuration information.

Parameterization		
Microphysics	**WSM6**	(Hong and Lim 2006)
Shortwave Radiation	**Dudhia**	(Dudhia 1989)
Longwave Radiation	**RRTM**	(Mlawer et al. 1997; Iacono et al. 2000)
Land Surface Model	**Noah**	(Chen and Dudhia 2001)
Planetary Boundary Layer	**MYJ**	(Mellor and Yamada 1982)
Model Parameters		
Time Step	**24 s**	
Vertical Levels	**35**	
Horizonal Grid Point Spacing	**4 km**	
Initial/Boundary Conditions		
Temperature, specific humidity, geopotential height, u-v wind, surface pressure	**Surface, 27 isobaric levels; 6-h intervals**	
Soil Temperature, Soil Moisture	**0–10, 10–40, 40–100, 100–200 cm; 6-h intervals**	

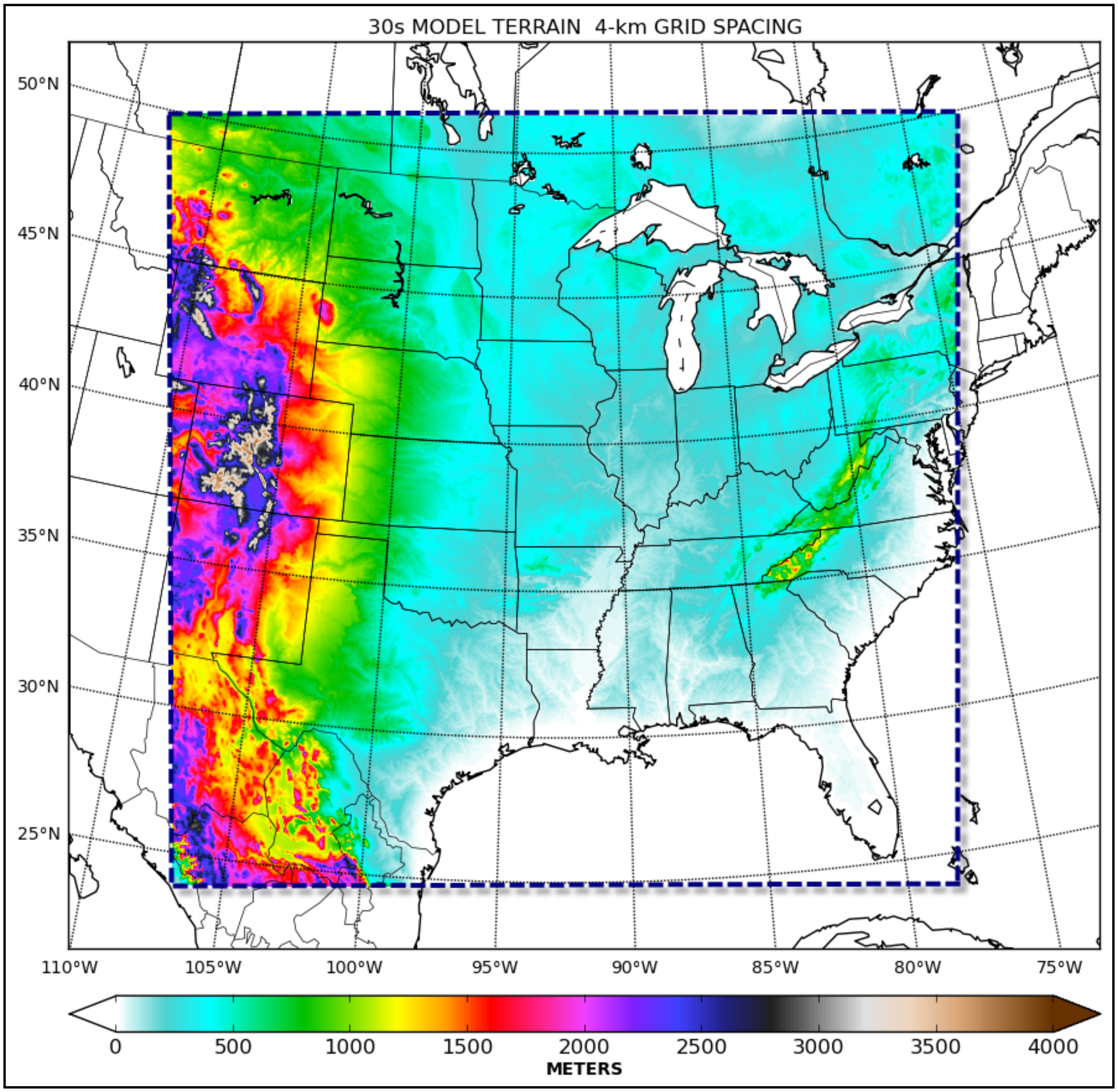

Fig. 3.1. Study region denoted by the dashed blue box.

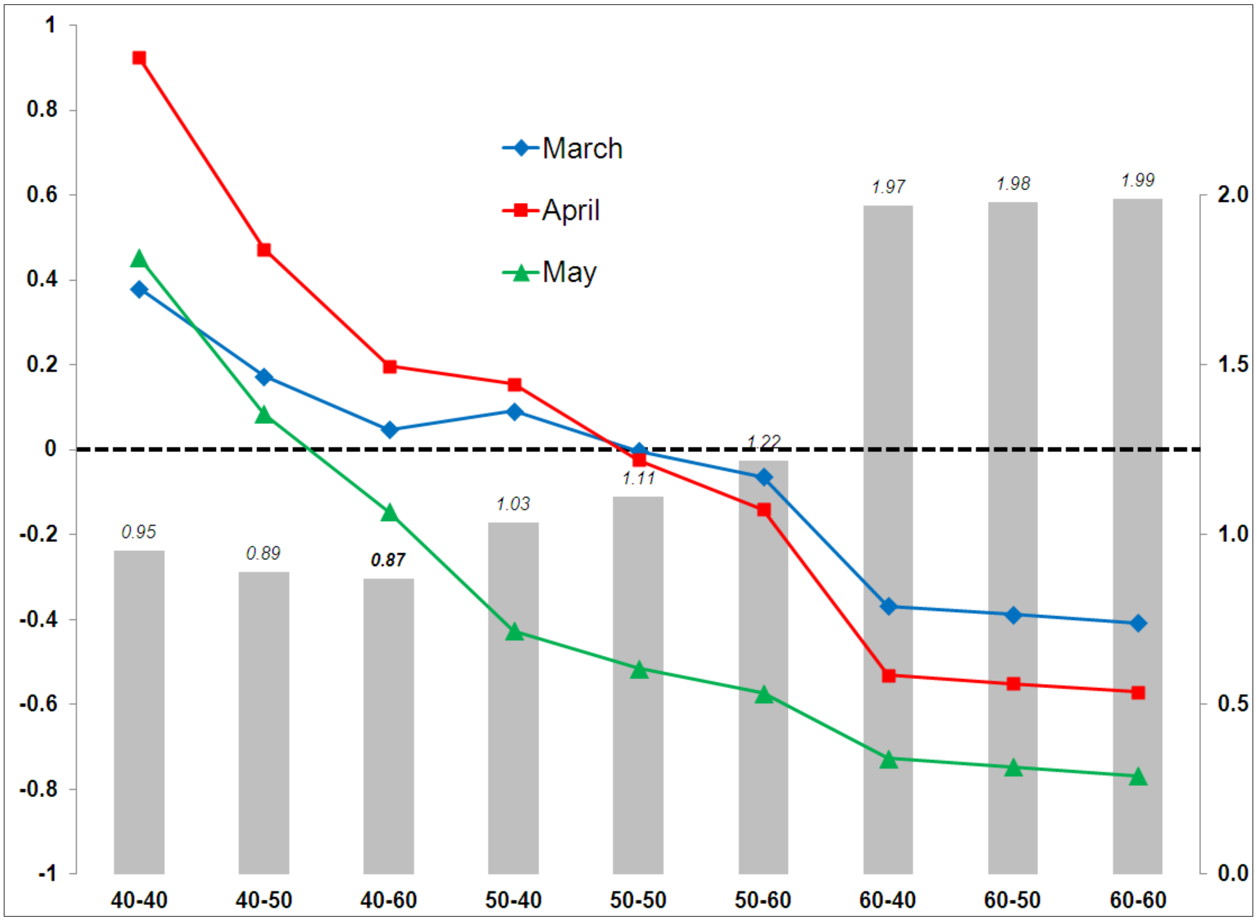

Fig. 3.2. Fractional gross error (grey bars; axis right) and mean bias (colored lines; axis left) by month for nine Z/UH pairs examined in this study.

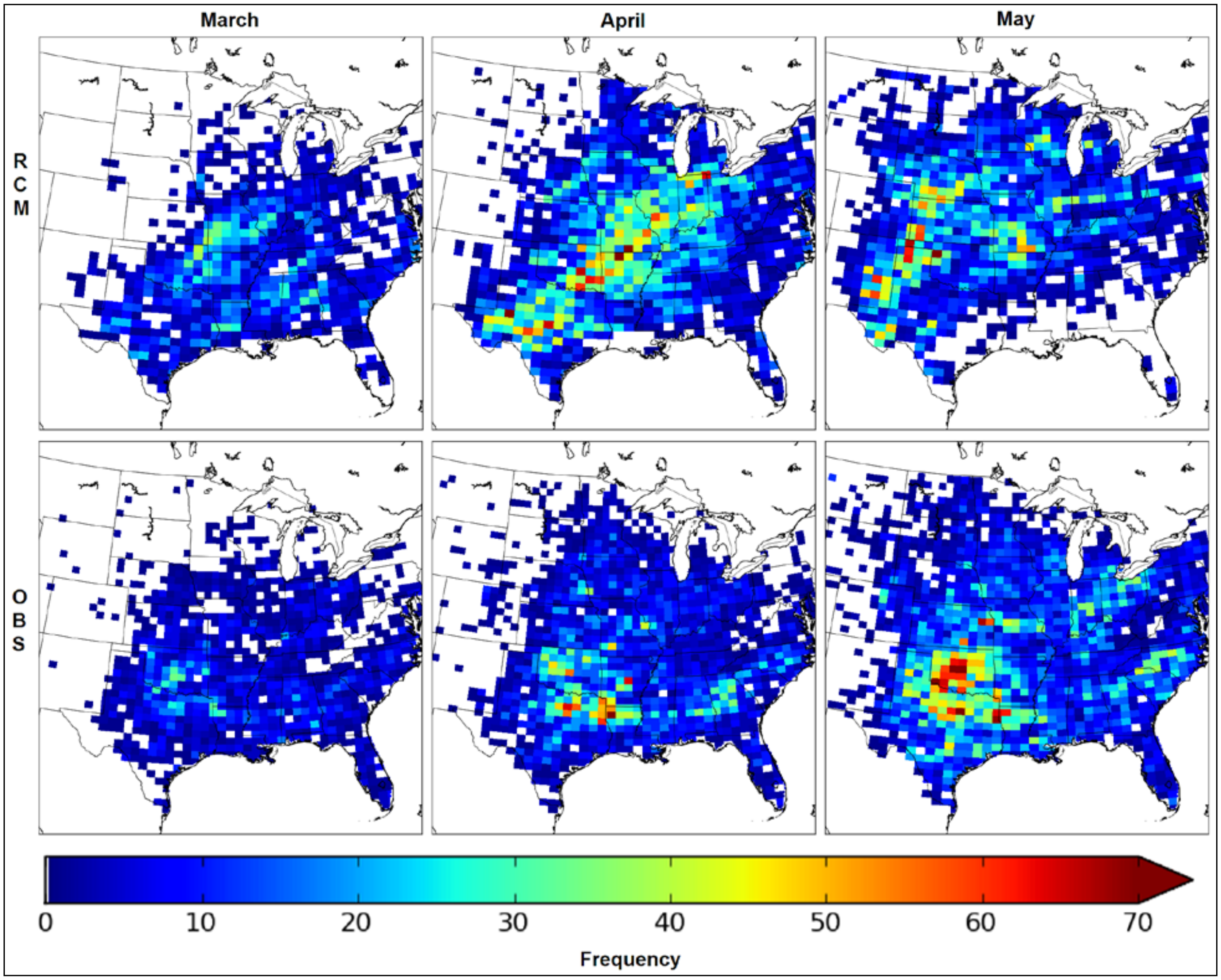

Fig. 3.3. 1980–1990 RCM simulated (top row) and observed (bottom row) severe weather reports.

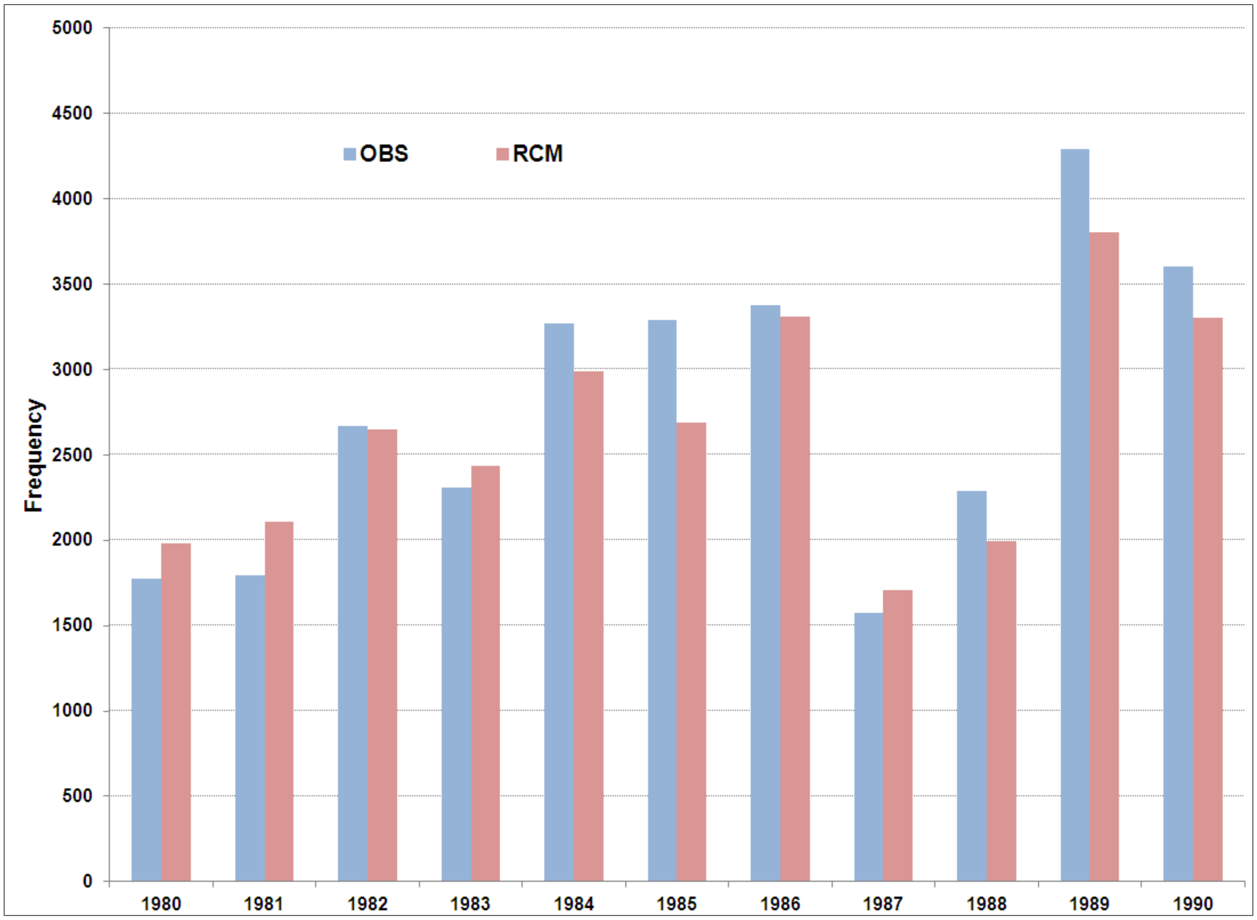

Fig. 3.4. Interannual variability of March–May HCW as depicted by a RCM and observations.

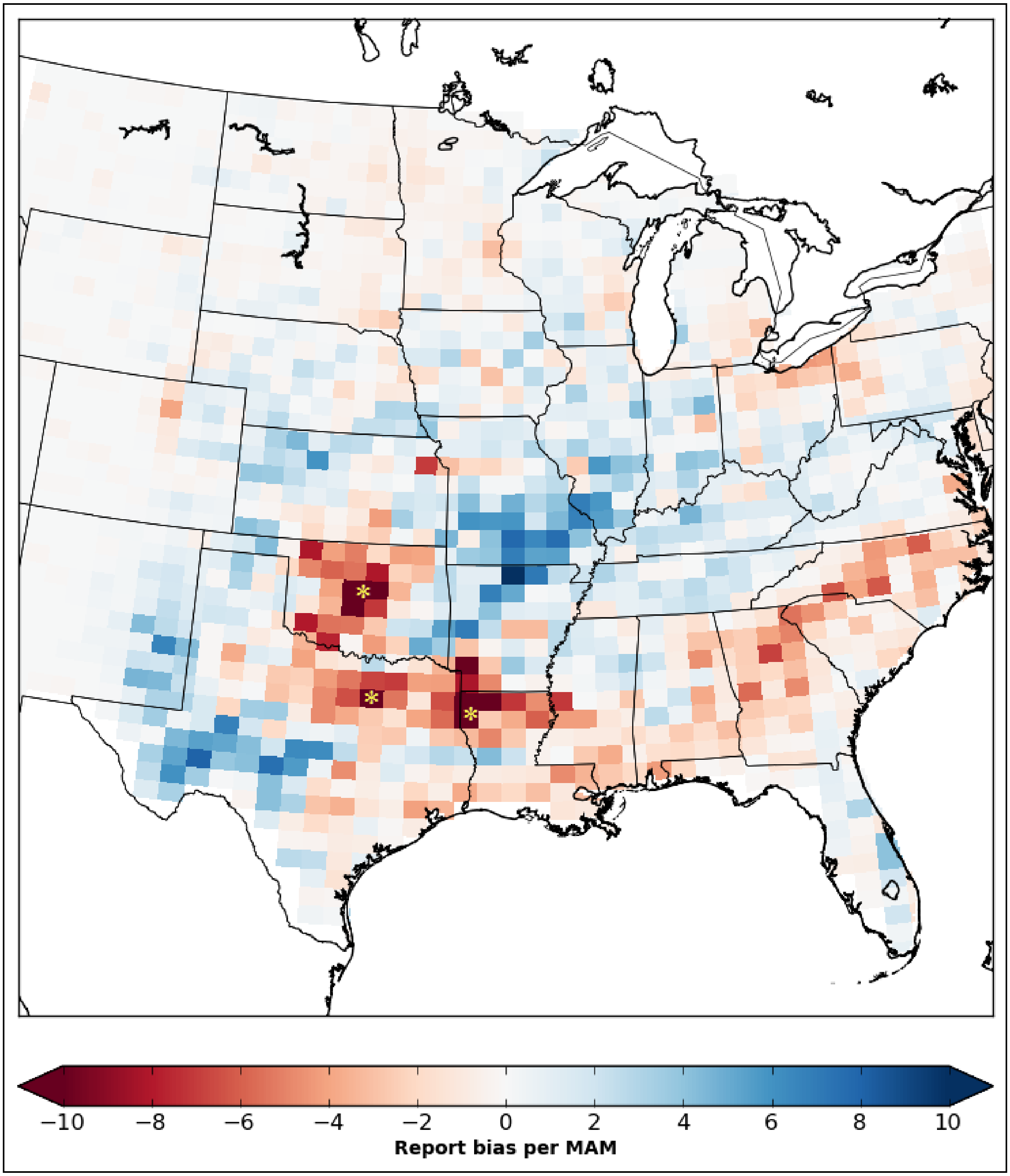

Fig. 3.5. Spatial difference between RCM proxy and observed severe weather reports for the period 1980–1990. Yellow "*" indicate the locations of Oklahoma City, OK, Dallas-Fort Worth, TX, and Shreveport, LA.

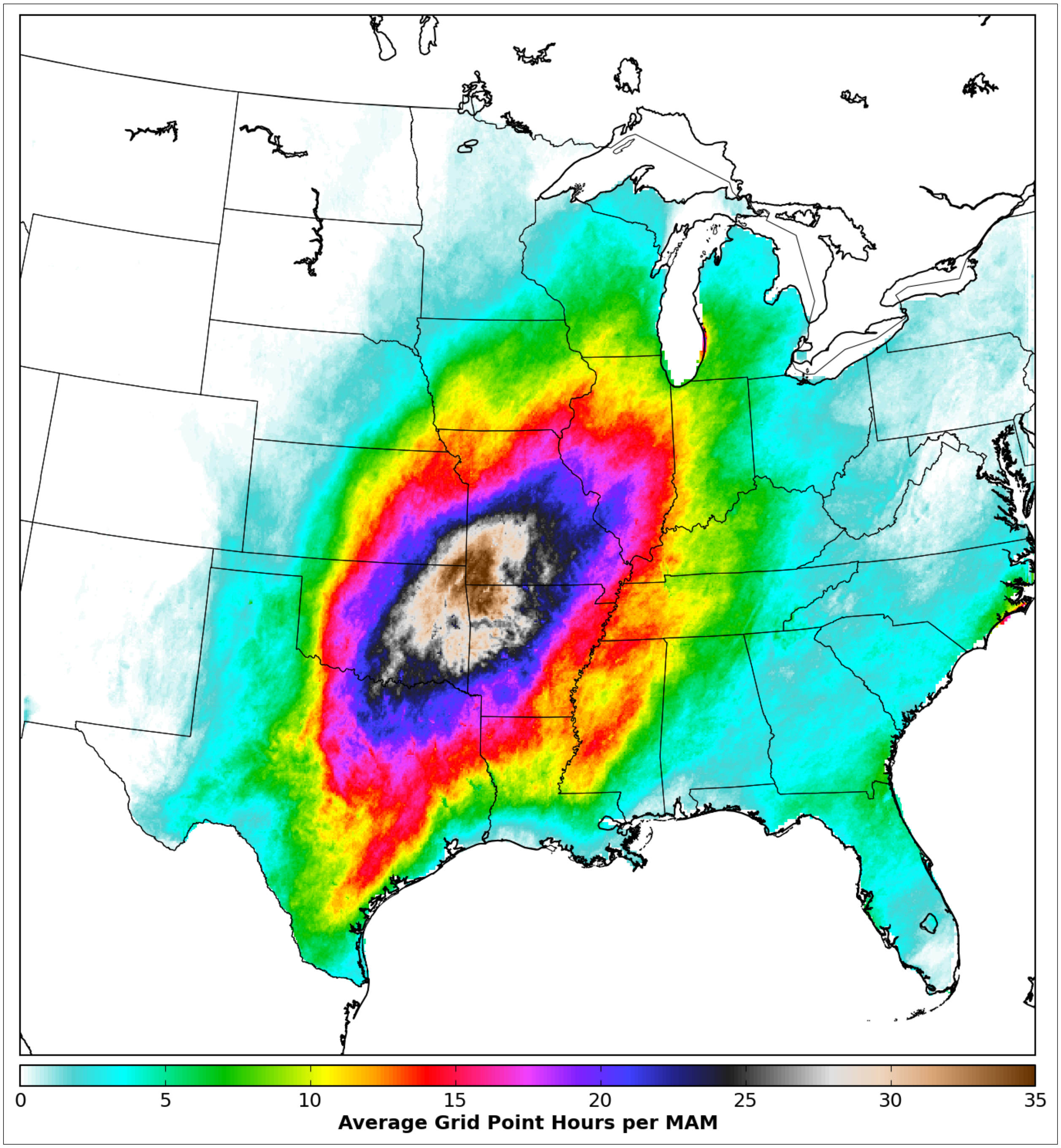

Fig. 3.6. 1980–1990 frequency of March–May (MAM) significant severe weather environments as simulated by a RCM.

Fig. 3.7. 0000 UTC domain-averaged proxy C-composite values (following Gensini and Ashley 2011) from the North American Regional Reanalysis and the RCM used in this study.

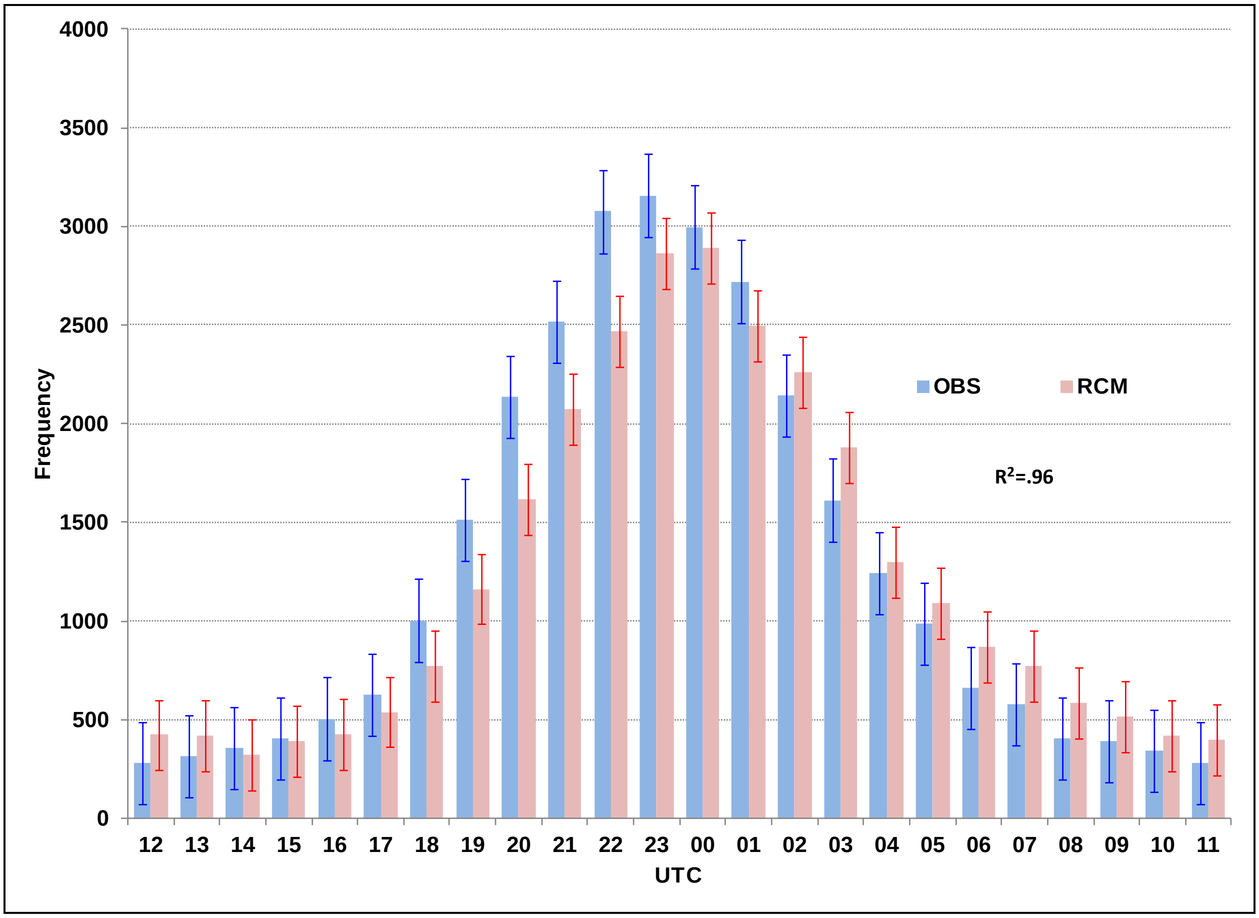

Fig. 3.8. Diurnal frequency comparison of RCM simulated and observed severe weather reports. Error bars the standard error.

CHAPTER 4

DYNAMICAL DOWNSCALING ANALYSIS OF FUTURE HAZARDOUS CONVECTIVE WEATHER[1]

[1] Gensini, V.A. and T. L. Mote. To be submitted to *Climatic Change.*

Abstract

High-resolution dynamical downscaling is used to explore 2080–2090 peak-season hazardous convective weather as simulated from the Community Climate System Model version 3. Downscaling to 4 km grid spacing is performed using the Weather Research and Forecasting model. Tornadoes, damaging wind gusts, and large hail are simulated using a model proxy at hourly intervals for locations east of the U.S. Continental Divide. Future period results are placed into context using 1980–1990 output. While a limited sample size exists, a statistically significant increase in synthetic severe weather activity is noted in March, whereas event frequency is shown to slightly increase in April, and stay the same in May. These increases are primarily found in the Mississippi, Tennessee, and Ohio River valleys. Diurnally, most of the increase in HCW activity is shown to be in the hours surrounding local sunset. Peak-season severe weather is also shown to be more variable in the future with a skewed potential toward larger counts. Finally, modeled proxy events are compared to environmental parameters known to generate HCW activity. These environmental conditions explain over 80% of the variance associated with modeled reports during March–May and show an increasing future tendency. Finally, challenges associated with dynamical downscaling for purposes of resolving severe local storms are discussed.

4.1 Introduction

A major point of discussion in severe weather climatology surrounds the future of deep, moist convection in an anthropogenically altered climate. Historically, the record of U.S. hazardous convective weather (HCW; i.e., tornadoes, wind gusts, and large hail) has been driven largely by reporting. Problems associated with the reporting process and population biases have made it difficult to determine trends from reports (see discussions in Doswell and Burgess 1988; Grazulis 1993; Brooks and Doswell 2001; Brooks and Doswell 2002; Verbout et al. 2006; and Doswell 2007).

Due to the uncertainty associated with reports, recent research has instead examined the variability of environmental conditions necessary for the formation of HCW. These studies suggest that environmental conditions related to hazardous convective weather will increase in response to elevated greenhouse forcing (Del Genio et al. 2007; Trapp et al. 2007a; Trapp et al. 2009; Van Klooster and Roebber 2009; Brooks 2013; Gensini et al. 2013; Diffenbaugh et al. 2013). Despite the mounting environmental evidence, recent climate change assessments have largely avoided any conclusions regarding potential changes of HCW in a future climate (see discussions in Alley et al. [2007] and Karl et al. [2009]). The latest Intergovernmental Panel on Climate Change (IPCC AR5) report lacks any definitive conclusions regarding extreme convective weather. This lack of confidence is primarily due to the opaque historical record of HCW reports and the inability to directly link environmental control parameters to events (Alexander and Coauthors 2013).

While Global Climate Model (GCM) output can simulate future environmental conditions favorable for the formation of HCW, the grid spacing (typically on the order of 100-

km) lacks the ability to resolve processes associated with HCW. However, new research indicates that synthetic reports produced by high-resolution (4 km; hourly) regional climate models can accurately capture the spatio-temporal variability of observed reports when forced with coarse resolution GCM-scale conditions (Trapp et al. 2011; Robinson et al. 2013; Gensini and Mote 2014). Dynamical downscaling for purposes of resolving HCW events has yet to be performed on GCM-scale future projections. Thus, this is the first study to compare historical and future synthetic severe weather reports from the same GCM.

4.2 Background

Dynamically downscaled global reanalysis data (similar to the coarse-resolution of many GCMs) has accurately represented HCW during the peak of the convective season (May–June; Trapp et al. 2011; Robinson et al. 2013). The Community Climate System Model version 3 (CCSM3) control run was also found to accurately portray spatial and temporal variability during March–May while correctly timing the diurnal hourly frequency of HCW (Gensini and Mote 2014). While dynamical downscaling GCM output for purposes of resolving HCW is in its infancy, these studies indicate a promising future of research.

Downscaling for HCW must be done at a grid spacing $\leq$ 4 km, as severe convective storms can be explicitly resolved at this scale (Weisman et al. 1997). The main challenge associated with dynamical downscaling continues to be its computationally expensive nature, though, there is little doubt this challenge will become increasingly less important in the future. Dynamical downscaling for HCW will become unnecessary when GCM grid spacing is reduced to 4 km. However, grid spacing from the latest suite of GCM models used for the IPCC AR5 report were simulated with latitude-longitude spacing that ranged from 4° by 5° to about 1° by 1°, indicating that dynamical downscaling will likely be pertinent for years to come.

As previously discussed, one must recognize several potential pitfalls when drawing conclusions from the recorded history of HCW. Studies using objective methods to determine the history of HCW activity indicate that environmental conditions (Gensini and Ashley 2011; Robinson et al. 2013) and modeled proxy reports (Robinson et al. 2013) have exhibited little to no trend, despite a significant increase in HCW reports over the past 30 years. Inflation in HCW reporting is well documented in the literature (e.g., Doswell and Burgess 1988; Grazulis 1993; Brooks and Doswell 2001; Brooks and Doswell 2002; Verbout et al. 2006; and Doswell 2007), and hence, recent increases in economic losses from severe thunderstorms (Changnon 2001) and tornadoes (Brooks and Doswell 2001; Changnon 2009) have been attributed to changes in the societal landscape (e.g., population, property value) rather than an increase in the frequency of HCW events (Bouwer 2011).

While no trends in HCW synthetic reports or environments exist over the past 30 years, Several GCMs project a bullish increase in the ingredients supportive of HCW by the late 21st Century (Del Genio et al. 2007; Trapp et al. 2007a; Trapp et al. 2009; Van Klooster and Roebber 2009; Diffenbaugh et al. 2013). Using dynamically downscaled data from the North American Regional Climate Change Assessment Program (NARCCAP; Mearns et al. 2009, 2012) project, similar increases in HCW environments were found across a large portion of the U.S. (Gensini et al. 2013). These studies agree that projected increases in HCW activity is largely a function of increases in convective available potential energy (CAPE), associated with augmentation in future period near-surface specific humidity values.

While an environmental approach has been commonly used to this point, results herein give researchers first glances into storm-scale responses to anthropogenically altered synoptic convective environments. High resolution dynamical downscaling for purposes of resolving HCW has yet to be performed for future period GCM scenarios, prior to the work presented here. Building from a previous historical scenario used in Gensini and Mote (2014), this study presents the first results of potential future changes in U.S. severe weather activity using synthetic reports derived from high-resolution dynamical downscaling.

4.3 Methodology

a. Model information

i. <u>Global climate model</u>

The CCSM3 is a coupled global climate spectral model consisting of atmosphere, land surface, sea-ice, and ocean components. CCSM3 uses an 85-wavenumber triangular truncation grid spacing (approximately 1.4° resolution at the equator) in the horizontal, and has 26 levels in the vertical (Collins et al. 2006). Available output includes a control run (no changes in external climate forcing), a 20th Century simulation (containing the observed changes of greenhouse gases, sulphate aerosols, volcanic aerosols, and solar irradiance from the 20th Century), and 21st Century scenarios (containing estimated changes in greenhouse gas and aerosol concentrations).

For the study presented here, two 11-year epochs were compared to evaluate potential changes in future HCW activity. The historical (1980–1990) and future (2080–2090) downscaled periods use data based on a simulation initialized in 1870 and simulated through the end of the 21st Century. This simulation utilizes data based on the special report for emissions scenario (SRES) A2 scenario, characterized by, “a very heterogeneous world with continuously increasing global population and regionally oriented economic growth that is more fragmented and slower than in other storylines" (Nakicenovic et al. 2000). This aggressive, but not worse case, scenario is chosen in an effort to assess potential changes in HCW to atmospheric responses associated with increasing anthropogenic carbon emissions.

ii. Regional climate model

Regional Climate Model (RCM) configurations were chosen following previous research downscaling CCSM3 historical fields (Gensini and Mote 2014). Thus, we again use the non-hydrostatic advanced research core of the Weather Research and Forecasting (WRF-ARW) model (Skamarock et al. 2008). Output fields from the CCSM3 at 0000 UTC on 1 March of each year are used to initialize the RCM. Integrations are then performed over a three-month period, providing CCSM3 boundary conditions to the RCM every six hours, while the first six hours of the simulation are discarded to account for model spin-up (Skamarock 2004). This longer integration time is desirable as it supports better representation of influences associated with longer-memory processes, such as soil moisture, known to influence surface fluxes in the climate system (Gensini and Mote 2014). RCM diagnostics, and parameterization schemes (Table 3.1) are based on previous WRF-model simulations of HCW in the United States (e.g., Weisman et al. 2008; Kain et al. 2006; Trapp et al. 2011; Robinson et al. 2013; Gensini and Mote 2014).

The model-based proxy used in this research follows that used in Trapp et al. (2011) and Gensini and Mote (2014), using hourly thresholds of updraft helicity (UH) and simulated composite radar reflectivity (Z) as described by Kain et al. (2008). Specifically, a synthetic HCW event occurs when an hourly RCM grid point contains UH values $\geq 60\ m^2 \cdot s^{-2}$ juxtaposed with Z values $\geq$ 40 dBZ (Fig. 4.1). This threshold UH/Z pair has been shown to best approximate HCW activity in the U.S. during a 1980–1990 historical simulation using CCSM3 (Gensini and Mote 2014). An animation of modeled composite reflectivity and HCW reports helps visualize this process (Fig. 4.2).

Synthetic HCW reports are spatially aggregated to a 50 km grid and summed to create two epoch (1980–1990; 2080–2090) climatologies for the months March–May. Based on observed HCW reports during the historical period, bias correction is applied to both historical and future periods. This is a desirable procedure when applying a downscaling framework to GCM data (Christensen et al. 2008). Finally, statistical significance was tested using the Mann-Whitney *U* test for the medians at the 95% confidence level.

b. Downscaling domain

Dynamical downscaling is applied to the same study region used in Gensini and Mote (2014), and contains all points in the U.S. east of the Continental Divide. This domain contains 490,000 grid points in a Lambert Conformal Conic projection, equating to between 4–4.25 km grid spacing depending on latitude. Given the central Great Plains has the highest annual frequency of HCW (Brooks et al. 2003b), it is hypothesized that potential changes in HCW activity will be most prominent in this high frequency region. Changes in HCW distributions may occur outside of this region due to a changing climate, but this study is not able to address such scenarios.

4.4 Results

We begin with modeled proxy reports of HCW. Raw counts of synthetic HCW reveal a 27% increase in future period events. Stratifying by month, most of this increase is found in

March (increases approaching 70%), whereas April shows a slight increase (15%) and May remains virtually unchanged (Fig. 4.3). This does not necessarily imply a shift in the temporal climax of HCW; rather, a greater probability of such events earlier in the annual cycle, and thus an increase in the overall frequency is depicted. Examinations of seasonal HCW changes suggest a future increase in the variability of peak-season events, indicated by a “fanning” of the cumulative frequency through the months examined (Fig. 4.4). This is further shown by nearly a doubling in standard deviation (778 to 1433 synthetic reports) from the historical to future epoch and an increase in the coefficient of variation from .29 to .43 respectively. From an environmental ingredients perspective, this variability is primarily a function of the polar jet stream location juxtapositioning with CAPE. Consequently, increases in peak-seasonal HCW variability suggest that synoptic scale controls, such as jet-stream location, are likely to be different in a future climate. This variability is broadly consistent with recent research relating arctic amplification with mid-latitude weather extremes (Francis and Vavrus 2012; Petoukhov et al. 2013; Screen and Simmonds 2013) due to a decline in Arctic sea-ice cover (Francis et al. 2009).

Similar to Gensini and Mote (2014), severe weather reports from the Storm Prediction Center’s severe weather database (Schaefer and Edwards 1999) were used to provide a simple bias correction factor to historical and future period proxy reports (Fig. 4.3), a necessary procedure when downscaling GCM data (Christensen et al. 2008). These corrections do not necessarily alter the change across epochs; they instead adjust the magnitudes of change into a context consistent with historical observed HCW reports. It should be noted that observed HCW reports, in particular, are a challenge to bias correct due to the nature of the reporting process.

Spatially, the largest increases in future period HCW are depicted across the Middle Mississippi, Lower Mississippi, Ohio, and Tennessee River valleys (Fig. 4.5). In these regions, results indicate increases of 2–8+ HCW reports per season on average. Some isolated points in and close to these regions depicted a statistically significant decrease. For example, a relative cluster of notable decrease in HCW activity is shown across Florida in this simulation. However, these statistically significant decreases (23 grid cells) are largely outweighed by roughly 6.5 times more grid cells that illustrated a statistically significant increase across the domain. Diurnally, the largest HCW frequency increases were found from 2100–0500 UTC (Fig. 4.6), which coincides with the typical maximum in HCW across the U.S. (Kelly et al. 1978).

Next, we focus on modeled composite reflectivity. While not a hazard itself, it can be used as a surrogate to gauge updraft and storm intensity. This is not a new process as meteorologists routinely use RADAR reflectivity to operationally imply storm intensity (Lemon 1977), objectively track thunderstorm echoes (Dixon and Wiener 1993; Johnson et al. 1998; Han et al. 2009) and classify potential hail size (Witt et al. 1998). The composite reflectivity value of 50 dBZ was chosen due its documented ability to discriminate for severe hail events when used with melting layer height (Donavon and Jungbluth 2007) and was again aggregated to a 50 km grid for comparison.

Significant increases in future period 50 dBZ values were found during the months of March and April, while May showed no significant change (Fig. 4.7). Most of the increases in March are identified in the southeast Great Plains through the southern and southeastern U.S., northward through the Mississippi and Ohio River valleys (Fig. 4.8). By April, a majority of the increase has shifted northward into the Ohio River valley, consistent with the northward climatological shift of severe weather as the season progresses (Brooks et al. 2003a; Gensini and Ashley 2011). Results herein suggest that late-century, early-season thunderstorms will be of greater intensity/frequency, likely a function of robust increases in CAPE and near-surface specific humidity depicted by several GCMs and RCMs (Del Genio et al. 2007; Trapp et al. 2007a; Trapp et al. 2009; Van Klooster and Roebber 2009; Diffenbaugh et al. 2013; Gensini et al. 2013).

We conclude with a discussion of environmental control parameters known to favor deep convection, specifically CAPE and 0–6-km bulk wind difference (BWD). An average increase of 236% is shown across all months of future period average frequencies of grid points with CAPE exceeding 2000 J kg^{-1} (Fig. 4.9). This robust increase in CAPE is consistent with recent studies examining ensembles of GCM output for convective purposes (Del Genio et al. 2007; Trapp et al. 2007a; Trapp et al. 2009; Diffenbaugh et al. 2013) during March–May. In addition, the product of CAPE and 0–6 km BWD has been widely used to discriminate potential significant severe weather environments for climatological purposes due to its ease of calculation (Brooks et al. 2003b). The calculation used herein follows the proximity Craven-Brooks composite methodology of Gensini and Ashley (2011), restricting events to CAPE values exceeding 100 J kg^{-1}. Similar to the synthetic HCW report distribution, the number of grid points with a product of CAPE and 0–6 km BWD exceeding 20,000 show a significant increase in March and April, with no meaningful change in May (Fig. 4.10). There are only a few distinguishable spatial shifts in the distribution of CAPE (Fig. 4.11a, Fig 4.11b) and significant severe weather environments (Fig. 4.11c, 4.11d) over the epochs examined. Rather, an overall general increase is noted from the historical to the future period.

These results are corroborated by the agreement between large-scale instability/shear parameters and modeled HCW reports. The product of CAPE and 0–6 km BWD exceeding 20,000 explains 81% of the variability associated with HCW reports over the historical and future periods examined (Fig. 4.12). This supports recent research depicting the ability of high-resolution dynamical downscaling to replicate large-scale conditions forcing interannual and sub-seasonal variability in HCW activity (Gensini and Mote 2014). This result is significant, as one of the main weaknesses in environmental analysis is the inability to discuss changes on the storm-scale. It appears, however, that environmental analysis is an efficient predictor of HCW occurrence across the domain and study periods analyzed.

4.5 Summary and conclusions

This study is the first to use dynamical downscaling for purposes of examining potential changes in hazardous convective weather under a business-as-usual emissions scenario. Using data from the Community Climate System Model version 3 downscaled by the Weather Research and Forecasting model, an artificial report proxy consisting of downscaled 2–5 km updraft helicity and composite reflectivity was used to simulate occurrences of tornadoes, damaging wind gusts, and large hail at hourly intervals over the eastern two-thirds of the U.S. during a historical (1980–1990) and future (2080–2090) period. Using observed severe weather reports to bias correct, a significant future increase in hazardous convective weather frequency and variability is revealed, especially during the afternoon hours during the months of March and April. The largest increase in future severe weather events is found across the Middle Mississippi, Lower Mississippi, Ohio, and Tennessee River valleys, with an overall frequency increase of 27%. Thus, this region would be poised to receive an additional 2–8+ severe weather reports per 50 km grid box during March–May. In addition, modeled composite reflectivity, a surrogate for storm intensity, is shown to significantly increase across a large portion of the analyzed domain, again specifically during the months of March and April.

These results, along with a quickly growing body of literature, suggest that late-century thunderstorms will be of greater intensity/frequency, likely a function of robust increases in CAPE and near-surface specific humidity depicted by several GCMs and RCMs (Del Genio et al. 2007; Trapp et al. 2007a; Trapp et al. 2009; Van Klooster and Roebber 2009; Diffenbaugh et al. 2013; Gensini et al. 2013). These previous studies are solidified by results presented herein, as large-scale environmental controls such as CAPE and deep-layer wind shear are shown to explain over 80% of the variability in modeled severe weather reports.

The main obstacle for this particular study is dataset length. Due to the computationally expensive nature of dynamical downscaling, it was only feasible to examine two ten-year periods. Ultimately, a multi-model ensemble approach over a period of 30 years would be most desirable for this type of study, and accordingly, we are limited with our ability to make definitive conclusions regarding severe weather in the late 21st Century. However, this study expands and existing body of literature indicating the potential for future increases in severe convective weather (Del Genio et al. 2007; Trapp et al. 2007a; Trapp et al. 2009; Van Klooster and Roebber 2009; Diffenbaugh et al. 2013; Gensini et al. 2013). Overall, dynamical downscaling for purposes of resolving mesoscale phenomenon, such as severe local storms, continues to emerge as an admirable methodological technique for climate change assessments.

4.6 References

Alexander, L., and Coauthors, 2013: Climate Change 2013: The Physical Science Basis. Contribution of Working Group I to the Fifth Assessment Report of the Intergovernmental Panel on Climate Change.

Alley, R., and Coauthors, 2007: Summary for policymakers. *Climate Change 2007: The Physical Science Basis*, S. Solomon, and Coauthors, Eds., Cambridge University Press, 1–18.

Bouwer, L. M., 2011: Have disaster losses increased due to anthropogenic climate change? *Bulletin of the American Meteorological Society*, **92,** 39–46.

Brooks, H. E., 2013: Severe thunderstorms and climate change. *Atmospheric Research*, **123,** 129–138.

Brooks, H. E., and C. A. Doswell III, 2001: Normalized damage from major tornadoes in the United States: 1890–1999. *Weather and Forecasting*, **16,** 168–176.

——, 2002: Deaths in the 3 May 1999 Oklahoma City tornado from a historical perspective. *Weather and Forecasting*, **17,** 354–361.

Brooks, H. E., C. A. Doswell III, and M. P. Kay, 2003a: Climatological estimates of local daily tornado probability for the United States. *Weather and Forecasting*, **18,** 626–640.

Brooks, H. E., J. W. Lee, and J. P. Craven, 2003b: The spatial distribution of severe thunderstorm and tornado environments from global reanalysis data. *Atmospheric Research*, **67–68,** 73–94.

Changnon, S. A., 2001: Damaging thunderstorm activity in the United States. *Bulletin of the American Meteorological Society*, **82,** 597–608.

——, 2009: Tornado losses in the United States. *Natural Hazards Review*, **10,** 145–150.

Christensen, J. H., F. Boberg, O. B. Christensen, and P. Lucas-Picher, 2008: On the need for bias correction of regional climate change projections of temperature and precipitation. *Geophysical Research Letters*, **35,** L20709.

Del Genio, A. D., M.-S. Yao, and J. Jonas, 2007: Will moist convection be stronger in a warmer climate? *Geophysical Research Letters*, **34,** L16703.

Diffenbaugh, N. S., M. Scherer, and R. J. Trapp, 2013: Robust increases in severe thunderstorm environments in response to greenhouse forcing. *Proceedings of the National Academy of Sciences*, **110,** 16361–16366.

Dixon, M., and G. Wiener, 1993: TITAN: Thunderstorm identification, tracking, analysis, and nowcasting-A radar-based methodology. *Journal of Atmospheric and Oceanic Technology*, **10,** 785–797.

Donavon, R. A., and K. A. Jungbluth, 2007: Evaluation of a technique for radar identification of large hail across the Upper Midwest and Central Plains of the United States. *Weather and Forecasting*, **22,** 244–254.

Doswell III, C. A., 2007: Small sample size and data quality issues illustrated using tornado occurrence data. *Electronic Journal of Severe Storms Meteorology*, **2,** 1–16.

Doswell III, C. A., and D. W. Burgess, 1988: On some issues of United States tornado climatology. *Monthly Weather Review*, **116,** 495–501.

Francis, J. A., and S. J. Vavrus, 2012: Evidence linking Arctic amplification to extreme weather in mid-latitudes. *Geophysical Research Letters,* **39,** L06801.

Francis, J. A., W. Chan, D. J. Leathers, J. R. Miller, and D. E. Veron, 2009: Winter Northern Hemisphere weather patterns remember summer Arctic sea-ice extent. *Geophysical Research Letters,* **36,** L07503.

Gensini, V. A., and W. S. Ashley, 2011: Climatology of potentially severe convective environments from the North American Regional Reanalysis. *Electronic Journal of Severe Storms Meteorology,* **6,** 1–40.

Gensini, V. A., C. Ramseyer, and T. L. Mote, 2014: Future convective environments using NARCCAP. *International Journal of Climatology*, **34,** 1699–1705.

Grazulis, T. P., 1993: *Significant tornadoes: 1680–1991.* Environmental Films, 1326 pp.

Han, L., S. Fu, L. Zhao, Y. Zheng, H. Wang, and Y. Lin, 2009: 3D convective storm identification, tracking, and forecasting-An enhanced TITAN algorithm. *Journal of Atmospheric and Oceanic Technology*, **26,** 719–732.

Johnson, J., P. L. MacKeen, A. Witt, E. D. W. Mitchell, G. J. Stumpf, M. D. Eilts, and K. W. Thomas, 1998: The storm cell identification and tracking algorithm: An enhanced WSR-88D algorithm. *Weather and Forecasting*, **13,** 263–276.

Kain, J. S., and Coauthors, 2008: Some practical considerations regarding horizontal resolution in the first generation of operational convection-allowing NWP. *Weather and Forecasting*, **23,** 931–952.

Karl, T. R., J. M. Melillo, and T. C. Peterson, 2009: *Global climate change impacts in the United States.* Cambridge University Press.

Kelly, D. L., J. T. Schaefer, R. P. McNulty, C. A. Doswell III, and R. F. Abbey Jr., 1978: An augmented tornado climatology. *Monthly Weather Review*, **106,** 1172–1183.

Mearns, L. O., W. Gutowski, R. Jones, R. Leung, S. McGinnis, A. Nunes, and Y. Qian, 2009: A regional climate change assessment program for North America. *Eos, Transactions American Geophysical Union,* **90,** 311.

Mearns, L. O., and Coauthors, 2012: The North American regional climate change assessment program: overview of phase I results. *Bulletin of the American Meteorological Society*, **93,** 1337–1362.

Nakicenovic, N., and Coauthors, 2000: Special report on emissions scenarios: a special report of Working Group III of the Intergovernmental Panel on Climate Change, 599 pp.

Petoukhov, V., S. Rahmstorf, S. Petri, and H. J. Schellnhuber, 2013: Quasiresonant amplification of planetary waves and recent Northern Hemisphere weather extremes. *Proceedings of the National Academy of Sciences,* **110,** 5336–5341.

Robinson, E. D., R. J. Trapp, and M. E. Baldwin, 2013: The geospatial and temporal distributions of severe thunderstorms from high-resolution dynamical downscaling. *Journal of Applied Meteorology and Climatology*, **52,** 2147–2161.

Schaefer, J. T., and R. Edwards, 1999: The SPC tornado/severe thunderstorm database. *11th Conference on Applied Climatology*, American Meteorological Society, 603–606

Screen, J. A., and I. Simmonds, 2013: Exploring links between Arctic amplification and mid-latitude weather. *Geophysical Research Letters*, **40,** 959–964.

Skamarock, W. C., 2004: Evaluating mesoscale NWP models using kinetic energy spectra. *Monthly Weather Review*, **132,** 3019–3032.

Skamarock, W. C., J. B. Klemp, J. Dudhia, D. O. Gill, D. M. Barker, W. Wang, and J. G. Powers, 2008: A description of the Advanced Research WRF version 3. NCAR Tech. Note NCAR/TN-475+STR, 113pp.

Trapp, R. J., N. S. Diffenbaugh, and A. Gluhovsky, 2009: Transient response of severe thunderstorm forcing to elevated greenhouse gas concentrations. *Geophysical Research Letters*, **36,** L01703.

Trapp, R. J., E. Robinson, M. Baldwin, N. Diffenbaugh, and B. Schwedler, 2011: Regional climate of hazardous convective weather through high-resolution dynamical downscaling. *Climate Dynamics*, **37,** 677–688.

Trapp, R. J., N. S. Diffenbaugh, H. E. Brooks, M. E. Baldwin, E. D. Robinson, and J. S. Pal, 2007a: Changes in severe thunderstorm environment frequency during the 21st century caused by anthropogenically enhanced global radiative forcing. *Proceedings of the National Academy of Sciences*, **104,** 19719–19723.

Van Klooster, S. L., and P. J. Roebber, 2009: Surface-based convective potential in the contiguous United States in a business-as-usual future climate. *Journal of Climate*, **22,** 3317–3330.

Verbout, S. M., H. E. Brooks, L. M. Leslie, and D. M. Schultz, 2006: Evolution of the U.S. tornado database: 1954–2003. *Weather and Forecasting*, **21,** 86–93.

Weisman, M. L., W. C. Skamarock, and J. B. Klemp, 1997: The resolution dependence of explicitly modeled convective systems. *Monthly Weather Review*, **125,** 527–548.

Witt, A., M. D. Eilts, G. J. Stumpf, J. Johnson, E. D. W. Mitchell, and K. W. Thomas, 1998: An enhanced hail detection algorithm for the WSR-88D. *Weather and Forecasting*, **13,** 286–303.

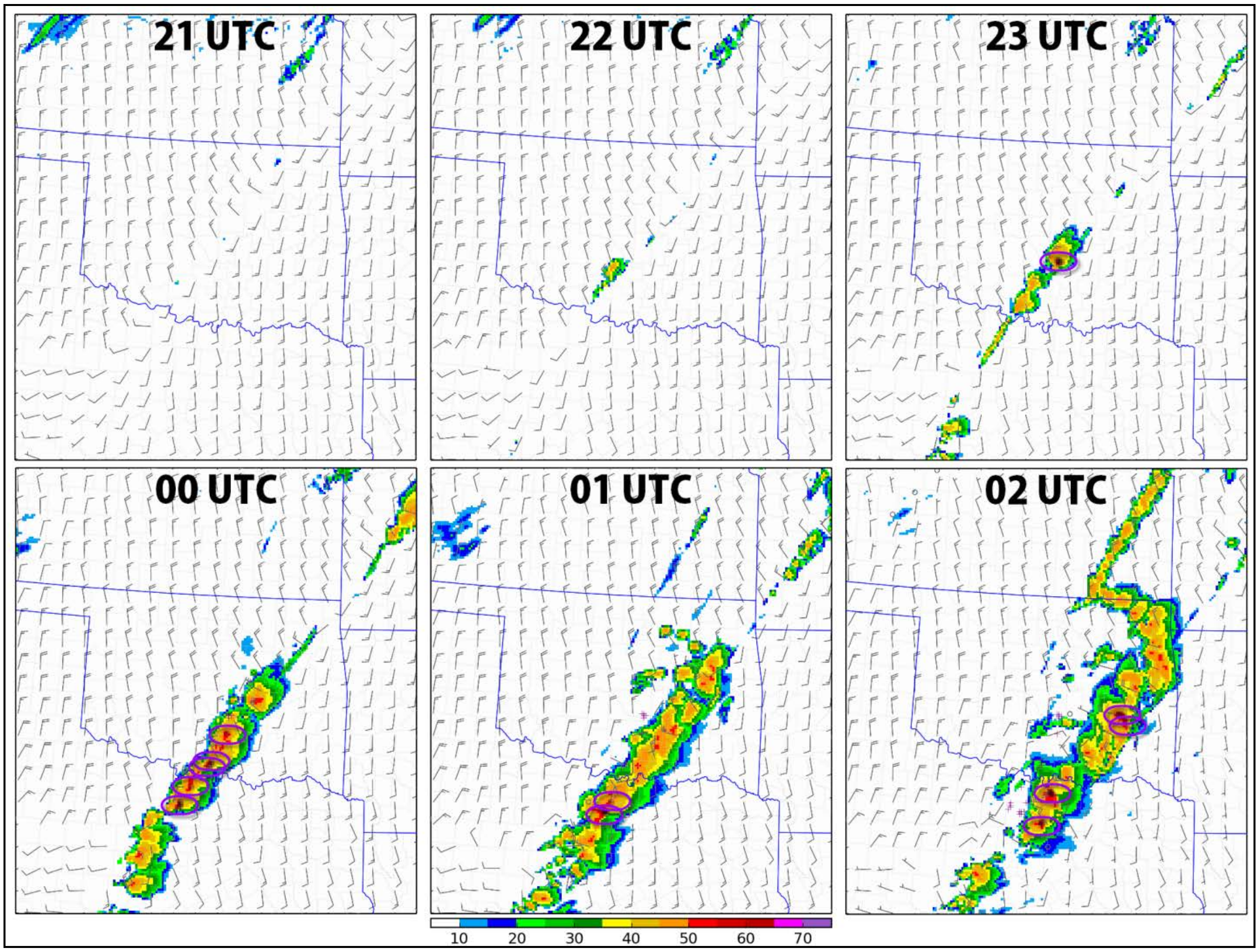

Fig. 4.1. Progression of composite reflectivity (dBZ; fill) and 10-m wind (knots) from 2100 UTC 2 May 2090 to 0200 UTC 3 May 2090. Purple ovals highlight areas of proxy-based severe convective weather reports.

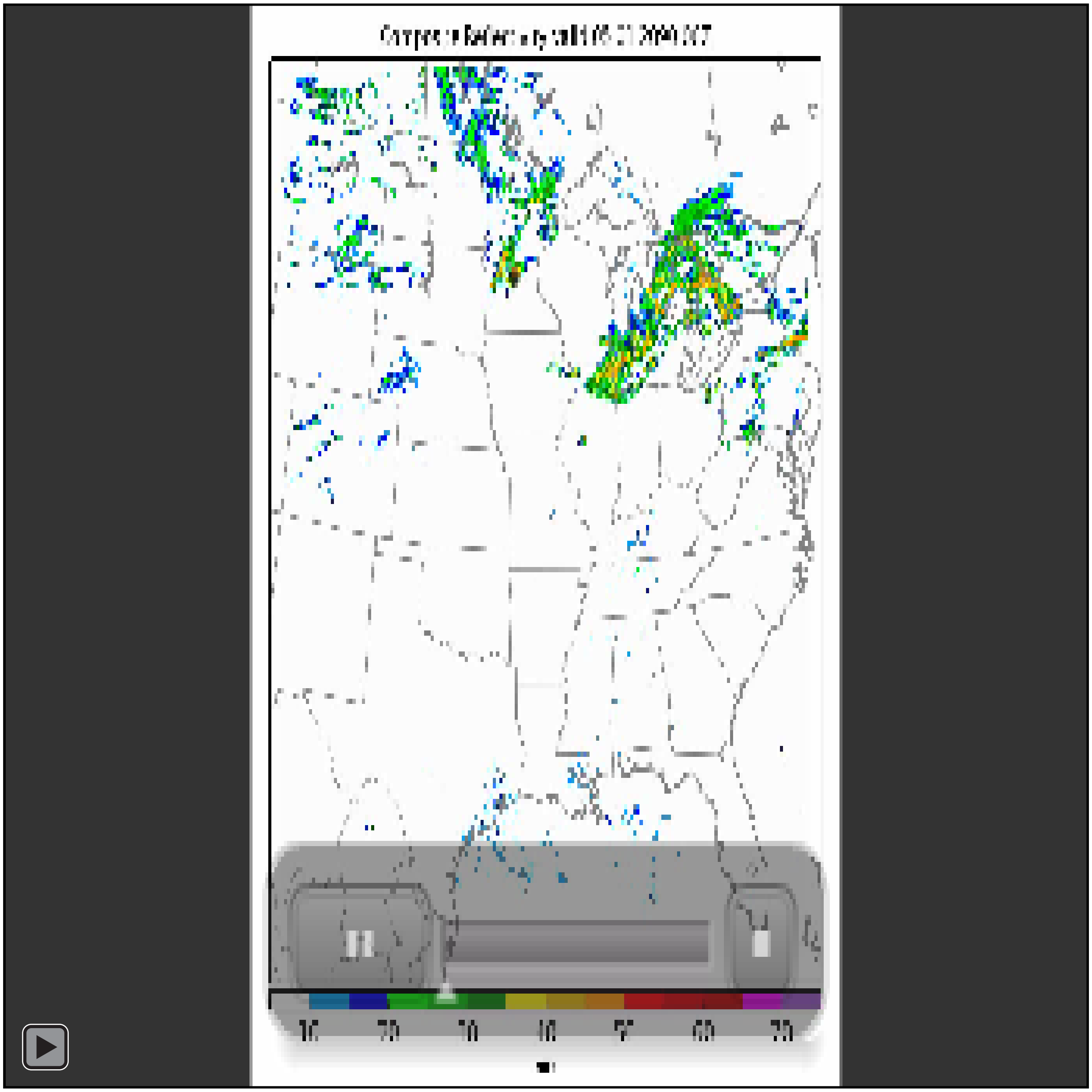

Fig. 4.2. Animation of modeled composite reflectivity (dBZ) for the period 0000 UTC 1 May 1990–0500 UTC 3 May 2090. Purple '+' symbols indicate locations of accumulating HCW reports. (*Click image to play animation on electronic device)*

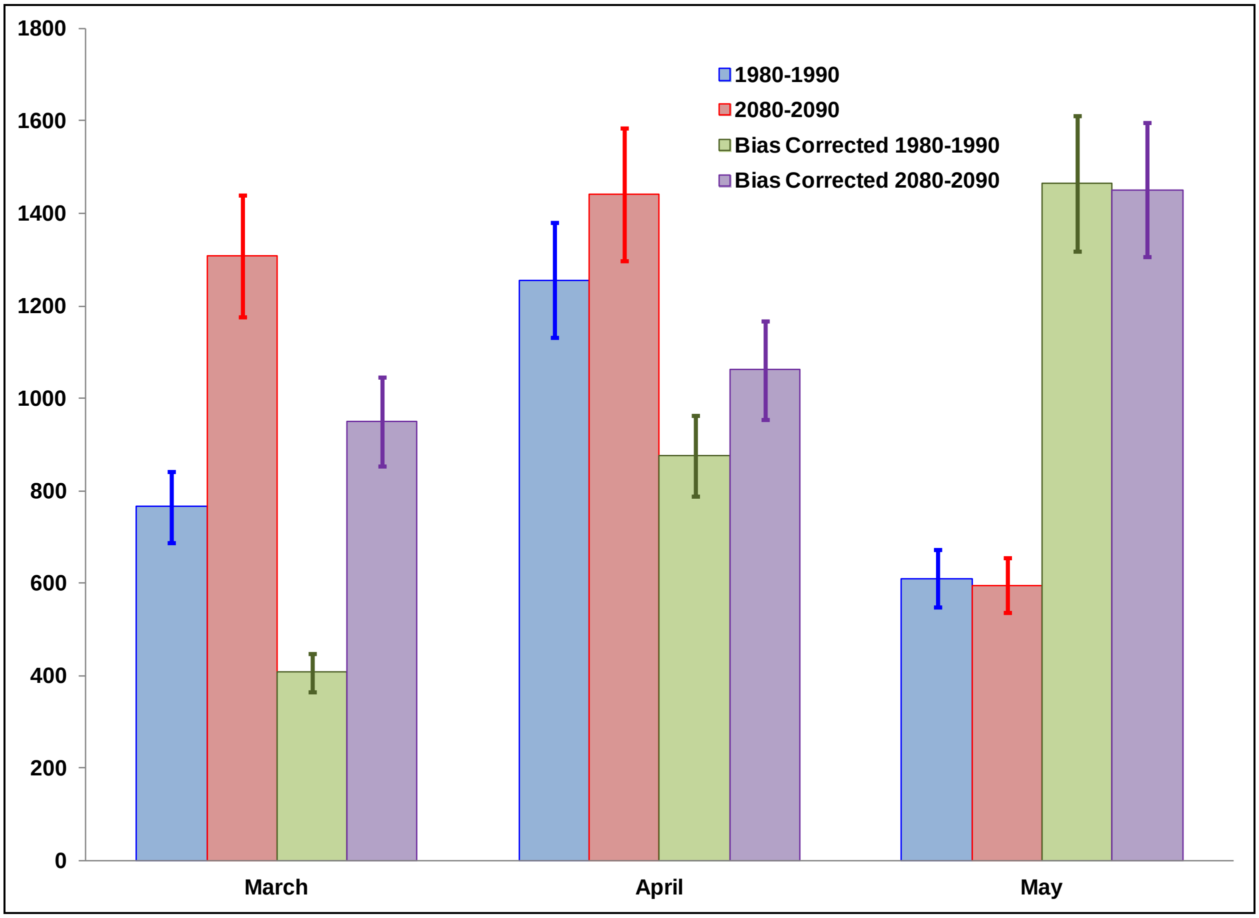

Fig. 4.3. Average monthly comparisons of raw and bias corrected synthetic severe weather reports. Error bars indicate the standard error.

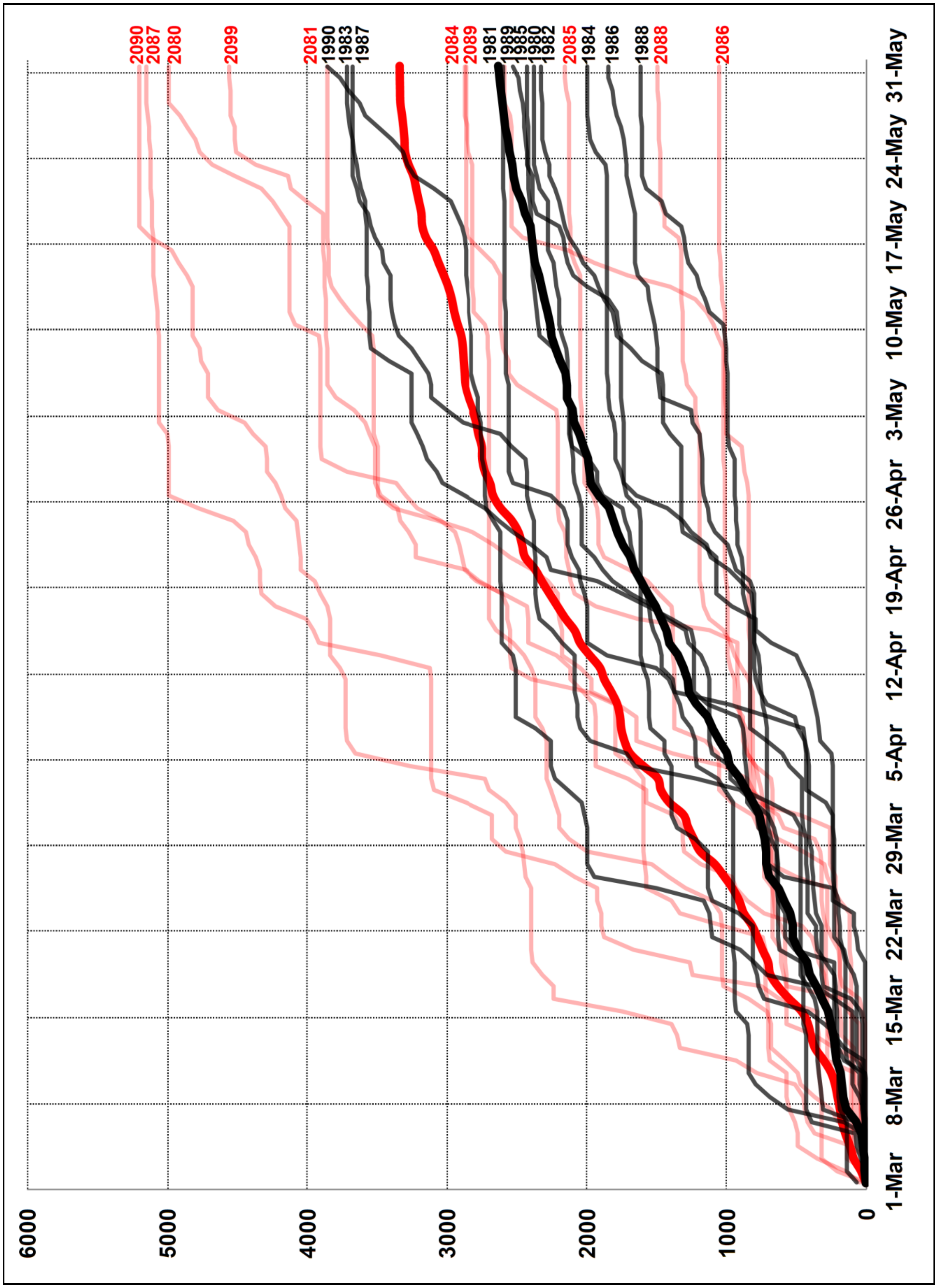

Fig. 4.4. Cumulative frequency of historical (black) and future (red) period synthetic hazardous convective weather reports. Thick black and red lines indicate averages for their respective period.

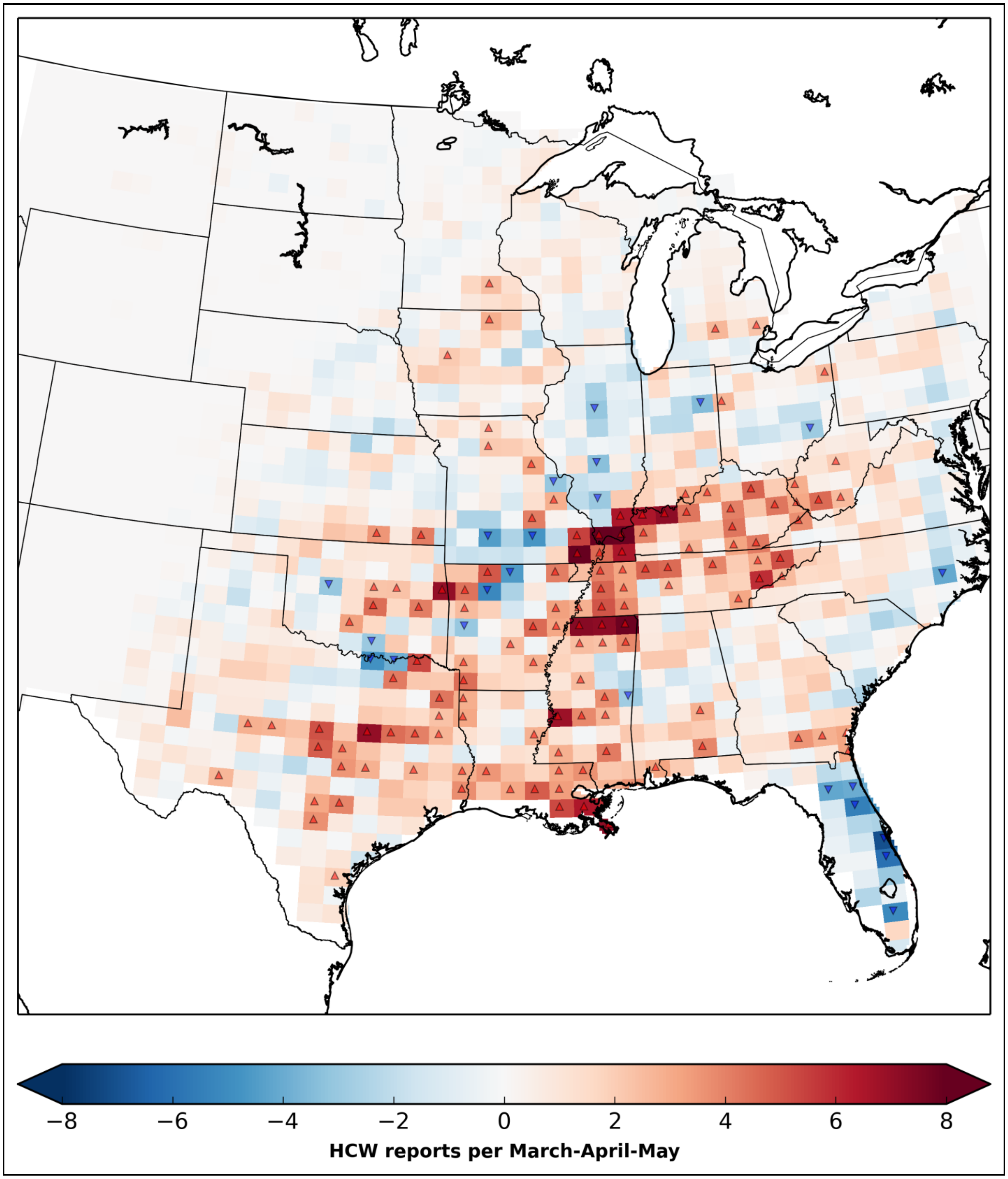

Fig. 4.5. Average difference between 2080–2090 and 1980–1990 modeled severe weather reports. Red (blue) grid cells indicate a positive (negative) change in the average number of modeled reports per season. Triangles indicate statistical significance at the 95% confidence level.

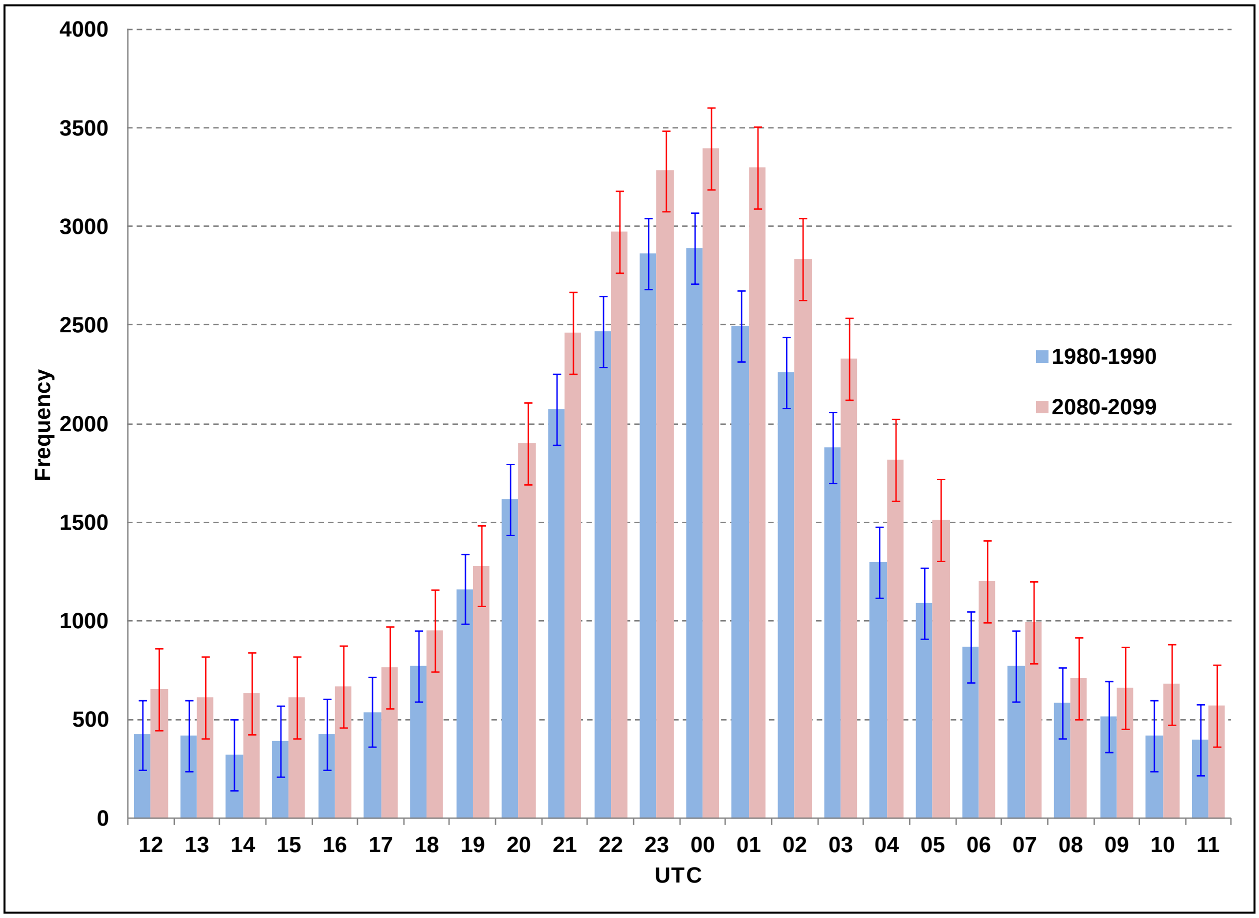

Fig. 4.6. Diurnal frequency comparison of historical (blue) and future (red) severe weather reports. Error bars indicate the standard error.

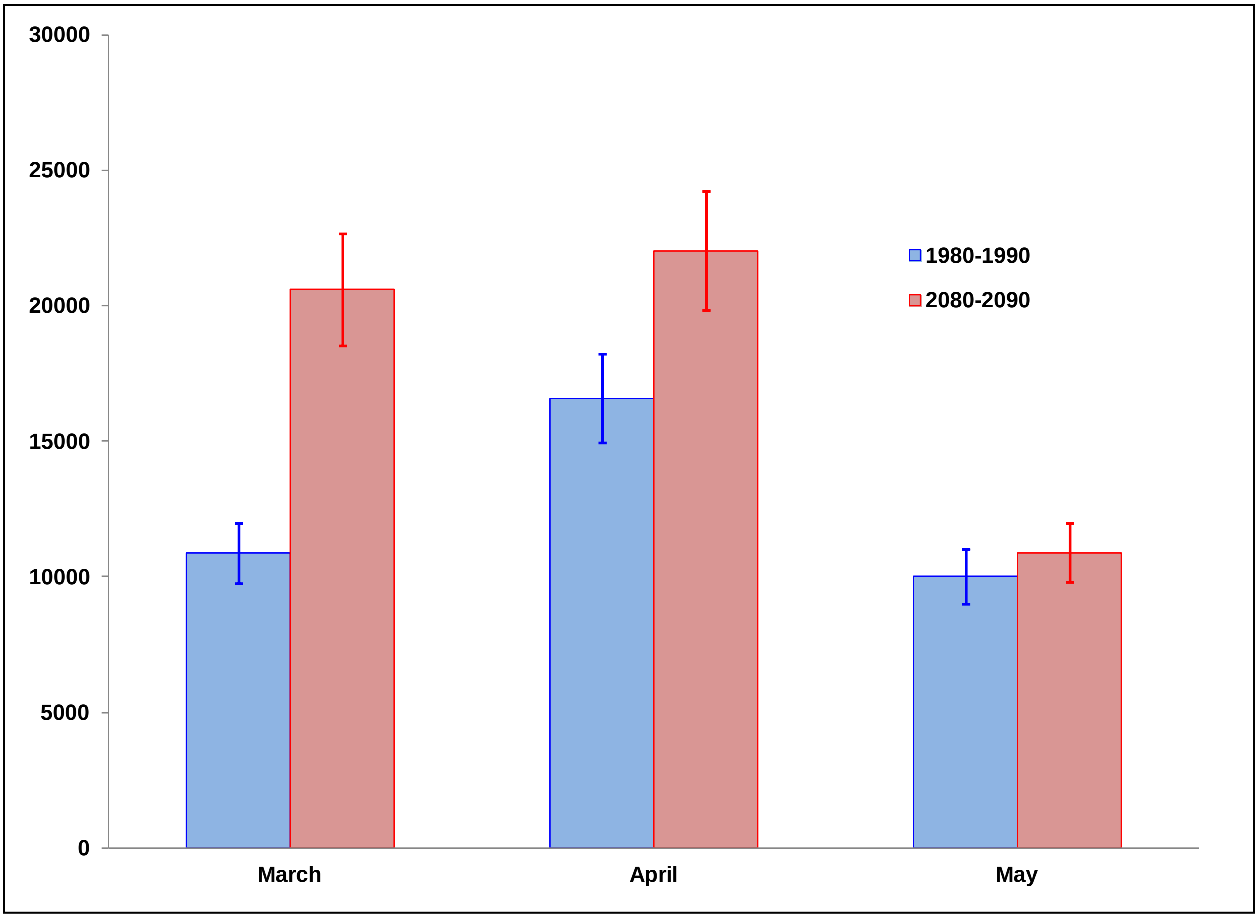

Fig. 4.7. Average monthly comparisons of historical and future period grid cell counts with modeled composite reflectivity (Z) ≥ 50 dBZ. Error bars indicate the standard error.

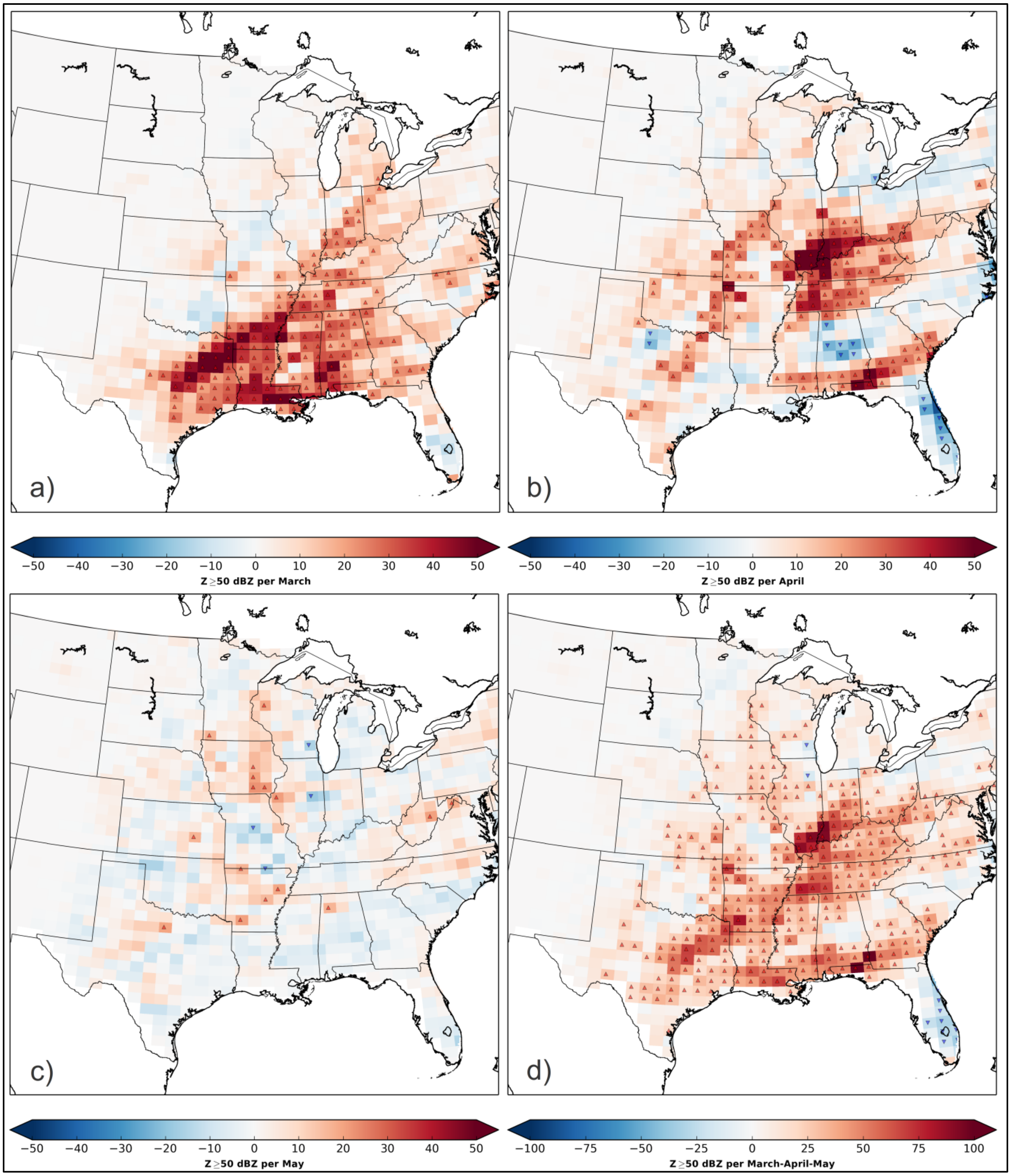

Fig. 4.8. Average difference between 2080–2090 and 1980–1990 modeled composite reflectivity values ≥ 50 dBZ for March (a), April (b), May (c), and March–May (d). Red (blue) grid cells indicate a positive (negative) change in the average number of modeled reports per season. Triangles indicate statistical significance at the 95% confidence level.

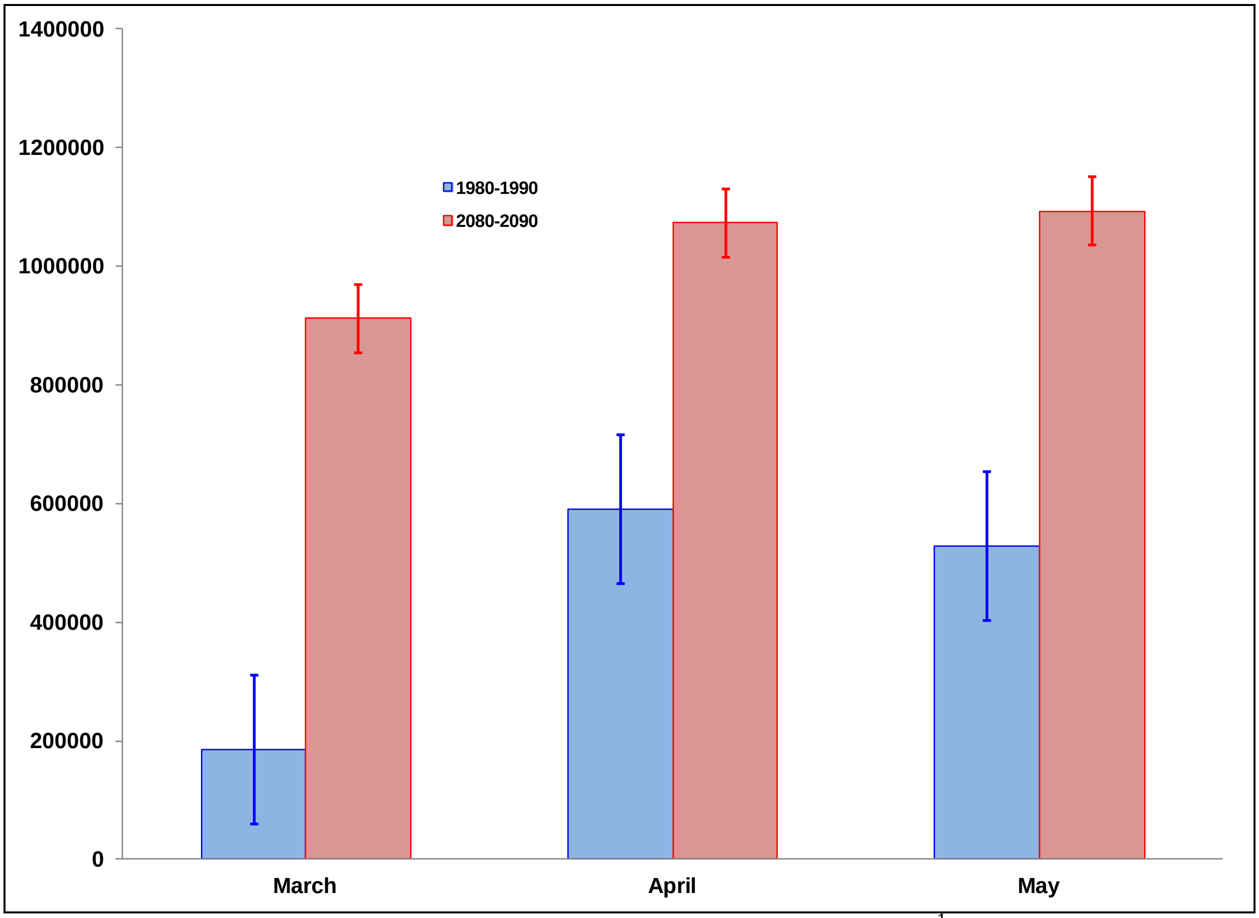

Fig. 4.9. As in Fig. 4.6, but for grid cell counts with CAPE ≥ 2,000 J kg^{-1}.

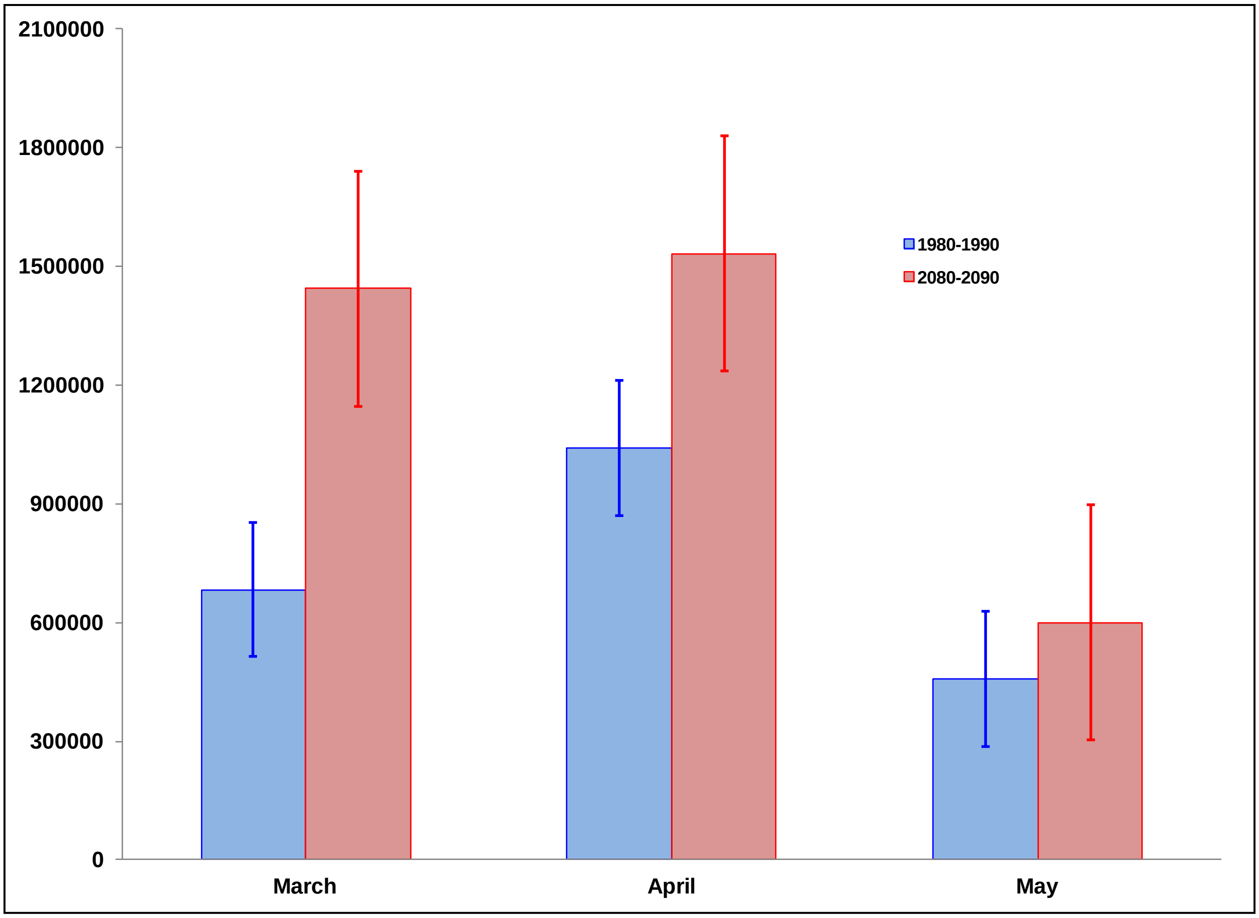

Fig. 4.10. As in Fig. 4.6, but for grid cell counts with CAPE × 0–6-km BWD ≥ 20,000 with CAPE ≥ 100 J kg^{-1}.

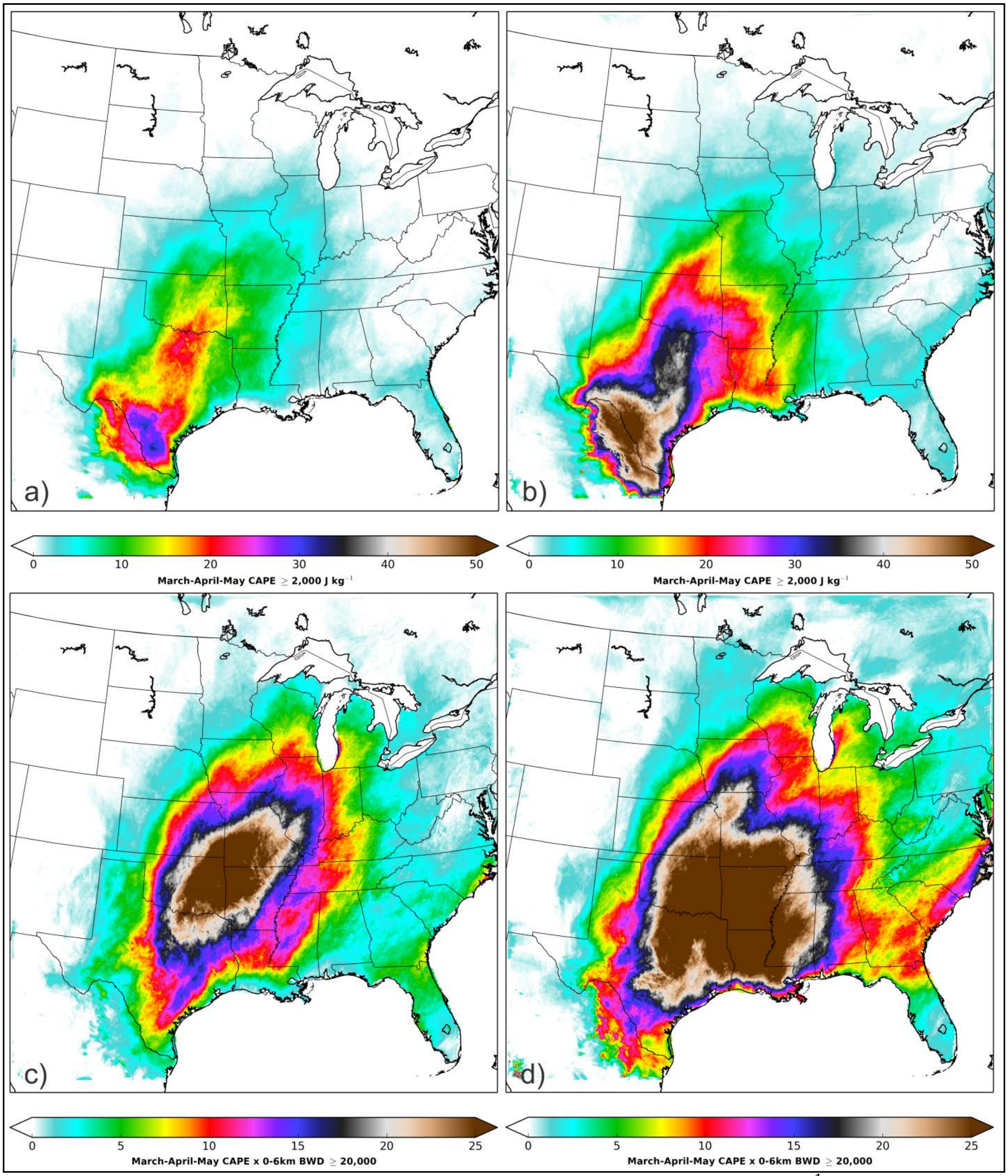

Fig. 4.11. Average frequency of March–May historical (a) CAPE ≥ 2,000 J kg^{-1} and (b) the product of CAPE and 0–6-km BWD exceeding 20,000. Panels (c) and (d) represent the future period respectively. In the case of CAPE × 0–6-km BWD, CAPE is constrained to only evaluate events with ≥100 J kg^{-1}.

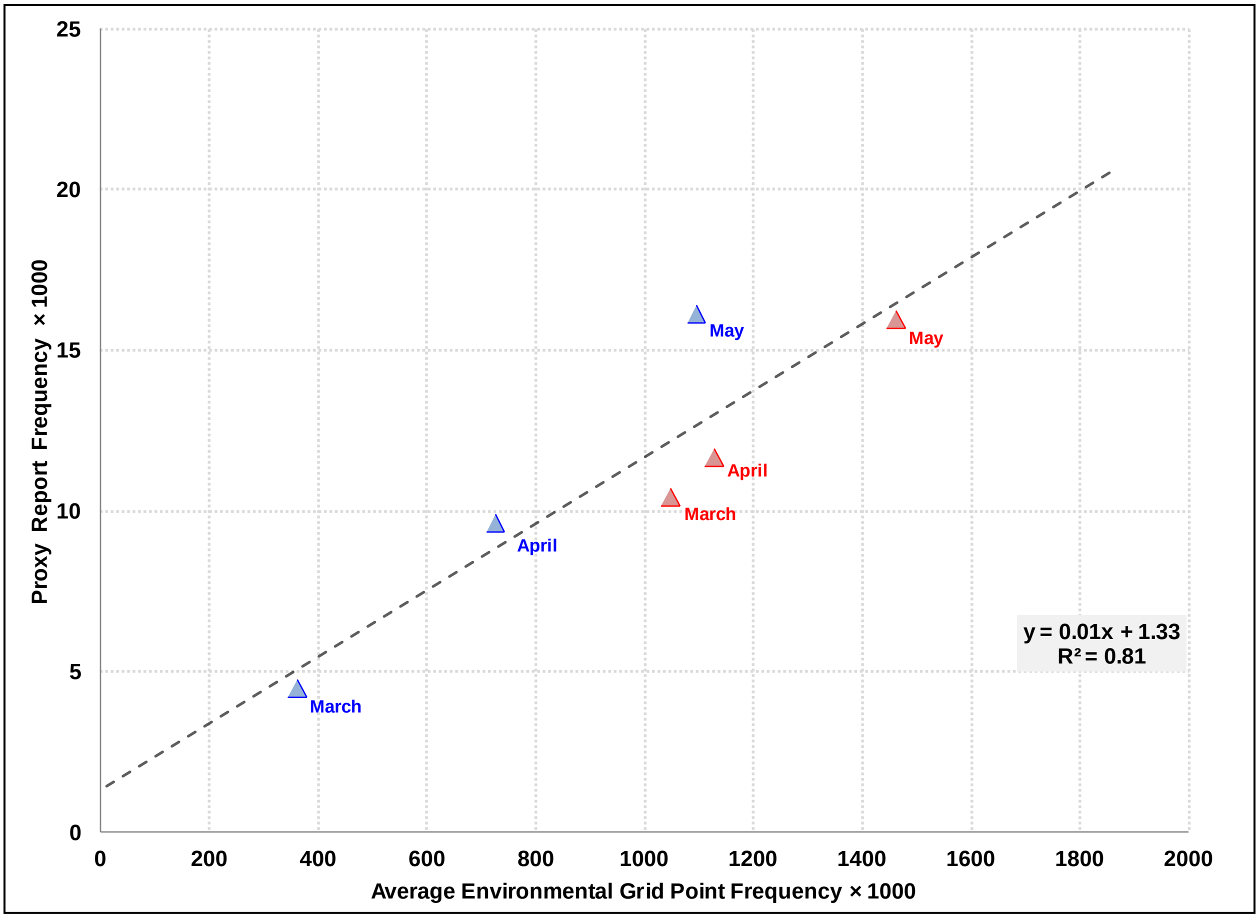

Fig. 4.12. Bias-corrected linear correlation between average grid point frequency with CAPE × 0–6-km BWD ≥ 20,000 and average synthetic report frequency by month. Blue triangles correspond to the period 1980–1990, while red triangles correspond to the period 2080–2090. The least-squares regression equation and coefficient of determination are displayed in the gray box.

CHAPTER 5

SUMMARY AND CONCLUSIONS

5.1 Overview

Thunderstorm wind gusts, large hail, and tornadoes (otherwise known as hazardous convective weather [HCW]) cause billions of dollars of economic loss and several fatalities across the U.S. each year. Despite their socio-economic impact, climate change summaries (e.g., reports from Intergovernmental Panel on Climate Change [IPCC] and the United States Climate Change Science Program [CCSP]) have avoided definitive conclusions regarding potential changes to their frequency and intensity in a future, anthropogenically altered, climate (Brooks 2013). Such climate assessments have expressed great uncertainty in late 21st Century HCW activity, owing to the poor observational record of severe weather events and inadequacies in grid spacing resolution of current Global/Regional Climate Models (RCMs/GCMs). Interestingly, despite these conclusions (or lack thereof), much speculation regarding future HCW (especially tornadoes) has percolated into the popular press.

To date, most of the scientific effort to understand future distributions of HCW has been limited to utilizing GCM or RCM output to analyze the large-scale convective environment that is known to favor severe convection. These studies indicate that an increase in HCW activity is likely in the future, due in large part to increases in convective available potential energy (CAPE; Del Genio et al. 2007; Trapp et al. 2007a; Trapp et al. 2009; Van Klooster and Roebber 2009;

Brooks 2013; Diffenbaugh et al. 2013; Gensini et al. 2013). However, novel research by Trapp et al. (2011) explored the use of high-resolution dynamical downscaling to advance methodological techniques for examining storm-scale processes from coarse-resolution initial and boundary conditions. Trapp et al. (2011) were successful in simulating accurate representations of HCW distribution, and further research confirmed its potential utility (Robinson et al. 2013; Gensini and Mote 2014).

The overall goals of this dissertation were to: 1) illustrate the relative utility of a reanalysis dataset to approximate convective environments (Chapter 2), 2) establish a historical baseline climatology of modeled HCW activity using dynamical downscaling (Chapter 3), and 3) investigate potential changes surrounding severe weather activity in a future climate altered by anthropogenic greenhouse warming (Chapter 4). These topics are timely and important, as no study has yet performed dynamical downscaling analysis on current or future period GCM output. Additionally, several devastating severe weather events occurred over the past year, including an EF-5 tornado that struck the town of Moore, OK on 20 May 2013. This event caused 24 fatalities, 377 injuries, and an estimated $2 billion in damages, causing some media responses speculating climate change was to blame. As noted in Brooks (2013), a singular severe thunderstorm event cannot be used as evidence of a trend. However, this dissertation helps extend a promising methodological approach to understanding late 21st Century severe weather projections in a business-as-usual carbon emissions scenario. The following is a summary of the major findings in this dissertation.

5.2 Summary

a. Reanalysis and the observed convective environment

Chapter 2 of this dissertation compared North American Regional Reanalysis (NARR; Mesinger et al. 2006) proxy soundings to observed radiosonde data for various stations across the U.S. during the period 2000–2011. This study was motivated by the need to quantify how well a reanalysis dataset approximates the observed convective environment, as reanalysis variables are typically sources of data for HCW climatological analysis. Most importantly, it is demonstrated that variables representing kinematic calculations are best approximated by NARR, while scalar thermal variables suffer from errors originating in boundary-layer moisture variables. These errors originate from the lack of vertical resolution in NARR and the convective parameterization scheme employed. This leads to errors in evaluation of the elevated mixed-layer and near-surface moisture content (both important features when forecasting for severe thunderstorms), and researchers wishing to use NARR fields to initialize model simulations should be aware of such potential errors. These results should prove useful for future climatological studies using NARR that use physical or derived variables relating to severe convection.

b. Downscaling estimates of historical severe weather

High-resolution dynamical downscaling was used to simulate the variability of HCW across the eastern two-thirds of the U.S. for the months March–May during the period 1980–1990 in Chapter 3 of this dissertation. Initialized by data from the Community Climate System Model version 3 (CCSM3), hourly synthetic severe weather reports were generated from the

Weather Research and Forecasting (WRF; Skamarock et al. 2008) model using values of modeled composite reflectivity and updraft helicity at 4-km grid spacing.

Similar to previous research, severe weather reports simulated by dynamical downscaling in this study depict accurate distributions of HCW during the months examined (Trapp et al. 2011; Robinson et al. 2013). These results are enhanced by evaluating an environmental parameter composed of convective available potential energy and deep-layer wind shear that exhibits strong interannual correlation between modeled reports and re-analyzed environments. Furthermore, hourly comparisons between modeled and observed HCW exhibit strong correlation, indicating that dynamical downscaling can replicate the diurnal cycle of severe convection.

Overall, this chapter indicates that dynamical downscaling of data with relatively coarse grid spacing (~100 km) to the resolution needed to explicitly resolve severe thunderstorms (~4 km) is a beneficial methodology. Such research will be fundamental to our understanding of potential changes in late 21st Century severe weather frequency/variability, and will serve as an augmentation to the previous estimated changes via environmental methods from GCMs and RCMs. This downscaling technique could also be useful to obtain high-resolution information from existing reanalysis datasets (e.g., those discussed in Chapter 2), or applied to other mesoscale atmospheric phenomena.

c. Future estimates of severe weather

Chapter 4 of this dissertation explored the use of dynamical downscaling for purposes of examining potential future changes in severe thunderstorms influenced by a business-as-usual anthropogenic carbon emissions scenario. Again using data from the CCSM3, historical (1980–

1990) data from Chapter 3 of this dissertation was compared to a future (2080–2090) period simulation. In general, a future increase in hazardous convective weather frequency and variability is revealed, especially during the months of March and April. The largest increase in future severe weather events is revealed across the same regions identified as most vulnerable to tornado fatalities by Ashley (2007). This is a significant result, suggesting that vulnerability to severe convective weather may increase due to alterations in physical risk, especially in geographic regions that are already considered to be exceedingly vulnerable.

A new result of Chapter 4 indicates that an increase in the interannual variability of HCW events is also possible in the future, potentially owing to variability in the position of the polar jet stream. This is suggested by nearly a doubling in the standard deviation of future period reports during March–May. During these months, it is the deep-tropospheric shear that governs the severity of events such as large hail and tornadoes (Brooks 2013). Finally, when added to an ever-growing body of literature, results in this chapter suggest that on average late 21st Century thunderstorms will be of greater frequency, especially during afternoon hours, likely a function of robust increases in CAPE and near-surface specific humidity depicted by several GCMs and RCMs (Del Genio et al. 2007; Trapp et al. 2007a; Trapp et al. 2009; Van Klooster and Roebber 2009; Diffenbaugh et al. 2013; Gensini et al. 2013). This study is the first to identify such an increase at the storm-scale and is a small, but significant step toward understanding potential changes in future severe thunderstorms.

5.3 Conclusions

Recent research has significantly increased our understanding of the potential changes associated with severe thunderstorms in a changing climate. Results from this dissertation extend our understanding of such potential modifications, especially in regards to storm-scale changes and linkages to the larger scale convective environment. It is shown that HCW is likely to be more frequent and variable in the late 21st Century. Confidence is instilled in previous research results conducted with environmental analysis, as over 80% of the variability associated with modeled severe convective weather is explained by the product of convective available potential energy and deep-layer (0–6 km) wind shear.

As computer processing continues to be less of an obstacle to this methodology, dynamical downscaling for purposes of examining extreme weather (convective or otherwise) will become feasible for more researchers. This will undoubtedly continue to paint a clearer picture of discussions surrounding severe thunderstorms and climate change, especially once such analysis is feasible in a multi-model ensemble setting. Ultimately, this research is a small, yet significant, step in such discussion. Climate change assessments should address results presented in the studies herein (and other recent research) relative to their discussions regarding severe thunderstorms in a future climate. Finally, these results could be utilized in a physical risk context for decision makers, to begin addressing changes in vulnerability associated with an increase in late 21st Century HCW frequency and variability.

REFERENCES

Alexander, L., and Coauthors, 2013: Climate Change 2013: The Physical Science Basis. Contribution of Working Group I to the Fifth Assessment Report of the Intergovernmental Panel on Climate Change.

Allen, J. T., and D. J. Karoly, 2014: A climatology of Australian severe thunderstorm environments 1979–2011: inter-annual variability and ENSO influence. *International Journal of Climatology*, **34,** 81–97.

Alley, R., and Coauthors, 2007: Summary for policymakers. *Climate Change 2007: The Physical Science Basis,* S. Solomon, and Coauthors, Eds., Cambridge University Press, 1–18.

Ashley, W. S., 2007: Spatial and temporal analysis of tornado fatalities in the United States: 1880–2005. *Weather and Forecasting*, **22,** 1214–1228.

Ashley, W. S., and T. L. Mote, 2005: Derecho hazards in the United States. *Bulletin of the American Meteorological Society,* **86,** 1577–1592.

Barrett, B. S., and V. A. Gensini, 2013: Variability of central United States April–May tornado day likelihood by phase of the Madden-Julian Oscillation. *Geophysical Research Letters*, **40,** 2790–2795.

Baumgardt, D. A., and K. Cook, 2006: Preliminary evaluation of a parameter to forecast environments conducive to non-mesocyclone tornadogenesis. *Preprints, 23rd Conf. on Severe Local Storms,* American Meteorological Society, 12.1.

Biggerstaff, M. I., and R. A. Houze Jr, 1991: Kinematic and precipitation structure of the 10–11 June 1985 squall line. *Monthly Weather Review,* **119,** 3034–3065.

Bluestein, H. B., and G. R. Woodall, 1990: Doppler-radar analysis of a low-precipitation severe storm. *Monthly Weather Review,* **118,** 1640–1665.

Bouwer, L. M., 2011: Have disaster losses increased due to anthropogenic climate change? *Bulletin of the American Meteorological Society*, **92,** 39–46.

Brooks, H. E., 2004: On the relationship of tornado path length and width to intensity. *Weather and Forecasting*, **19,** 310-319.

——, 2013: Severe thunderstorms and climate change. *Atmospheric Research*, **123,** 129–138.

Brooks, H. E., and C. A. Doswell III, 2001: Normalized damage from major tornadoes in the United States: 1890–1999. *Weather and Forecasting*, **16,** 168–176.

——, 2002: Deaths in the 3 May 1999 Oklahoma City tornado from a historical perspective. *Weather and Forecasting*, **17,** 354–361.

Brooks, H. E., C. A. Doswell III, and M. P. Kay, 2003a: Climatological estimates of local daily tornado probability for the United States. *Weather and Forecasting*, **18,** 626–640.

Brooks, H. E., J. W. Lee, and J. P. Craven, 2003b: The spatial distribution of severe thunderstorm and tornado environments from global reanalysis data. *Atmospheric Research*, **67–68,** 73–94.

Brooks, H. E., A. R. Anderson, K. Riemann, I. Ebbers, and H. Flachs, 2007: Climatological aspects of convective parameters from the NCAR/NCEP reanalysis. *Atmospheric Research*, **83,** 294–305.

Browning, K. A., 1962: Cellular structure of convective storms. *Meteorological Monographs,* **91,** 341–350.

——, 1977: The structure and mechanisms of hailstorms. *Meteorological Monographs*, **16,** 1–43.

Changnon, S. A., 2001: Damaging thunderstorm activity in the United States. *Bulletin of the American Meteorological Society,* **82,** 597–608.

——, 2009: Tornado losses in the United States. *Natural Hazards Review*, **10,** 145–150.

Chen, F., and J. Dudhia, 2001: Coupling an advanced land surface-hydrology model with the Penn State-NCAR MM5 modeling system. Part I: Model implementation and sensitivity. *Monthly Weather Review,* **129,** 569–585.

Christensen, J. H., F. Boberg, O. B. Christensen, and P. Lucas-Picher, 2008: On the need for bias correction of regional climate change projections of temperature and precipitation. *Geophysical Research Letters,* **35,** L20709.

Church, C., D. Burgess, C. Doswell, and R. P. Davies-Jones, 1993: *The tornado: its structure, dynamics, prediction, and hazards.* Vol. 79, American Geophysical Union.

Clark, A. J., W. A. Gallus Jr, and T.-C. Chen, 2007: Comparison of the diurnal precipitation cycle in convection-resolving and non-convection-resolving mesoscale models. *Monthly Weather Review,* **135,** 3456–3473.

Collins, W. D., and Coauthors, 2006: The Community Climate System Model Version 3 (CCSM3). *Journal of Climate,* **19,** 2122–2143.

Concannon, P. R., H. E. Brooks, and C. A. Doswell III, 2000: Climatological risk of strong and violent tornadoes in the United States. *Preprints, 2nd Symp. on Environmental Applications,* Long Beach, CA, American Meteorological Society, 212–219.

Craven, J. P., H. E. Brooks, and J. A. Hart, 2004: Baseline climatology of sounding derived parameters associated with deep, moist convection. *National Weather Digest*, **28,** 13–24.

Crisp, C. A., 1979: Training guide for severe weather forecasters, 73 pp.

Cutter, S. L., B. J. Boruff, and W. L. Shirley, 2003: Social vulnerability to environmental hazards. *Social Science Quarterly*, **84,** 242–261.

Davies-Jones, R., 1984: Streamwise vorticity: The origin of updraft rotation in supercell storms. *Journal of the Atmospheric Sciences*, **41,** 2991–3006.

Davies-Jones, R. P., D. W. Burgess, and M. Foster, 1990: Test of helicity as a tornado forecast parameter. *Preprints, 16th Conf. on Severe Local Storms*, American Meteorological Society, 588–592.

Del Genio, A. D., M.-S. Yao, and J. Jonas, 2007: Will moist convection be stronger in a warmer climate? *Geophysical Research Letters*, **34,** L16703.

Deser, C., 2000: On the teleconnectivity of the "Arctic Oscillation". *Geophysical Research Letters*, **27,** 779–782.

Dial, G. L., J. P. Racy, and R. L. Thompson, 2010: Short-term convective mode evolution along synoptic boundaries. *Weather and Forecasting*, **25,** 1430–1446.

Diffenbaugh, N. S., M. Scherer, and R. J. Trapp, 2013: Robust increases in severe thunderstorm environments in response to greenhouse forcing. *Proceedings of the National Academy of Sciences*, **in press.**

Dixon, M., and G. Wiener, 1993: TITAN: Thunderstorm identification, tracking, analysis, and nowcasting-A radar-based methodology. *Journal of Atmospheric and Oceanic Technology*, **10,** 785–797.

Donavon, R. A., and K. A. Jungbluth, 2007: Evaluation of a technique for radar identification of large hail across the Upper Midwest and Central Plains of the United States. *Weather and Forecasting*, **22,** 244–254.

Doswell III, C. A., 1980: Synoptic-scale environments associated with high plains severe thunderstorms. *Bulletin of the American Meteorological Society*, **61,** 1388–1400.

——, 1987: The distinction between large-scale and mesoscale contribution to severe convection: A case study example. *Weather and Forecasting*, **2,** 3–16.

——, 1996: What is a supercell? *Preprints, 18th Conf. on Severe Local Storms*, San Francisco, CA, American Meteorological Society, 161–172.

——, 2001: Severe convective storms—An overview. *Severe Convective Storms*, C. A. Doswell III, Ed., American Meteorological Society, 1–26.

——, 2007: Small sample size and data quality issues illustrated using tornado occurrence data. *Electronic Journal of Severe Storms Meteorology*, **2,** 1–16.

Doswell III, C. A., and D. W. Burgess, 1988: On some issues of United States tornado climatology. *Monthly Weather Review*, **116,** 495–501.

Doswell III, C. A., and E. N. Rasmussen, 1994: The effect of neglecting the virtual temperature correction on CAPE calculations. *Weather and Forecasting*, **9,** 625–629.

Doswell III, C. A., and P. M. Markowski, 2004: Is buoyancy a relative quantity? *Monthly Weather Review*, **132,** 853–863.

Doswell III, C. A., and D. M. Schultz, 2006: On the use of indices and parameters in forecasting severe storms. *Electronic Journal of Severe Storms Meteorology*, **1,** 1–22.

Doswell III, C. A., S. J. Weiss, and R. H. Johns, 1993: Tornado forecasting: A review. *The Tornado: Its Structure, Dynamics, Prediction, and Hazards,* American Geophysical Union, 557–571.

Doswell III, C. A., H. E. Brooks, and R. A. Maddox, 1996: Flash flood forecasting: An ingredients-based methodology. *Weather and Forecasting,* **11,** 560–581.

Dudhia, J., 1989: Numerical study of convection observed during the winter monsoon experiment using a mesoscale two-dimensional model. *Journal of the Atmospheric Sciences*, **46,** 3077–3107.

Elsner, J. B., and H. M. Widen, 2014: Predicting spring tornado activity in the central Great Plains by March 1st. *Monthly Weather Review*, **142,** 259–267.

Evans, J. S., and C. A. Doswell III, 2001: Examination of derecho environments using proximity soundings. *Weather and Forecasting,* **16,** 329–342.

Francis, J. A., and S. J. Vavrus, 2012: Evidence linking Arctic amplification to extreme weather in mid-latitudes. *Geophysical Research Letters*, **39,** L06801.

Francis, J. A., W. Chan, D. J. Leathers, J. R. Miller, and D. E. Veron, 2009: Winter Northern Hemisphere weather patterns remember summer Arctic sea-ice extent. *Geophysical Research Letters*, **36,** L07503.

Fujita, T. T., 1978: *Manual of downburst identification for project NIMROD.* Satellite and Mesometeorology Research Project, Department of the Geophysical Sciences, University of Chicago.

Galway, J. G., and A. Pearson, 1981: Winter tornado outbreaks. *Monthly Weather Review*, **109,** 1072–1080.

Gensini, V. A., and W. S. Ashley, 2011: Climatology of potentially severe convective environments from the North American Regional Reanalysis. *Electronic Journal of Severe Storms Meteorology*, **6,** 1–40.

Gensini, V. A., C. A. Ramseyer, and T. L. Mote, 2014: Future convective environments using NARCCAP. *International Journal of Climatology*, **34**, 1699–1705.

Gensini, V. A., and T. L. Mote, 2014: Examination of historical hazardous convective weather using dynamical downscaling. *Journal of Climate*, **submitted.**

Grazulis, T. P., 1993: *Significant tornadoes: 1680–1991.* Environmental Films, 1326 pp.

Hales, J. E., 1988: Improving the watch/warning system through the use of significant event data. *Preprints, 24th Conference on Severe Local Storms*, Baltimore, MD, American Meteorological Society, 165–168.

Han, L., S. Fu, L. Zhao, Y. Zheng, H. Wang, and Y. Lin, 2009: 3D convective storm identification, tracking, and forecasting-An enhanced TITAN algorithm. *Journal of Atmospheric and Oceanic Technology*, **26,** 719–732.

Hart, J. A., and W. Korotky, 1991: The SHARP workstation version 1.5, A skew-t / hodograph analysis and research program for the IBM and compatible PC. 58 pp.

Higgins, R. W., and S. D. Schubert, 1996: Simulations of persistent North Pacific circulation anomalies and interhemispheric teleconnections. *Journal of the Atmospheric Sciences*, **53,** 188–207.

Hilgendorf, E. R., and R. H. Johnson, 1998: A study of the evolution of mesoscale convective systems using WSR-88D data. *Weather and Forecasting*, **13,** 437–452.

Hohenegger, C., P. Brockhaus, and C. Schar, 2008: Towards climate simulations at cloud-resolving scales. *Meteorologische Zeitschrift*, **17,** 383–394.

Hong, S.-Y., and J.-O. J. Lim, 2006: The WRF single-moment 6-class microphysics scheme (WSM6). *Journal Korean Meteorological Society*, **42,** 129–151.

Houze Jr, R. A., 2004: Mesoscale convective systems. *Reviews of Geophysics*, **42,** RG4003.

Hunter, J. D., 2007: Matplotlib: A 2D graphics environment. *Computing in Science and Engineering***,** 90–95.

Iacono, M. J., E. J. Mlawer, S. A. Clough, and J. J. Morcrette, 2000: Impact of an improved longwave radiation model, RRTM, on the energy budget and thermodynamic properties of the NCAR community climate model, CCM3. *Journal of Geophysical Research*, **105,** 14873–14890.

Janjić, Z. I., 1990: The step-mountain coordinate: Physical package. *Monthly Weather Review*, **118,** 1429–1443.

——, 1994: The step-mountain eta coordinate model: Further developments of the convection, viscous sublayer, and turbulence closure schemes. *Monthly Weather Review*, **122,** 927–945.

Johns, R. H., 1982: A synoptic climatology of northwest flow severe weather outbreaks. Part I: Nature and significance. *Monthly Weather Review*, **110,** 1653–1663.

——, 1984: A synoptic climatology of northwest-flow severe weather outbreaks. Part II: Meteorological parameters and synoptic patterns. *Monthly Weather Review*, **112,** 449–464.

Johns, R. H., and W. D. Hirt, 1987: Derechos: Widespread convectively induced windstorms. *Weather and Forecasting*, **2,** 32–49.

Johns, R. H., and C. A. Doswell III, 1992: Severe local storms forecasting. *Weather and Forecasting*, **7,** 588–612.

Johnson, J., P. L. MacKeen, A. Witt, E. D. W. Mitchell, G. J. Stumpf, M. D. Eilts, and K. W. Thomas, 1998: The storm cell identification and tracking algorithm: An enhanced WSR-88D algorithm. *Weather and Forecasting*, **13,** 263–276.

Kain, J. S., and Coauthors, 2008: Some practical considerations regarding horizontal resolution in the first generation of operational convection-allowing NWP. *Weather and Forecasting*, **23,** 931–952.

Kalnay, E., and Coauthors, 1996: The NCEP/NCAR 40-year reanalysis project. *Bulletin of the American Meteorological Society*, **77,** 437–471.

Karl, T. R., J. M. Melillo, and T. C. Peterson, 2009: *Global climate change impacts in the United States.* Cambridge University Press.

Kelly, D. L., J. T. Schaefer, R. P. McNulty, C. A. Doswell III, and R. F. Abbey Jr., 1978: An augmented tornado climatology. *Monthly Weather Review*, **106,** 1172–1183.

Kendon, E. J., N. M. Roberts, C. A. Senior, and M. J. Roberts, 2012: Realism of rainfall in a very high-resolution regional climate model. *Journal of Climate*, **25**, 5791–5806.

Knupp, K. R., and W. R. Cotton, 1987: Internal structure of a small mesoscale convective system. *Monthly Weather Review*, **115,** 629–645.

Langhans, W., J. Schmidli, O. Fuhrer, S. Bieri, and C. Schar, 2013: Long-Term Simulations of Thermally Driven Flows and Orographic Convection at Convection-Parameterizing and Cloud-Resolving Resolutions. *Journal of Applied Meteorology & Climatology*, **52**, 1490–1510.

Lanicci, J. M., and T. T. Warner, 1991: A synoptic climatology of the elevated mixed-layer inversion over the southern Great Plains in spring. Part I: Structure, dynamics, and seasonal evolution. *Weather and Forecasting*, **6,** 198–213.

Lee, J. W., 2002: Tornado proximity soundings from the NCEP/NCAR reanalysis data, Meteorology, University of Oklahoma, 61 pp.

Lemon, L. R., 1977: New severe thunderstorm radar identification techniques and warning criteria. D. o. Defense, Ed., Air Weather Service, 67.

Liu, C., M. W. Moncrieff, J. D. Tuttle, and R. E. Carbone, 2006: Explicit and parameterized episodes of warm-season precipitation over the continental United States. *Advances in Atmospheric Sciences*, **23,** 91–105.

Madden, R. A., and P. R. Julian, 1972: Description of global-scale circulation cells in the tropics with a 40–50 day period. *Journal of the Atmospheric Sciences*, **29,** 1109–1123.

Maddox, R. A., 1983: Large-scale meteorological conditions associated with midlatitude, mesoscale convective complexes. *Monthly Weather Review*, **111,** 1475–1493.

Mahoney, K., M. Alexander, J. D. Scott, and J. Barsugli, 2013: High-resolution downscaled simulations of warm-season extreme precipitation events in the Colorado Front Range under past and future climates. *Journal of Climate*, **26**, 8671–8689.

Markowski, P., and Y. Richardson, 2011: *Mesoscale Meteorology in Midlatitudes.* Wiley-Blackwell, 407 pp.

Mearns, L. O., W. Gutowski, R. Jones, R. Leung, S. McGinnis, A. Nunes, and Y. Qian, 2009: A regional climate change assessment program for North America. *Eos, Transactions American Geophysical Union,* **90,** 311.

Mearns, L. O., and Coauthors, 2012: The North American regional climate change assessment program: overview of phase I results. *Bulletin of the American Meteorological Society*, **93,** 1337–1362.

Mellor, G. L., and T. Yamada, 1982: Development of a turbulence closure model for geophysical fluid problems. *Reviews of Geophysics*, **20,** 851–875.

Mesinger, F., and Coauthors, 2006: North American Regional Reanalysis. *Bulletin of the American Meteorological Society*, **87,** 343–360.

Miller, R. C., 1972: Notes on analysis and severe-storm forecasting procedures of the Air Force Global Weather Central. D. o. Defense, Ed., Air Weather Service Tech. Rept. 200 (Rev.), 190.

Mlawer, E. J., S. J. Taubman, P. D. Brown, M. J. Iacono, and S. A. Clough, 1997: Radiative transfer for inhomogeneous atmospheres: RRTM, a validated correlated-k model for the longwave. *Journal of Geophysical Research,* **102,** 16663–16682.

Moncrieff, M. W., and M. J. Miller, 1976: The dynamics and simulation of tropical cumulonimbus and squall lines. *Quarterly Journal of the Royal Meteorological Society*, **102,** 373–394.

Nakicenovic, N., and Coauthors, 2000: Special report on emissions scenarios: a special report of Working Group III of the Intergovernmental Panel on Climate Change, 599 pp.

Parker, M. D., and R. H. Johnson, 2000: Organizational modes of midlatitude mesoscale convective systems. *Monthly Weather Review*, **128,** 3413–3436.

Petoukhov, V., S. Rahmstorf, S. Petri, and H. J. Schellnhuber, 2013: Quasiresonant amplification of planetary waves and recent Northern Hemisphere weather extremes. *Proceedings of the National Academy of Sciences*, **110,** 5336–5341.

Prein, A. F., G. J. Holland, R. M. Rasmussen, J. Done, K. Ikeda, M. P. Clark, and C. H. Liu, 2013: Importance of regional climate model grid spacing for the simulation of heavy precipitation in the Colorado Headwaters. *Journal of Climate*, **26**, 4848–4857.

Rasmussen, E. N., 2003: Refined supercell and tornado forecast parameters. *Weather and Forecasting*, **18,** 530–535.

Rasmussen, E. N., and D. O. Blanchard, 1998: A baseline climatology of sounding-derived supercell and tornado forecast parameters. *Weather and Forecasting*, **13,** 1148–1164.

Rasmussen, E. N., and J. M. Straka, 1998: Variations in supercell morphology. Part I: Observations of the role of upper-level storm-relative flow. *Monthly Weather Review*, **126,** 2406–2421.

Robinson, E. D., R. J. Trapp, and M. E. Baldwin, 2013: The geospatial and temporal distributions of severe thunderstorms from high-resolution dynamical downscaling. *Journal of Applied Meteorology and Climatology***,** in press.

Rotunno, R., 1981: On the evolution of thunderstorm rotation. *Monthly Weather Review*, **109,** 577–586.

Sato, T., H. Miura, M. Satoh, Y. N. Takayabu, and Y. Wang, 2009: Diurnal cycle of precipitation in the tropics simulated in a global cloud-resolving model. *Journal of Climate*, **22**, 4809–4826.

Schaefer, J. T., and R. Edwards, 1999: The SPC tornado/severe thunderstorm database. *11th Conference on Applied Climatology*, American Meteorological Society, 603–606

Screen, J. A., and I. Simmonds, 2013: Exploring links between Arctic amplification and mid-latitude weather. *Geophysical Research Letters*, **40,** 959–964.

Skamarock, W. C., 2004: Evaluating mesoscale NWP models using kinetic energy spectra. *Monthly Weather Review*, **132,** 3019–3032.

Skamarock, W. C., J. B. Klemp, J. Dudhia, D. O. Gill, D. M. Barker, W. Wang, and J. G. Powers, 2008: A description of the Advanced Research WRF version 3. NCAR Tech. Note NCAR/TN-475+STR, 113pp.

Smull, B. F., and R. A. Houze Jr, 1985: A midlatitude squall line with a trailing region of stratiform rain: Radar and satellite observations. *Monthly Weather Review*, **113,** 117–133.

Thompson, R. L., C. M. Mead, and R. Edwards, 2007: Effective storm-relative helicity and bulk shear in supercell thunderstorm environments. *Weather and Forecasting*, **22,** 102–115.

Thompson, R. L., R. Edwards, J. A. Hart, K. L. Elmore, and P. Markowski, 2003: Close proximity soundings within supercell environments obtained from the Rapid Update Cycle. *Weather and Forecasting*, **18,** 1243–1261.

Trapp, R. J., N. S. Diffenbaugh, H. E. Brooks, M. E. Baldwin, E. D. Robinson, and J. S. Pal, 2007a: Changes in severe thunderstorm environment frequency during the 21st century caused by anthropogenically enhanced global radiative forcing. *Proceedings of the National Academy of Sciences*, **104,** 19719–19723.

Trapp, R. J., B. A. Halvorson, and N. S. Diffenbaugh, 2007b: Telescoping, multimodel approaches to evaluate extreme convective weather under future climates. *Journal of Geophysical Research*, **112,** D20109.

Trapp, R. J., N. S. Diffenbaugh, and A. Gluhovsky, 2009: Transient response of severe thunderstorm forcing to elevated greenhouse gas concentrations. *Geophysical Research Letters*, **36,** L01703.

Trapp, R. J., E. Robinson, M. Baldwin, N. Diffenbaugh, and B. Schwedler, 2011: Regional climate of hazardous convective weather through high-resolution dynamical downscaling. *Climate Dynamics*, **37,** 677–688.

Trapp, R. J., N. S. Diffenbaugh, H. E. Brooks, M. E. Baldwin, E. D. Robinson, and J. S. Pal, 2007a: Changes in severe thunderstorm environment frequency during the 21st century caused by anthropogenically enhanced global radiative forcing. *Proceedings of the National Academy of Sciences*, **104,** 19719–19723.

Uccellini, L. W., and D. R. Johnson, 1979: The coupling of upper and lower tropospheric jet streaks and implications for the development of severe convective storms. *Monthly Weather Review*, **107,** 682–703.

Van Klooster, S. L., and P. J. Roebber, 2009: Surface-based convective potential in the contiguous United States in a business-as-usual future climate. *Journal of Climate*, **22,** 3317–3330.

Verbout, S. M., H. E. Brooks, L. M. Leslie, and D. M. Schultz, 2006: Evolution of the U.S. tornado database: 1954–2003. *Weather and Forecasting*, **21,** 86–93.

Warrach-Sagi, K., T. Schwitalla, V. Wulfmeyer, and H.-S. Bauer, 2013: Evaluation of a climate simulation in Europe based on the WRF–NOAH model system: precipitation in Germany. *Climate Dynamics*, **41,** 755–774.

Weisman, M. L., and J. B. Klemp, 1982: The dependence of numerically simulated convective storms on vertical wind shear and buoyancy. *Monthly Weather Review*, **110,** 504–520.

Weisman, M. L., and J. B. Klemp, 1984: The structure and classification of numerically simulated convective storms in directionally varying wind shears. *Monthly Weather Review*, **112,** 2479–2498.

Weisman, M. L., W. C. Skamarock, and J. B. Klemp, 1997: The resolution dependence of explicitly modeled convective systems. *Monthly Weather Review*, **125,** 527–548.

Weisman, M. L., C. Davis, W. Wang, K. W. Manning, and J. B. Klemp, 2008: Experiences with 0–36-h Explicit Convective Forecasts with the WRF-ARW Model. *Weather and Forecasting*, **23,** 407–437.

Wilks, D. S., 1995: *Statistical Methods in the Atmospheric Sciences.* Academic Press, 467 pp.

Witt, A., M. D. Eilts, G. J. Stumpf, J. Johnson, E. D. W. Mitchell, and K. W. Thomas, 1998: An enhanced hail detection algorithm for the WSR-88D. *Weather and Forecasting*, **13,** 286–303.

Zipser, E. J., 1982: Use of a conceptual model of the life-cycle of mesoscale convective systems to improve very-short-range forecasts. Academic Press, 191–204.